## ABSTRACT

BOPPA, VENUGOPAL. Characterization of Structure and Tensile Properties of Electrospun Web. (Under the direction of Dr. Bhupender S. Gupta.)

Electrospinning has been considered a versatile method for producing nanofibers, which have generated great interest for use in many areas, including those of tissue engineering and filtration, due to their high surface area to volume ratio and high porosity. Mechanical properties of these materials are important for these and many other applications. Although much work has been carried out in the area of electrospinning technology over the past decade, little has been focused on the structure of electrospun webs and their mechanical properties. This work was undertaken to close a part of this gap in the literature.

Using PEO as the polymer and water as the solvent, a series of electrospun webs were produced. The primary variables used were polymer concentration and time of spinning and properties measured were peak stress-peak strain, initial modulus and yield point. It was found necessary to adjust voltage and the distance between the needle and collector plate to get a stable Taylor cone, which was essential for forming uniform fibers. Three levels of concentrations, 8, 10 and 12.5% PEO were used to produce electrospun webs and these led to nanofibers of diameter 210nm, 325nm and 550nm, respectively. Increase in concentration resulted in decrease in stress and modulus values, and increase in strain values. The time of spinning was varied to simply vary the areal density of the web that was expected to have an influence on peak force; areal density was particularly an important input parameter for the model used for predicting the tensile properties of a web.

The model to predict the tensile properties of web required single fiber stress-strain properties. Difficulty of conducting tensile test on single fibers required the use of an alternative way, tensile testing of aligned fiber bundles. Aligned fiber bundles were produced using collector strips separated with a gap. For these fibers, effects of concentration and spinning distance on fiber morphology and mechanical properties were investigated. Concentration showed similar effect, as found in the case of unoriented webs, increase in concentration fiber led to diameter increase, and stress and modulus values decreased. With increase in spinning distance, fiber diameter decreased, and stress and modulus values increased.

A mathematical model is developed and proposed for predicting the stress-strain behavior of electrospun webs. The analysis method used was the “Force method”. Peak stress values were predicted using single fiber stress-strain properties in conjunction with the model. Predicted values of peak stress matched closely with the measured values within a correction factor of less than two. Reasons are given for the small differences noted between the measured and predicted values. The results noted in the measured values of peak stress and the difference found between the predicted and the measured values suggest that the fibers in the electrospun webs are bonded to some extent at the cross-over points. This leads to the suggestion that the structural model used for characterizing the tensile behavior should be modified by including bonding at the cross-over points.

# Characterization of Structure and Tensile Properties of Electrospun Web

by
Venugopal Boppa

A thesis submitted to the Graduate Faculty of
North Carolina State University
in partial fulfillment of the
requirements for the Degree of
Master of Science

Textile Engineering

Raleigh, North Carolina

2009

APPROVED BY:

| | |
|---|---|
| _____ | _____ |
| Dr. Hechmi Hamouda | Dr. Jeffrey Ray Thompson |

_____
Dr. Bhupender S. Gupta
Chair of Advisory Committee

# DEDICATION

Dedicated to my family and friends for being a source of immense inspiration, for their undying support and steadfast belief.

# BIOGRAPHY

Venugopal Boppa was born in Siddipet, India. He completed his Bachelor of Technology, in Textile Technology from University College of Technology, Osmania University, Hyderabad in 2004. After completing his under graduation, he obtained professional experience as a Technical Trainee at Reid and Taylor, Mysore. He came to the United States to pursue his Master of Science degree in Textile Engineering at North Carolina State University in Spring 2007. He was inducted in the Phi-Kappa-Phi society in the year 2008, in recognition of maintaining an overall GPA of 4.00 during the course of his Master's degree. Currently he is working towards completing the requirements for the Master's degree.

# ACKNOWLEDGMENTS

I would like to thank the people who have immense importance in my life and have made me the person I am today.

I would like to express my heartfelt gratitude to my mentor Dr. Bhupender S. Gupta, for his valuable guidance and constant support during my Master's degree. Without his encouraging presence this work would not have been possible. I truly feel privileged to have worked under him.

I would like to thank my committee members Dr. Hechmi Hamouda and Dr. Jeffrey Ray Thompson for their encouragement and belief in my potential to undertake this work successfully. I would like to thank the NTC and the College of Textiles for funding this research.

I cannot express in words my gratitude to my parents, brother and sister for their unconditional love, unwavering support and limitless faith that they had in me. Though physically far away you have this knack of making me feel that you are around as and when I need your presence and encouragement.

My heartfelt thanks to Dr. Russell Gorga and Dr. Martin King for giving me access to the Instron machine. I would like to offer my high appreciation to the physical testing lab manager Dr. Jan E. Pegram, the lab assistant Ms. Teresa J White, analytical lab manager Ms.

Birgit Andersen, Graduate secretary Ms. Angie Brantley and SEM Lab Manager Mr. Charles B Mooney for their technical help and coordination in conducting studies.

Thanks to all my friends Ajit, Dnyanada, Neha, Nilesh, Ravikanth, Rupesh, Syamal, Vamsi, and Vijay without whose cheerful presence, my life in Raleigh would have not been half as enjoyable.

# TABLE OF CONTENTS

# LIST OF TABLES

# LIST OF FIGURES

# 1. INTRODUCTION

In the electrospinning field, most of the attention has been focused on producing uniform fibers and how the diameter values and their distribution may vary with the materials and the processing conditions. Little is known about the structure of nanofibers, the accompanying mechanical properties, and how these vary with the processing conditions. Due to their high surface area to the volume ratio, high porosity and interconnected pore network, electrospun nanofibers, have been drawing interest in a range of applications, including filtration, biomedical products (drug delivery systems, tissue scaffolds), optical fibers, composite materials and protective clothing. Accordingly, due to this increasing popularity and potential of even broader applications, it is important that one is able to fully understand the nature of structure and the tensile properties found in electrospun webs and be able to model and predict the latter.

A primary requirement to succeed in modeling and predicting the mechanical properties will be that one understands the nature of fiber distribution, determine the number of fibers in the specimen actually gripped in the jaws of the tester and supporting the load. One of the variables of the study is the width of specimen that directly influences the number of fibers gripped in the jaws. Another variable is the areal density of the web that for a given material and set of processing conditions varies with the length of time of deposition of the fibers on the collector plate or device. An increase in the areal density can be assumed to cause an increase in the number of fibers in a given interval of angular orientation. Another variable affecting the mechanical properties is the fiber diameter. Change in the processing conditions

of electrospinning, such as concentration of polymer and voltage applied, can cause a change in the internal structure of fiber and its diameter. Modeling and predicting the tensile properties of electrospun web would require the properties of constituent elements the web is composed of, which are the individual nanofibers. Accordingly, measuring the mechanical properties of not only the webs produced but also of the individual fibers it is made up of will be necessary. Though electrospinning is an old process of making nanofibers, much less has been investigated and published on the mechanical properties of electrospun webs and of the single nanofibers, most probably due to the difficulty involved in handling the delicate and tiny size materials.

In this thesis project the objectives are as follows:

1. Set-up the electrospinning apparatus to produce uniform nanofiber webs made up of different fiber diameters, by varying polymer concentration and voltage applied.

2. Evaluate the structure of the web produced in terms parameters required for modeling tensile properties – i.e. fiber diameter and web thickness.

3. Conduct tensile tests on the webs to find the effect of concentration, width of test specimen.

4. Determine single fiber stress-strain properties by conducting tensile tests on aligned nanofiber bundles produced using collector strips separated with gap.

5. Find the effect of process variables, like concentration of polymer solution, distance between the collector plate and needle on the fiber size, web thickness and tensile properties.
6. Model the structure of the electrospun web and its tensile properties.
7. Compare the predicted values with those measured.

In this thesis, the chapters listed are as follows:

Chapter 2 covers the literature review on the history and fundamentals of electrospinning, effect of processing parameters on the electrospinning process, methods of testing single nanofiber mechanical properties, mechanical properties of electrospun web. As no literature existed on the prediction of tensile properties of electrospun webs, the literature found on the non-woven materials was reviewed to get an insight on the structural mechanics.

Model developed to predict the number of fibers supporting load at different orientations and their contribution to the web tensile properties is given in detail in Chapter 3. There are two approaches that might be used to model and predict mechanical properties: the Force method and the Energy method. The first attempt made was using the Force method. This is included in Chapter 3. Energy method was also used, but since no computations were made using it, the equations derived are included in Appendix A.

Chapter 4 elucidates the experimental procedures followed in this research. It gives details about the materials used, the procedures followed to produce random web and aligned

fiber bundles, and the process variables studied. This chapter also covers the technique used for preparing the samples, conducting tests, and characterizing the data obtained.

Results are presented and discussed in Chapter 5.

The last chapter includes conclusions obtained based on this research as well as a list of recommendations for further work in this area.

# 2. LITERATURE REVIEW

## 2.1 Electrospinning

Polymer nanofibers are in demand due to their potential advanced applications. Electrospinning is an emerging method for producing nanofibers. Electrospun fibers with their high surface area to volume ratio and small pores, are drawing interest in vast variety of applications, some being, filtration products, scaffolds for tissue engineering, wound dressings, drug release materials, fiber reinforcement composites, protective clothing (Ramakrishna, 2005).

### *2.1.1 History*

In 1700s influence of electrostatics was observed on water behavior and an electric charge influenced the excitation of dielectric liquid. This probably led to the invention of electrospinning to produce fibers in the early 1900s by Cooley and Morton. In one of the earliest electrospinning inventions, Cooley patented a set-up that used auxiliary electrodes to direct the electrospinning jet onto a rotating collector. In the 1930s, Formhals has introduced several innovative set-ups to produce yarns from electrospun fibers, including designs that did not require the use of a spinneret (Teo, 2006) and patented his invention relating to the process and the apparatus. In 1940, Formhals patented another method for producing composite fiber webs from multiple polymer substrates by electrostatically spinning polymer fibers on a moving base substrate. In 1969, Taylor studied the shape of the polymer droplet produced at the tip of the needle when an electric field was applied and showed that it was a

cone and the jets ejected from the vortices of the cone. This cone was later referred to as the 'Taylor cone'. The effects of electric field, experimental conditions and the factors affecting the atomization and fiber stability were studied (Subbiah, Bhat, Tock, Parameswaran, & Ramkumar, 2005). For the fiber industries, one important consideration is the rate of fiber production. Electrospinning, compared to the popular industrial fiber spinning processes, has very low production rates (Teo, 2006). Industrial dry spinning has a yarn take-up rate of 200–1500 m $min^{-1}$ while yarn fabricated from electrospinning has a take-up speed of 30 m $min^{-1}$. Thus, before 1990, there was very little industrially oriented research interest found on electrospinning. Melt spinning being the preferred method for producing synthetic fibers, efforts were made to electrospin fibers using polymer melts, but difficulties were encountered in fabricating fibers with nanometer diameters and, therefore, little progress was made in this specific approach. Nevertheless, Dalton *et al* (Dalton, Klinkhammer, Salber, Klee, & Moller, 2006) recently succeeded in depositing electrospun polymer melt fibers directly on to cells to form layered tissue constructs for tissue engineering. This eliminated the introduction of cytotoxic solvents into the cell culture when the fibers were deposited. While there have been patents filed for various electrospinning set-ups since the 1900s, it is only in the last decade that academia got heavily involved in using electrospinning to fabricate various nano-fibrous assemblies for a range of potential applications.

### *2.1.2 Electrospinning fundamentals*

The formation of nanofibers through electrospinning is based on the uniaxial stretching of a visco-elastic solution due to electrostatic charges. Polymer solution or the melt that has to

be spun is forced through a syringe pump to form a pendant droplet of the polymer at the tip of the capillary where the polymer exits. High voltage potential of 10-30kV is applied to the polymer material inside the syringe through an immersed electrode, thereby inducing charges into the polymer solution. Taylor showed that jet will erupt from the droplet forming a conical shaped surface (the 'Taylor cone') with an angle of 49.3° when a critical potential is reached. This disturbs the equilibrium of the droplet at the tip of the capillary, and initiates ejection (Subbiah et al., 2005). Due to the critical voltage, applied potential reaches a critical value and the repulsive force within the charged solution exceeds surface tension and a jet erupts from the tip of the cone. These charged ions in the polymer jet move in response to the applied electric field towards the electrode of opposite polarity, thereby transferring tensile forces to the polymer jet making the latter undergo a chaotic motion or bending instability with whipping action. The jet moves towards the opposite charged collector, which collects the charged fibers. The jet ejected from the apex of the cone continues to thin down along the path of its travel towards the collector. As the jet travels through the atmosphere, the solvent evaporates, leaving behind a dry fiber on the collecting device. The structure formation happens on a millisecond scale (Dersch, Liu, Schaper, Greiner, & Wendorff, 2003). An important step within production of the fibers is the elongation taking place within the jet with a strain rate as high as $10^4$ $sec^{-1}$ (Subbiah et al., 2005).

Similar to conventional fiber spinning methods, the spinning of the solution to form the fiber will continue as long as there is enough polymer solution to feed the electrospinning jet. Thus without any disruption to the electrospinning jet, the formation of the fiber will be

continuous. Fiber assembly changes with the type of collector. A review paper by Teo *et al* (Teo, 2006) explains various concepts to get different fibrous assemblies.

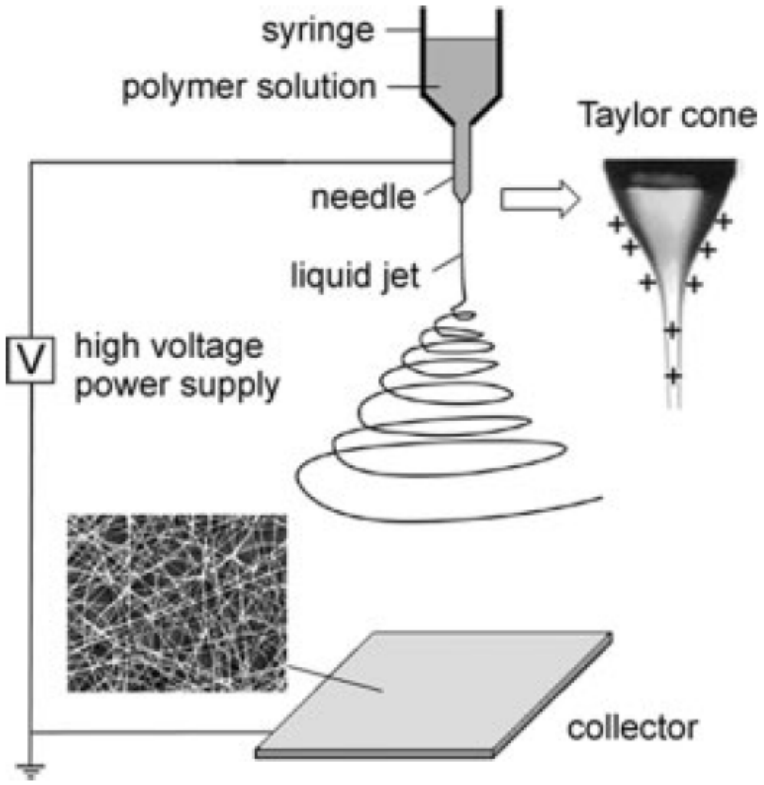


**Figure 2.1:** Schematic illustration of electrospinning setup (D. Li & Xia, 2004)

A typical electrospinning setup only requires a high voltage power supply, a syringe, a flat tip needle and a conducting collector as shown in Figure 2.1. Electrospinning is able to produce continuous nanofibers from a wide range of materials. But there are many parameters which affect the fiber morphology and properties in electrospinning. The main parameters are polymer parameters and processing conditions (Ramakrishna, 2005).

### *2.1.3 Processing parameters*

2.1.3.1 Polymer Solution parameters

Polymer molecular weight, polymer concentration, solution viscosity, surface tension and solution conductivity are some that fall under this category and influence the fiber morphology. Higher molecular weight polymer dissolved in solvent has higher viscosity than solution of the same material but with lower molecular weight. Polymer molecular weight represents the chain length of the polymer which in turn influences the entanglements, hence the viscosity of the solution. Polymer solution is stretched during electrospinning from the needle tip to the collector plate. These entanglements prevent the jet from breaking up during the process. Low viscous polymer solution jet breaks up into small droplets or creates beaded fibers. As the viscosity increases, the number of entanglements increases and results in uniform fibers without beads as shown in Figure 2.2 . If, however, the viscosity is too high, it will be difficult to pump the solution through the capillary and the solution may dry up or drip at the tip. (Ramakrishna, 2005)

Similar effects can be observed also with the polymer concentration as the factor. When the polymer concentration is increased, number of polymer chains increases and results in more chain entanglements as noted above when the molecular weight is increased. Both lead to an increase in the viscosity of the polymer solution and produce somewhat similar effects.

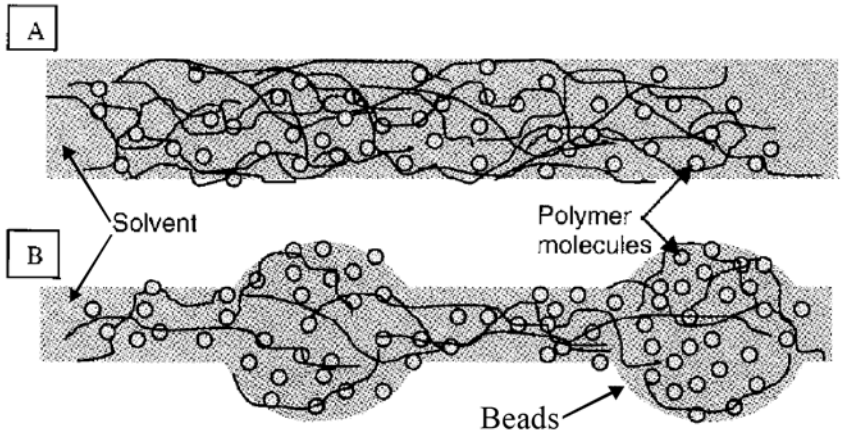


**Figure 2.2:** (A) At higher viscosity, the solvent molecules are distributed over the entangled polymer molecules where as, (B) with a lower viscosity, the solvent molecules tend to congregate under the action of surface tension

In addition to the formation of beads or uniform fibers, another effect of viscosity is the deposition area on collector plate. Higher concentration polymer solution has more entanglements and resists the bending instability to some extent and the collected mass spreads over a smaller area. The reduced jet path, on the other hand, causes less stretching of the solution and results in larger fiber diameter (Ramakrishna, 2005).

To erupt a jet from the tip of needle, surface tension has to be overcome by the electric forces due to the charges in the solution. Surface tension causes the surface area per unit mass of the solution to decrease and forces it to form a spherical droplet. In case of less concentration of polymer solution, high ratio of solvent molecules have greater tendency to congregate and form a spherical shape due to surface tension. This causes beads in fibers collected. In higher viscous solution, there is greater interaction between polymer and solvent

molecules. Solvent molecules will spread over the entangled polymer molecules and uniform fibers will deposit on the collector. To form bead free uniform fibers, low surface tension solvents should be used in forming the polymer solution.

Repulsion of charges at the surface of polymer solution causes stretching of the jet. If the conductivity of the solution is increased by addition of ions, more charges can be carried by the jet. Addition of small amount of salt or polyelectrolyte to the polymer solution would increase the stretching and assists in forming smooth fibers in place of beaded fibers. This additional stretching also reduces the fiber diameter. Further, the presence of extra ions in the solution increases the conductivity and reduces the required critical voltage for electrospinning. The increased conductivity also results in greater bending instability and increase in deposition area of fibers (Moghe, 2008).

2.1.3.2 Processing conditions

Processing conditions include the voltage applied, the feed rate, distance between needle tip and collector, diameter of needle and type of collector etc. These factors are known to affect the electrospinning process.

High voltage induces required charges on the solution to cause the jet to emerge from the tip of needle. Higher voltage than required will cause the jet to accelerate faster, more volume of solution to be drawn, and result in smaller Taylor cone. Effect of voltage on diameter of fiber is uncertain. In some cases, higher voltage will lead to greater stretching of the solution due to the greater columbic forces and to smaller diameter fibers. In some other

cases, lower voltage reduces the acceleration of the jet and increases the flight time which may favor formation of finer fibers. More research is needed to ascertain these exact effects.

Amount of solution available between the needle and the collector plate for electrospinning is determined by the feed rate. With the increase in latter, diameter of fiber or bead size increases. But there is limit to the increase of fiber diameter because to maintain a stable Taylor cone, voltage also needs to be increased with the feed rate. This increase in voltage causes more stretching of solution which counters the increased diameter due to the increase in feed rate. Increased feed rate may also cause fusing of fibers due to improper evaporation of solvent before the fiber is collected.

Distance between the collector plate and needle tip affects the flight time and electric field strength. The reduction in the distance causes shorter flight time for the jet. So the jet may not have enough time to solidify and result in fusing of fibers. Decreasing the distance has the same effect as increasing the voltage: in both cases the electric field strength increases. If the field strength is too high, increased instability in jet causes bead formation. Diameter of fiber is also affected by the distance between tip and collector. Increase in distance means longer flight time for the solution to be stretched and the fiber diameter will decrease. But if the distance is further increased, low field strength causes less stretching and increase in fiber diameter. So, field strength below some optimum value will cause decrease in stretching and, therefore, increase in fiber diameter.

Diameter of the orifice also has an effect. Smaller internal diameter reduces the clogging due to less exposure of solution to the atmosphere. Reduction in diameter of needle causes the surface tension of the solution to increase as the droplet size decreases. This causes the acceleration of the jet to decrease. So jet gets more flight time before deposition and has more stretching and elongation; this results in smaller diameter fibers.

The above parameters are the major factors affecting the fiber morphology and web properties in electrospinning. Another factor is the design of the collector. Regular electrospinning yields randomly aligned nanofibers. Control on the geometry of deposition of fiber or getting other desired fiber patterns can be achieved with change in design of collectors. One of these is parallel bars with a gap between the two that leads to aligned nanofibers. Li *et al* (D. Li, Wang, & Xia, 2003) used this set-up for producing aligned fiber bundles. Two strips of electrical conductors with a gap whose size can be varied is shown in Figure 2.3(A).

Electric field lines split into two parts near the collectors pointing towards opposite edges of the gap, as shown in the cross-sectional view of the electric field strength vectors between needle and collector (Figure 2.3(B)). The visco-elastic polymer has charged elements within it and is subjected to two forces while depositing on to the electrode. First force ($F_1$) originates from the splitting electrical field and the second one ($F_2$) exists between the charged fiber and opposite charged electrode surface (Figure 2.3(C)). The attraction between the opposite charges of the fiber and electrode pulls the ends of a fiber segment towards the two electrodes. The force, $F_1$, further straightens the fiber and deposits perpendicular to the

edges of each electrode. The fibers suspended across the gap will remain charged even after deposition, and the repulsion between the deposited and upcoming fibers further enhances the parallel alignment (D. Li et al., 2003)(Tan, Ng, & Lim, 2005).

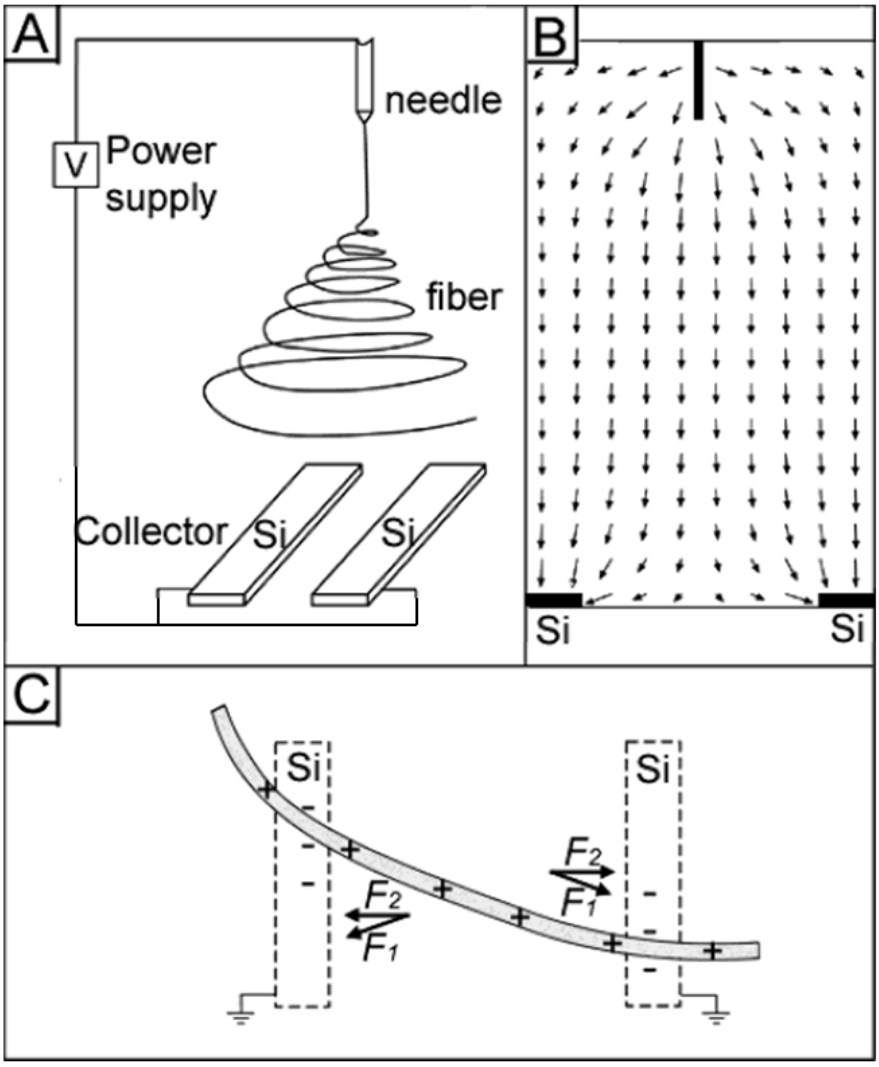


**Figure 2.3:** (A) Electrospinning with two strips of electrodes to collect aligned fibers, (B) Profile of electric field, (C) Forces acting on the fiber between the electrodes (D. Li et al., 2003)

## 2.2 Mechanical properties

Mechanical properties of electrospun nanofibers are important as their applications in products should provide long life durability and structural integrity. Traditional testing methods can be applied for tensile testing of electrospun web but modeling and validating their behavior that requires the results of a test on a single fiber is challenging. Little has been published on the tensile properties of nanofiber webs.

### *2.2.1 Single nanofiber testing*

Difficulty in handling single nanofiber without damaging it and non-availability of sensitive enough equipment (sensitive force transducers) to measure the minute loads (Nanonewtons) on the fiber are the main reasons for lack of publications in this area. Following testing techniques have however been tried to measure mechanical properties of single nanofibers. They are the nano tensile and bending test methods.

Nano Tensile Test:

Tan *et al* (Tan et al., 2005) used Piezo-resistive AFM tip to perform tensile test on single electrospun fiber. For this, one end of aligned electrospun fiber was glued to inverted microscope stage, used as actuator to apply stretch to the nanofiber. The other end of the fiber was glued to the AFM cantilever tip (Figure 2.4). When the microscope stage is moved to give elongation to the fiber, the deflection in the cantilever tip results in a linear change in resistance. This resistance can be converted to load readings by connecting a multimeter to

the piezo-resistive cantilever tip. This test was conducted on PEO nanofiber of 700 nm diameter, the stress-strain curve obtained is shown in Figure 2.5.

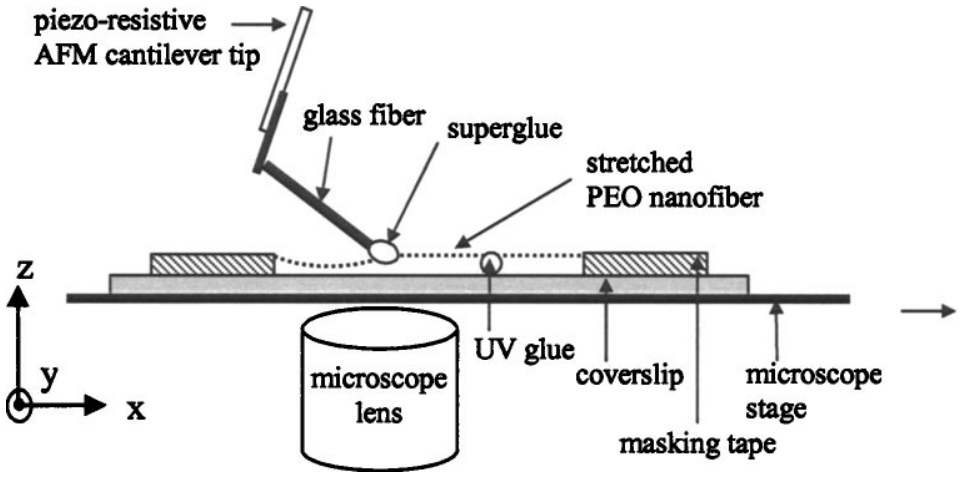


**Figure 2.4:** Tensile testing of nanofiber using piezo-resistive AFM cantilever tip (Tan, Goh, Sow, & Lim, 2005)

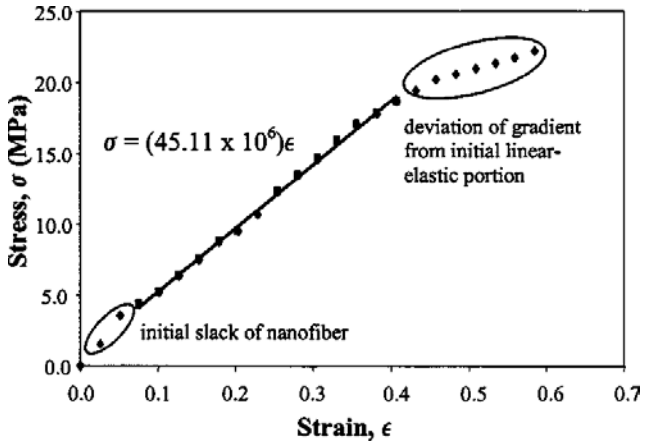


**Figure 2.5:** Stress-strain plot of PEO nanofiber of diameter 700 nm. (Tan et al., 2005)

A commercial nano tensile testing system (Nano Bionix System, MTS) can be used to conduct tensile test on single nanofiber (Figure 2.6). Tan *et al* (Tan et al., 2005) and Inai *et al* (Inai, Kotaki, & Ramakrishna, 2005) used this testing method to conduct tests on polycaprolactone (PCL) and poly (L-lactic acid) (PLLA) fibers, respectively. Single fiber collected on cardboard frame is mounted on the tester, the edges of the frame are cut before the test is conducted.

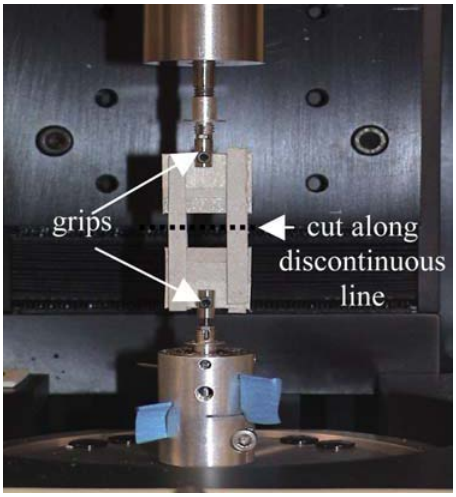


**Figure 2.6:** Nano tensile tester with a sample mounted on it (Tan et al., 2005)

From the data generated, stress-strain curves of different diameter PCL fibers could be constructed as shown in Figure 2.7. It was found that smaller diameter fibers had higher strength but lower elongation at break.

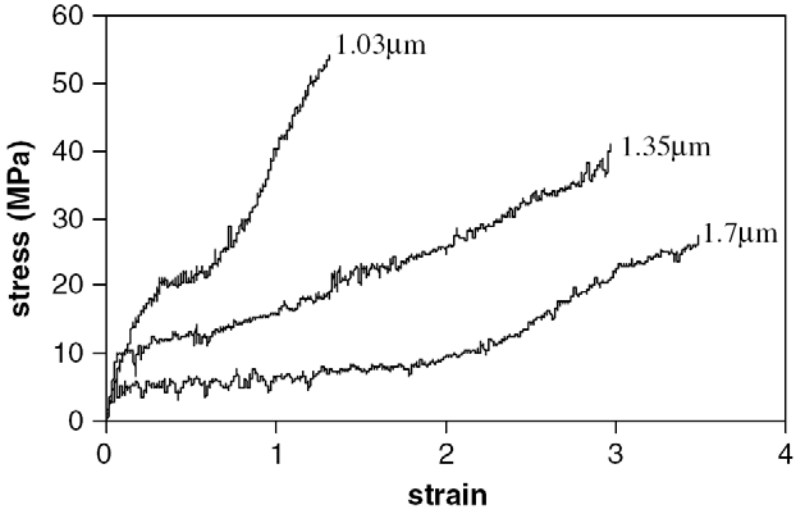


**Figure 2.7:** Stress-strain plot of PCL fibers at various fiber diameters. (Tan et al., 2005)

Bending test:

A three point bending test was conducted on PLLA nanofiber by Tan *et al* (Tan & Lim, 2004) to measure the Young's modulus of the fiber. A single nanofiber was suspended over a microsized etched groove in a silicon wafer and the ends were fixed to the substrate. An AFM cantilever tip was used to apply a small deflection at the midspan of the fiber (Figure 2.8). Known values of the spring constant, 0.15N/m, of the cantilever, the force applied, and the deflection of the fiber, facilitated the calculation of the elastic modulus ($E$) of the fiber using the following formula.

$$E = \frac{FL^3}{192 \cdot \delta \cdot I}$$

where $F$ is the maximum force applied, $L$ is the suspended length of fiber, $\delta$ is the deflection of the fiber at midspan, and $I$ is the second moment of area of fiber.

$I = \frac{\pi D^4}{64}$, where $D$ is the fiber diameter.

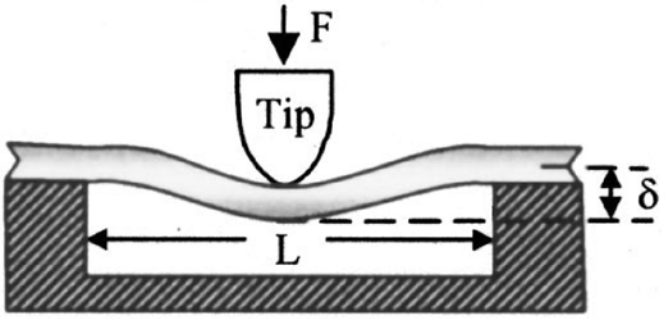


**Figure 2.8:** Schematic representation of nano fiber deflected at the mid span by an AFM tip (Tan & Lim, 2004)

Nanoindent technique is one way to measure the hardness of the fiber (Tan & Lima, 2004). These custom made complex and expensive equipments can be used to measure the tensile properties of the single micro and nano diameter fibers.

### *2.2.2 Electrospun web testing*

Tensile testing of electrospun web is not as difficult as that of testing single fiber because of sufficient strength and ease of handling due to larger size. Attempts concerning such have been made in the literature. The specimens were prepared in two different shapes: rectangular shape (Z. Huang, Zhang, Ramakrishna, & Lim, 2004; W. Li, Laurencin, Caterson, Tuan, & Ko, 2002; Ohgo, Zhao, Kobayashi, & Asakura, 2003; Zong, Ran, Fang, Hsiao, & Chu, 2003) and dumbbell shape (Bhattarai, Cha, Bhattarai, Khil, & Kim, 2003; Khil, Kim, Kim, Park, & Lee, 2004; K. H. Lee, Kim, Khil, Ra, & Lee, 2003; K. H. Lee, Kim, La, Lee, & Sung, 2002; Pedicini & Farris, 2003; Wnek, Carr, Simpson, & Bowlin, 2003). In the former, stress is

concentrated in the vicinity of the grip that could have some impact on the results (Ramakrishna, 2005). Use of dumbbell shape specimen alleviates the issue of stress concentration at the grips but preparation of the dumbbell specimen is tedious and interpretation of results difficult particularly on randomly oriented unbonded webs. The specimens prepared by either of the method are taken for tensile tests on an Instron machine.

Mechanical properties of different polymer webs were published in recent years to determine the effect of some variables (Table 2.1 and Table 2.2). Moon *et al* (Moon, Ryu, Choi, Jo, & Farris, 2009) conducted tests on sodium alginate and PEO blend nanofiber webs for their mechanical properties. Webs prepared from only PEO had 10.4MPa tensile strength with the fiber diameter of 306 nm. By the addition of sodium alginate to PEO, the tensile strength was found to increase to 20.9MPa due to the improvement in the fiber morphology. Ohgo et al (Ohgo et al., 2003) conducted tests on Bombyx mori silk and Samia Cynthia ricini silk nanofiber webs and got tensile strengths of 15MPa and 20MPa and elongation at break of 40% and 20%, respectively. Huang *et al* investigated mechanical properties of gelatin fibers of 5, 7.5, 10 and 12.5% concentrations and obtained maximum tensile strength of 4.75MPa for 7.5% concentration.

Pedicini *et al* compared the mechanical properties of polyurethane electrospun nanofibers with the bulk film. Fibers in the electrospun web seemed to have more oriented polymer molecules than in the film. This is because the tensile strength in web was higher, i.e. 10MPa at 300% ultimate strain (Figure 2.9). Up to 50% strain, however, the web showed lower stress values than did the film, but later the stress values greatly improved for the web

because after initial stretch randomly oriented fibers become oriented in the direction of strain and contributed to the strength. Due to higher molecular orientation in fibers of electrospun web, web had relatively higher stress and low strain values.

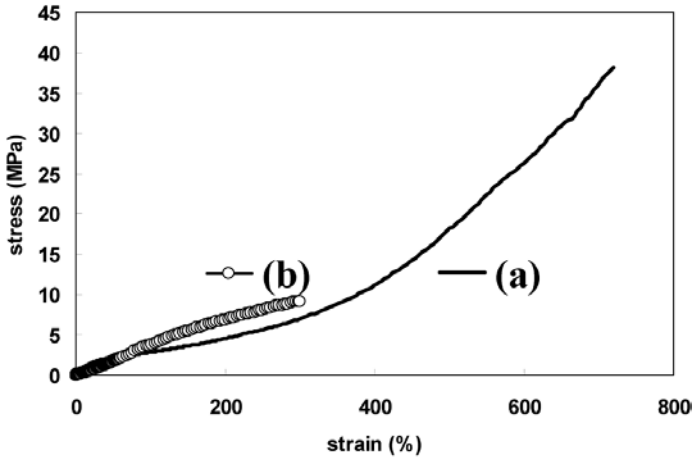


**Figure 2.9:** Stress-strain curves of polyurethane (a) bulk film and (b) electrospun web

Huang *et al* (Chaikof, 2001) conducted tests on collage-PEO blends of different proportions. Pure PEO web had tensile strength of 90 KPa and modulus of 7 MPa where as these values for 1:2 collagen-PEO blend were 270 KPa and 8 MPa and for 1:1 blend were 370 KPa and 12 MPa. Differences in these properties ascribed to the differences in the blend morphology: the 1:1 blend with maximum intermolecular interactions between PEO and collagen components resulted in high modulus values. In similar way, tests were conducted on other polymers and their combinations. The tensile properties data are summarized in Table 2.1 & Table 2.2. In these investigations two types of collectors were used, flat plate and rotating drum. With rotating drum, fibers were expected to be aligned in the machine direction. Mechanical tests were conducted in machine direction (L) and transverse direction

(T) for the webs collected on the rotating drum. But not much difference was found in the mechanical properties between the tests on these two directions, as noted in Table 2.1. It may be due to the jet speed that was much higher than the drum rotating speed and low alignment of fibers.

Studies were conducted on the mechanical properties of electrospun webs for different combinations of solvents and polymers but much less has been published on the effect of concentration or of fiber diameter on mechanical properties of the web.

**Table 2.1:** Mechanical properties of electrospun webs produced from different polymers collected on rotating drum. (Bhattarai et al., 2003; Khil et al., 2004; K. H. Lee et al., 2003; K. H. Lee et al., 2002; Wnek et al., 2003)

| Material | Fiber Orientation | Fiber Diameter (nm) | Modulus (MPa) | Strength (MPa) | Reference |
|---|---|---|---|---|---|
| Poly(p-dioxanone-co-L-lactide)-block-poly(ethylene glycol) | Aligned | 380 | $E_L = 30$<br>$E_T = 30$ | $\sigma_L = 1.2$<br>$\sigma_T = 1.4$ | (Bhattarai et al., 2003) |
| Polycaprolactone (PCL) | | Not specified (between 200~5500nm) | $E_L = 3.7$<br>$E_T = 2.7$ | $\sigma_L = 1.4$<br>$\sigma_T = 1.2$ | ( K. H. Lee et al., 2003) |
| Poly(vinyl chloride) (PVC) | | Unknown | $E_L = 7.8$<br>$E_T = 7.8$ | $\sigma_L = 1.8$<br>$\sigma_T = 1.7$ | (K. H. Lee et al., 2002) |
| Poly(trimethylene terephthalate) (PTT) | | 400 | $E_L = 0.7$<br>$E_T = 1.1$ | $\sigma_L = 2.2$<br>$\sigma_T = 4.1$ | (Khil et al., 2004) |
| Poly(vinyl alcohol) (PVA) cross-linked by glyoxal (0~10wt%) | | 280 | ---------- | $\sigma_L =$ 7~8.5<br>$\sigma_T =$ 9.5~10.5 | (Ramakrishna , 2005) |
| Acrylate modified Elastomeric Protein (degree of protein cross-linking) | | 300~1500 | 700 (Uncross-linked)<br>1800 (cross-linked) | 16 (Uncross-linked)<br>43 (cross-linked) | (Ramakrishna , 2005) |
| Fibrinogen | | 700 | 80 | 2 | Wnek et. al. (2003) |

**Table 2.2:** Mechanical properties of electrospun webs collected randomly on round plate. (Chaikof, 2001; L. Huang et al., 2000; Z. Huang et al., 2004; W. Li et al., 2002; Moon et al., 2009; Ohgo et al., 2003; Pedicini & Farris, 2003; Zong et al., 2003)

| Material | Fiber Orientation | Fiber Diameter (nm) | Modulus (MPa) | Strength (MPa) | Reference |
|---|---|---|---|---|---|
| Bombyx mori | Random | 200 ~ 400 | 0.6 | 15 | (Ohgo et al., 2003) |
| PEO<br>PEO:Sodium alginate=2:1 | | 300<br>150 | | 10.4<br>20.9 | (Moon et al., 2009) |
| Poly(lactic-glycolic) acid (PLGA) | | 400 & 1000 | 71 (400nm)<br>87 (1000nm) | 6 (400nm)<br>4.9 (1000nm) | ( Zong et al., 2003) |
| | | 500 ~ 800 | 323 | 23 | (W. Li et al., 2002) |
| Gelatin | | 100 ~ 1900 | 117 (100nm)<br>123 (1900nm) | 2.9 (100nm)<br>3.4 (1900nm) | (Z. Huang et al., 2004) |
| PEO<br>PEO : Collagen = 2:1<br>1:1 | | 100 ~ 150 | 7<br>8<br>12 | 0.09<br>0.27<br>0.37 | (Z. Huang et al., 2004) |
| Peptide Polymer | | 450 | 1800 | 35 | (L. Huang et al., 2000) |
| Polyurethane | | 100 ~ 500 | 3.7 | 10 | (Pedicini & Farris, 2003) |

## 2.3 Mathematical Models for predicting tensile properties

As mentioned, the mechanical behavior is important for materials used in tissue engineered scaffolds, reinforcement and filtration etc. For example, mechanical properties of the fibrous scaffold used for tissue engineering can affect cell morphology, proliferation and differentiation. Predicting the mechanical properties by considering the parameters affecting it is beneficial in many ways. Models allow one to know the properties of fabrics and parameters to be changed to get desired properties of end product. Many models have been proposed to predict the mechanical properties of nonwovens but no work has been done on modeling the behavior of electrospun webs.

In 1960, work done by Backer *et al.* (Backer & Petterson, 1960; Petterson & Backer, 1963) introduced elastic theory of orthotropic materials and fiber web theory to the nonwoven materials. The objective of orthotropic theory was to predict the directional material constants if modulus of elasticity, shear modulus and Poisson's ration in two principle directions of the material were given. For this, modeling the properties of a thin sheet of orthotropic material was considered whose primary axes of symmetry were *L* and *T*. Directions of interest were *x* and *y* which are perpendicular to each other with *y* making angle $\theta$ with the axis *L* as shown in (Figure 2.10). Strains along x and y creates strains in the *L* and *T* directions. These strains produce stresses in the *L* and *T* directions and the relation can be expressed by Hooken behavior for small strains.

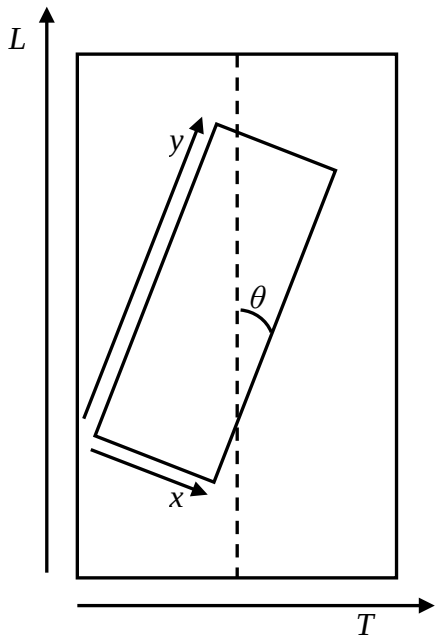


**Figure 2.10:** Axes of the material considered for orthotropic theory

$$\varepsilon_L = \frac{\sigma_L}{E_L} - \frac{\nu_{LT}\sigma_T}{E_L}$$

$$\varepsilon_T = \frac{\sigma_T}{E_T} - \frac{\nu_{TL}\sigma_L}{E_T}$$

$$\gamma_{LT} = \frac{\tau_{LT}}{G_{LT}}$$

where, $\sigma$ is the stress, $\varepsilon$ is the strain, $E$ is the elastic modulus, $\tau$ is the shear stress, $G$ is the shear modulus and $\gamma$ is the shear strain of the web in the direction of the given subscript. The subscripts used are $_L$ for longitudinal, $_T$ for transverse, $_x$ for $x$ and $_y$ for $y$ directions. $\nu_{LT}$ is Poisson's ratio due to the stress in $L$ direction and similarly $\nu_{TL}$ is the Poisson's ratio in the $T$ direction, $G_{LT}$, the shear modulus, the ratio of shear stress $\tau_{LT}$, to shear strain, $\gamma_{LT}$, in the $LT$ direction.

These stresses are resolved in *x* and *y* directions. The overall transformations take the following form:

$$\varepsilon_x = b_{11}\sigma_x + b_{12}\sigma_y + b_{13}\tau_{xy}$$
$$\varepsilon_y = b_{21}\sigma_x + b_{22}\sigma_y + b_{23}\tau_{xy}$$
$$\gamma_{xy} = b_{31}\sigma_x + b_{32}\sigma_y + b_{33}\tau_{xy}$$

where, the coefficients *b* are functions of $E_L$, $E_T$, $\nu_{LT}$, $\nu_{TL}$ and $G_{LT}$.

For uniaxial tension in the *y* direction, the transformation of all these equations reduces to

$$\varepsilon_x = b_{12}\sigma_y$$
$$\varepsilon_y = b_{22}\sigma_y$$
$$\gamma_{xy} = b_{32}\sigma_y$$

where,

$$b_{22} = \frac{\cos^4\theta}{E_L} + \frac{\sin^4\theta}{E_T} + \left[\frac{1}{G_{LT}} - \frac{2\nu_{LT}}{E_L}\right]\sin^2\theta\cos^2\theta$$
$$b_{12} = -\frac{\nu_{LT}}{E_L} + \left[\frac{1}{E_L} + \frac{1}{E_T} + \frac{2\nu_{LT}}{E_L} - \frac{1}{G_{LT}}\right]\sin^2\theta\cos^2\theta$$
$$b_{32} = \left[\frac{1}{G_{LT}} - \frac{2\nu_{LT}}{E_L} - \frac{2}{E_L}\right]\sin\theta\cos^3\theta - \left[\frac{1}{G_{LT}} - \frac{2\nu_{LT}}{E_L} - \frac{2}{E_T}\right]\sin^3\theta\cos\theta$$

But this orthotropic theory has definite limitations: it does not allow for complete design of a nonwoven web starting with the properties of the fiber elements and structural geometry of the web. It does not also permit the prediction of the plastic behavior of the web.

The fiber web theory assumes a distribution of straight fibers in terms of orientation relative to the machine direction of the nonwoven and the known fiber stress-strain properties. The steps used are: (1) calculate the strain in fibers due to a given strain in fabric, (2) determine fiber stress corresponding this strain, and (3) resolve all the fiber stresses to fabric stress in the direction of the strain.

Fiber strain, $\varepsilon_f$, in a fiber lying at an angle $\theta$ to the longitudinal direction *y* due to the longitudinal fabric strain, $\varepsilon_y$, is given by the following relationship. (*x* and *y* are longitudinal and lateral directions of fabric)

$$\varepsilon_f = \varepsilon_y \left( \cos^2 \theta - \nu_{xy} \sin^2 \theta \right)$$

The stress contribution of this fiber is determined from the fiber stress-strain curve. The number of fibers lying at the angle is found from the know fiber orientation distribution function $\phi(\theta)$. The stress contribution of all fibers, oriented at different angles, to the fabric in *y*-direction is given as follows:

$$\sigma_y = E_f \varepsilon_y \int_{-\pi/2}^{\pi/2} \left[ \cos^2 \theta - \nu_{xy} \sin^2 \theta \right] \cos^2 \theta \;\; \phi(\theta) \, d\theta$$

The stress build-up in *x*-direction is given as follows:

$$\sigma_x = E_f \varepsilon_y \int_{-\pi/2}^{\pi/2} \left[ \cos^2 \theta - \nu_{xy} \sin^2 \theta \right] \sin^2 \theta \;\; \phi(\theta) \, d\theta$$

But since the loading is uniaxial, considered in the *y*-direction, $\sigma_x = 0$. By rearranging the equation for $\sigma_x$, it gives value of Poisson's ratio $\nu_{xy}$ of nonwoven fabric. By substituting the value of $\nu_{xy}$ in the stress of fabric in y-direction, one obtains

$$\frac{\sigma_y}{\varepsilon_y} = E_y = E_f \int_{-\pi/2}^{\pi/2} \left[ \cos^4\theta - \nu_{xy} \cos^2\theta \, \sin^2\theta \, . \, \frac{\int_{-\pi/2}^{\pi/2} \sin^2\theta \cos^2\theta \;\; \phi(\theta)\, d\theta}{\int_{-\pi/2}^{\pi/2} \sin^4\theta \;\; \phi(\theta)\, d\theta} \right] \phi(\theta)\, d\theta$$

The above equation gives stress-strain relationship for a nonwoven fabric as proposed by Backer & Petterson (Backer & Petterson, 1960).

Several researchers worked on predicting tensile properties of nonwoven webs. The above model, i.e. by Backer and Petterson, is basically for straight fiber segments between bonds. Petterson's fiber network theory explains the nonwoven behavior for smaller strains and larger strains; for the latter, lateral contraction involving Poisson's ratio is considered. Later, Hearle and Stevenson (Hearle & Stevenson, 1964) modified Petterson's fiber network theory by introducing fiber curl factor, which is shown to have a great effect on the value of the initial modulus. Curl factor is the ratio of the length of curved fiber segment to the length of the chord between bonds. Graph shown (Figure 2.11) by Adanur *et al* (Adanur & Liao, 1999) explains the effect of curl factor on the stress-strain behavior of a fabric. The behavior is represented by the coarse line, which is affected by the level of curl in fibers. Fibers with curl contribute to the strength of material only after the curl has been taken up by the required amount of strain.

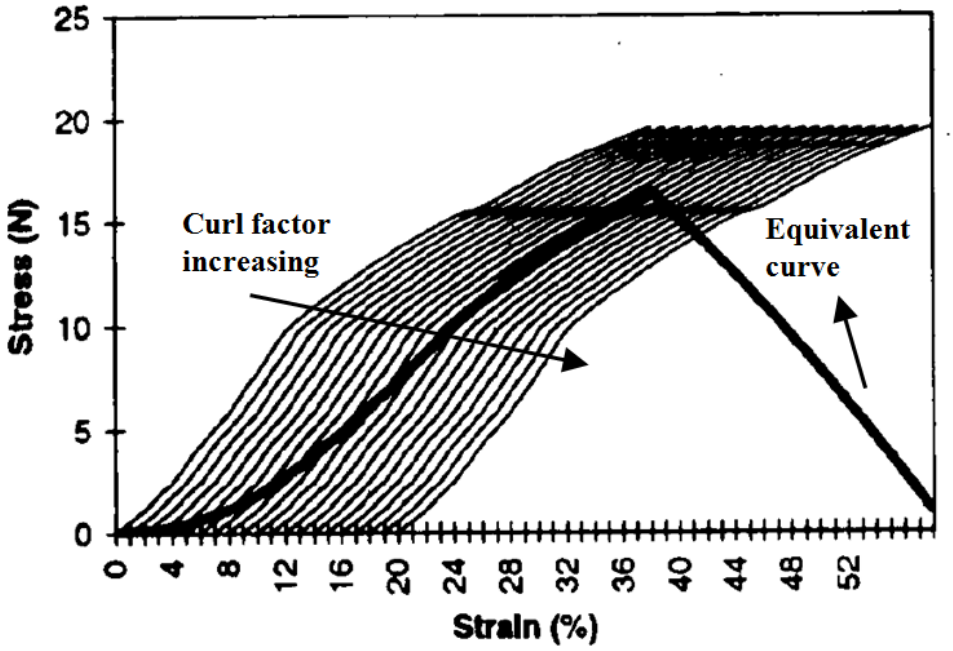


**Figure 2.11:** Graph showing the effect of fiber curl on the initial modulus of fabric (Adanur & Liao, 1999)

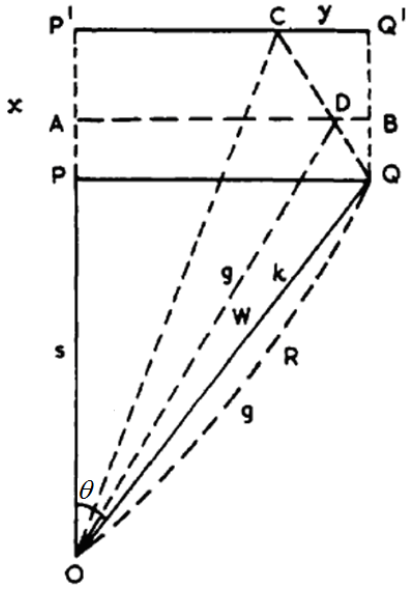


**Figure 2.12:** Deformation of fiber curvature

As shown in Figure 2.12, let ORQ be a curved fiber segment bonded at the points O and Q. Let length of fiber segment ORQ=g and the length of the chord OWQ=k.

Curl factor, $c = g/k$

Due to a given fabric strain, $\varepsilon_y$, points P and Q move to P′ and Q′, respectively.

$$\varepsilon_y = \frac{\mathrm{PP'}}{\mathrm{OP}} = \frac{x}{s}$$

The strain $\varepsilon_y$ straightens and elongates the fiber to OC.

CQ′= *y* is lateral contraction.

From the Pythagoras theorem, $\mathrm{OC}^2 = \mathrm{OP'}^2 + \mathrm{CP'}^2 = \mathrm{OP'}^2 + (\mathrm{PQ} - \mathrm{CQ'})^2$

$$\mathrm{OC}^2 = (s+x)^2 + (s\tan\theta - y)^2 = (s+x)^2 + (s\tan\theta - x\nu_{xy}\tan\theta)^2$$

Fiber strain, $\varepsilon_f = \dfrac{(\mathrm{OC} - g)}{g} = \dfrac{\left[(s+x)^2 + \tan^2\theta\,(s - x\nu_{xy})^2\right]^{1/2} - cs/\cos\theta}{cs/\cos\theta}$

since $g = ck = c.\dfrac{s}{\cos\theta}$

$$\varepsilon_f = \frac{1}{c}\left[(1+\varepsilon_y)^2\cos^2\theta + (1-\nu_{xy}\varepsilon_y)^2\sin^2\theta\right]^{1/2} - 1 \qquad (2.1)$$

The above equation transforms larger or smaller fabric strains to fiber strains at different angles of orientation. For smaller strains Poisson's ratio may be assumed zero.

Fiber stress $\sigma_f$ is a function of fiber strain which can be read directly from fiber stress-strain curve or from Hooke's law for low strains (Hearle & Stevenson, 1964). The next step then is to transform fiber stresses to fabric stress. If fiber orientation distribution function is expressed by $\phi(\theta)$, then the stress contribution of fibers lying at an angle $\theta$ is,

$$\sigma_\theta = \sigma_f \, \phi(\theta) \cos^2\theta$$

Total fabric stress $\sigma = \sum_{i=1}^{n} \sigma_f \, \phi(\theta) \cos^2\theta$

The assumptions for the above theory are that (1) the mean bond to bond distance is constant for a fabric, (2) bonds are at least as strong as fibers, (3) fiber curl is allowed to be taken up at negligible force compared to the force required to stretch the fiber, and (4) extension of binder is ignored.

Experimental values are matched with theoretically predicted values at small strains (Figure 2.13(a)). But as the strain increases, the theoretical values of stresses become greater than the experimental values. Limiting fiber stress to certain extent made the agreement with the experimental values also better at high strains (Figure 2.13(b)).

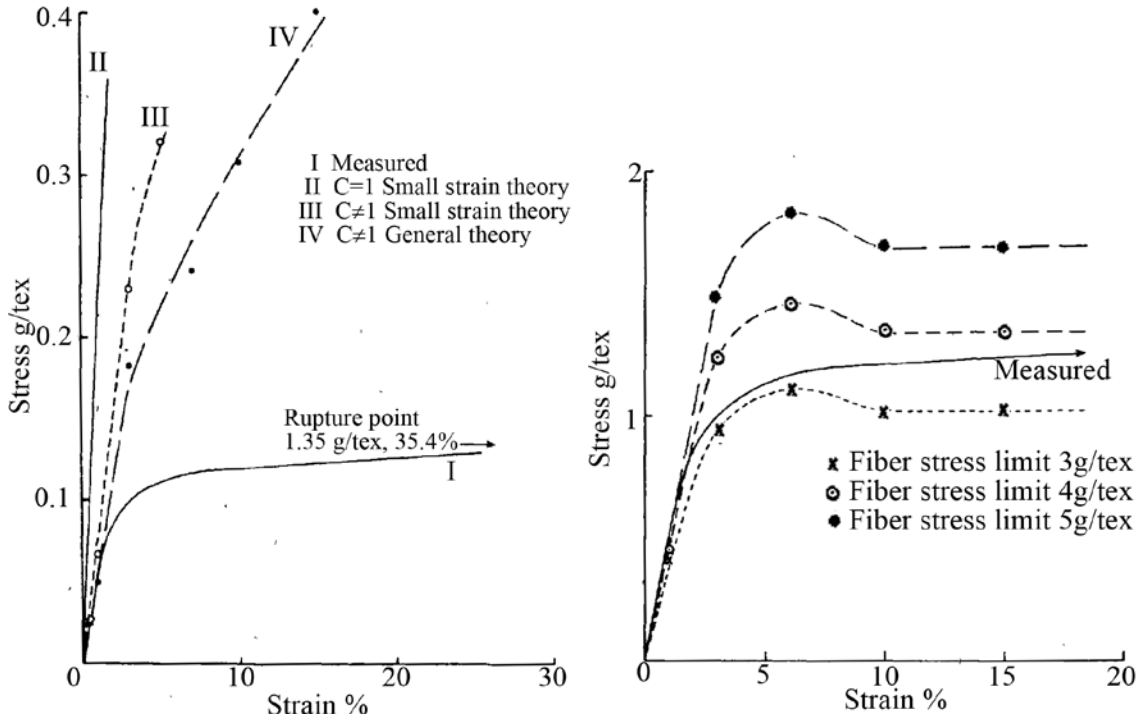


**Figure 2.13:** Theoretical and experimental stress-strain curves for cross-laid nonwoven fabric (a) without limiting fiber stress (b) with limiting the fiber stress (Hearle & Stevenson, 1964)

In Figure 2.13(a), Curve-I is the stress-strain curve of measured fabric, Curve-II is theoretically predicted behavior when curl factor and Poisson's ratio are ignored, Curve-III is theoretical behavior when curl factor is introduced and Poisson's ratio ignored and Curve-IV is predicted behavior from the full model which has curl factor and Poisson's ratio in it. In Figure 2.13(b), fiber stresses were limited to the values given in the plot for full model.

Later Hearle and Newton (Hearle & Newton, 1967) introduced energy method for performing structural mechanics of nonwoven fabrics. Energy method is simpler as it allows

one to avoid assumption of constant modulus and other approximations. The following simple treatment shows the simplicity of the energy method.

Let us consider a fabric specimen (Figure 2.14) deformed uniformly to a strain $\varepsilon_L$ without transverse contraction. Due to this strain, fiber element of length *l* lying at an angle $\theta$ to the loading axis in the fabric deforms by strain $\varepsilon_f$. Let *a* and *b* be the projected lengths of fiber parallel and perpendicular to length of fabric, respectively. From Pythagoras theorem,

$$l^2 = a^2 + b^2$$
$$2l.dl = 2a.da \qquad (b \text{ is constant})$$

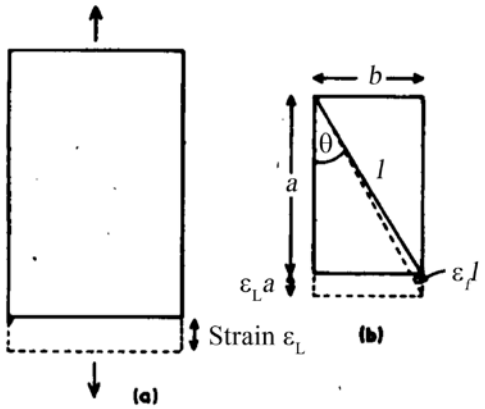


**Figure 2.14:** (a) Deformation of fabric specimen, (b) deformation of fiber element in it

Fiber strain $\varepsilon_f = \frac{dl}{l} = \frac{a.da}{l^2} = \varepsilon_L \cos^2\theta$

Energy is given by the area under the force-elongation curve.

If fibers follow Hooke's law, then

$$Energy = \frac{1}{2} Force \ . \ Displacement = \frac{1}{2} Specific\ stress \ . \ Strain \ . \ Mass$$

Energy per unit mass in the fiber = $U_f = \frac{1}{2}\sigma_f \varepsilon_f = \frac{1}{2} Y_f \varepsilon_f^{\ 2} = \frac{1}{2} Y_f \varepsilon_L^{\ 2} \cos^4\theta$

where, $Y_f$ is the Fiber Young's modulus.

If $\theta$ represents the distribution of fiber orientation, then the average elastic energy per unit mass in the fabric is given by $\overline{U} = \frac{1}{2} Y_f \varepsilon_L^2 \ \overline{\cos^4\theta}$ .

The total stored energy must equal the work done in the fabric by the applied tension. From this, energy per unit mass is given by $\overline{U} = \frac{1}{2} Y_F \varepsilon_L$ where, $Y_F$ is Fabric modulus.

By equating the above two equations, one gets:

$$Y_F = Y_f \overline{\cos^4\theta} \ .$$

This expression is similar to the result given by the fiber web theory when lateral contraction is ignored.

The principle of the energy method is that the work done on a specimen by the forces will be equal to the summation of energy changes that occur in individual elements of the specimen. As an example, consider a fabric specimen acted on by external forces $P_i$

( $P_1, P_2, .....P_n$ ) on $n$ points, and these elements undergo displacements of $S_i$ ($S_1, S_2, .....S_n$) in the direction of the forces. The work done by force $P_i$ for a change $dS_i$ in $S_i$ will equal $P_i.dS_i$. This work must be stored in the fabric as elastic deformation energy or dissipated as inelastic deformation energy. If the fabric is divided into $N$ elements denoted by suffix $j$, and energy stored in an element is given by $E_j$, then the

total stored energy = $\sum_{j=1}^{N} E_j$ .

For a displacement $dS_i$, change in stored energy $= \left( \frac{\partial}{\partial S_i} \sum_{j=1}^{N} E_j \right)_{S_1, S_2, .....S_{i-1}, S_{i+1} .....S_n} dS_i$

$$= \left( \sum_{j=1}^{N} \frac{\partial E_j}{\partial S_i} \right)_{S_1, S_2, .....S_{i-1}, S_{i+1} .....S_n} dS_i$$

By equating work done and energy change, $P_i = \left( \sum_{j=1}^{N} \frac{\partial E_j}{\partial S_i} \right)_{S_1, S_2, .....S_{i-1}, S_{i+1} .....S_n}$

This gives the general form of equation which can be applied to any set of forces acting on any type of specimen of any fabric deforming elastically. The equation can be modified to different forms as shown below.

1. When energy change in fibrous elements is known, $P_i = \sum_{j=1}^{N} \frac{\partial E_j}{\partial \varepsilon_j} \left( \frac{\partial \varepsilon_j}{\partial S_i} \right)$

2. When energy change in fibrous elements per unit mass is known,

$$P_i = \sum_{j=1}^{N} \mu_j \frac{\partial U_j}{\partial \varepsilon_j} \left( \frac{\partial \varepsilon_j}{\partial S_i} \right)$$

3. When fiber stress-strain relation is known, $P_i = \sum_{j=1}^{N} \mu_j \sigma_j \left( \frac{\partial \varepsilon_j}{\partial S_i} \right)$

where, $\sigma_j$ - stress in fibrous element *j*, $\varepsilon_j$ - strain in element *j*, $\mu_j$ - mass of element *j*, $U_j$ - energy per unit mass.

The above equations can be further simplified if shape of the specimen is known and forces and displacements can be converted into stresses and strains. If we consider a rectangular specimen of length *L* and width *B*, having mass per unit area *w*, with force $P_i$ applied to the edge of width *B* causing displacement $S_i$, then *wB* gives the mass per unit length.

Specific stress in the specimen = $\sigma_i = P_i / wB$ and strain $\varepsilon_i = S_i / L$.

$$\sigma_i = \left( \sum_{j=1}^{N} \frac{\partial E_j}{\partial (\varepsilon_i . L)} \right)_{S_1, S_2, \ldots S_{i-1}, S_{i+1} \ldots S_n} \Big/ wB = \frac{1}{wBL} \sum_{j=1}^{N} \left( \frac{\partial E_j}{\partial \varepsilon_i} \right)_{\varepsilon_1, \varepsilon_2, \ldots \varepsilon_{i-1}, \varepsilon_{i+1} \ldots \varepsilon_n}$$

$$\sigma_i = \frac{1}{wBL} \sum_{j=1}^{N} \mu_j \left( \frac{\partial U_j}{\partial \varepsilon_i} \right)_{\varepsilon_1, \varepsilon_2, \ldots \varepsilon_{i-1}, \varepsilon_{i+1} \ldots \varepsilon_n}$$

$$\sigma_i = \frac{1}{wBL} \sum_{j=1}^{N} \mu_j \frac{\partial U(\varepsilon_j)}{\partial \varepsilon_j} \left( \frac{\partial \varepsilon_j}{\partial \varepsilon_i} \right)_{\varepsilon_1, \varepsilon_2, \ldots \varepsilon_{i-1}, \varepsilon_{i+1} \ldots \varepsilon_n} \qquad (2.2)$$

where, $\partial U(\varepsilon_j)$ is energy change per unit mass due to strain $\varepsilon_j$.

If $\sigma(\varepsilon_j)$ is specific stress in the element due to strain $\varepsilon_j$, $t_j$ is mass per unit length of element and $l_j$ is length of an element, then

$$dU(\varepsilon_j) = \left[ t_j \sigma(\varepsilon_j) l_j d\varepsilon_j \right] \Big/ \mu_j = \sigma(\varepsilon_j) d\varepsilon_j \qquad (\because t_j l_j = \mu_j)$$

$$\text{or, } \sigma_i = \frac{1}{wBL} \sum_{j=1}^{N} \mu_j \sigma(\varepsilon_j) \left( \frac{\partial \varepsilon_j}{\partial \varepsilon_i} \right)_{\varepsilon_1, \varepsilon_2, \ldots\ldots \varepsilon_{i-1}, \varepsilon_{i+1} \ldots\ldots \varepsilon_n} \qquad (2.3)$$

As an alternative to digital summation equations, integral equations can be developed for the energy method.

$$\sum_{i=1}^{n} \int_0^{\varepsilon_i} \sigma_i d\varepsilon_i = \frac{1}{wBL} \sum_{j=1}^{N} \mu_j \int_0^{\varepsilon_j} \sigma(\varepsilon_j) d\varepsilon_j \qquad (2.4)$$

The above Equations 2.3 and 2.4 are used in the energy method when the specimen is of the mentioned shape and parameters. By assuming simple fiber network in nonwoven fabric, appropriate equations that apply can be derived using the energy method. Assumptions are,

1. fabric is made up two dimensional sheet
2. the sheet consists of networks of fiber elements lying between bonding points
3. there is an affine uniformity in fabric deformation, and
4. stored energy derives only from the change of length of fiber elements between bonded points.

As shown previous by Equation 2.1, strain in fibrous elements can be calculated from

$$\varepsilon_j = \frac{1}{c_j}\left[(1+\varepsilon_L)^2\cos^2\theta_j + (1+\varepsilon_T)^2\sin^2\theta_j\right]^{1/2} - 1, \text{ for biaxial loading and}$$

$$\varepsilon_j = \frac{1}{c_j}\left[(1+\varepsilon_L)^2\cos^2\theta_j + (1-\nu_{LT}\varepsilon_L)^2\sin^2\theta_j\right]^{1/2} - 1, \text{ for uniaxial loading where } c_j \text{ is the}$$

curl factor.

By substituting the value of $\varepsilon_j$ in $\frac{\partial\varepsilon_j}{\partial\varepsilon_T}$ for transverse or $\frac{\partial\varepsilon_j}{\partial\varepsilon_L}$ for longitudinal strain one obtains different equations for biaxial loading. And, for uniaxial loading

$$\left(\frac{\partial\varepsilon_j}{\partial\varepsilon_L}\right)_{\nu_{LT}} = \frac{\left[(1+\varepsilon_L)\cos^2\theta_j - \nu_{LT}(1-\nu_{LT}\varepsilon_L)\sin^2\theta_j\right]}{c_j\left[(1+\varepsilon_L)^2\cos^2\theta_j + (1-\nu_{LT}\varepsilon_L)^2\sin^2\theta_j\right]^{1/2}}$$

By substituting the above equation in, $\sigma_i = \frac{1}{wBL}\sum_{j=1}^{N}\mu_j\sigma(\varepsilon_j)\left(\frac{\partial\varepsilon_j}{\partial\varepsilon_i}\right)_{\varepsilon_1,\varepsilon_2,.....\varepsilon_{i-1},\varepsilon_{i+1}.....\varepsilon_n}$, and rearranging, longitudinal stress $\sigma_L$ caused by fabric strain $\varepsilon_L$ can be obtained,

$$\sigma_L = \frac{(1+\varepsilon_L)}{\sum_{j=1}^{N}\mu_j}\sum_{j=1}^{N}\frac{\mu_j\sigma_j\cos^2\theta_j}{c_j^2\ (1+\varepsilon_j)}$$

The above equation is solved by assuming minimum energy condition for Poisson's ratio.

The energy method can be applied to a fabric containing a blend of fibers as well. If a fabric is made up of $N_1$, $N_2$,…… fibers of different types, then the stress in the fabric will be as follows:

$$\sigma_L = \frac{(1+\varepsilon_L)\left[\sum_{j=1}^{N_1} \frac{\mu_j \sigma_{j1} \cos^2\theta_j}{c_j^2\ (1+\varepsilon_j)} + \sum_{j=1}^{N_2} \frac{\mu_j \sigma_{j2} \cos^2\theta_j}{c_j^2\ (1+\varepsilon_j)} + .....\right]}{\sum_{j=1}^{N_1} \mu_j + \sum_{j=1}^{N_2} \mu_j + .....}$$

Based on the equation given above, experiments were conducted and the results obtained by the authors (Hearle & Newton, 1968) were compared with those obtained experimentally. The predicted values matched with the experimental values up to certain value of extension, beyond which the departure started to occur. The reason for the latter was the role played by the binder content. In modeling, the assumption made was that the bond was at least as strong as fiber, which consequently means no slippage at bonds when loaded. But in practical case there might be some fiber slippage. With increase in binder content, agreement improved between theoretical and experimental values of stress at higher strains as shown in Figure 2.15 (Hearle & Newton, 1968).

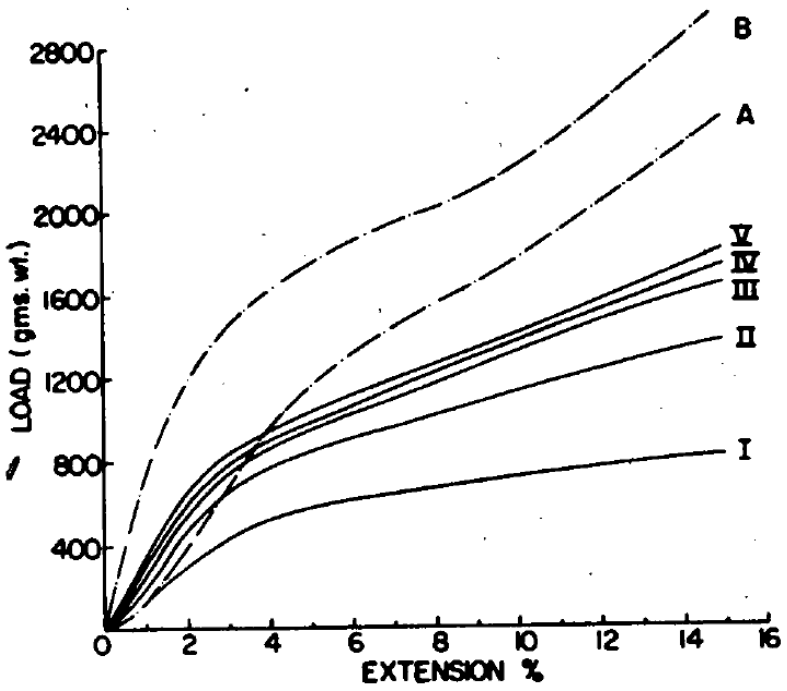


**Figure 2.15:** Theoretical and experimental curves of random laid nonwoven fabrics with different binder contents: Curves I-V are experimental curves with increase in binder content; Curve-A is theoretical curve including curl factor and Curve-B is theoretical curve excluding curl factor. (Hearle & Newton, 1968)

The model was further modified by Hearle *et al* by incorporating binder deformation in the model similar to deformation in fiber element (Hearle & Ozsanlav, 1979b).

Work done by Paradkar (Paradkar, 1987) on prediction of rupture properties of unbonded webs provides direction for modeling the behavior of complex structures. The work was performed on two types of webs, fully oriented web and unoriented web. It was shown that the web sample mechanical properties depended greatly on the number of fibers gripped at both ends in the jaws of tensile tester.

The deformation given to the web is transferred to fibers. Strain in a fiber is function of strain in the web ($\varepsilon_y$). As shown earlier in Hearle's fiber network model, the strain in a fiber oriented at an angle $\theta$ is

$$\varepsilon_{f,\theta} = \left[ (1+\varepsilon_y)^2 \cos^2\theta + \sin^2\theta \right]^{1/2} - 1$$

If strain is small, lateral contraction can be neglected. This strain gives the value of stress or force developed in the fiber from fiber stress-strain behavior (Paradkar, 1987).

Force in the fiber is a function of strain or elongation. $P_f(\varepsilon_{f,\theta}) = \textit{function of}\,(\varepsilon_{f,\theta})$

After elongation, the angle made by fiber to the longitudinal strain direction decreases. This angle $\theta' = \tan^{-1}\left[\dfrac{\tan\theta}{1+\varepsilon_y}\right]$.

Force in the web due to the fibers oriented at an angle $\theta$ is

$$P(\varepsilon_{f,\theta}) = \alpha\left(\theta, l, \varepsilon_y, L^*\right).P_f(\varepsilon_{f,\theta}).\cos\left(\tan^{-1}\left[\frac{\tan\theta}{1+\varepsilon_y}\right]\right)$$

where, $\alpha\left(\theta, l, \varepsilon_y, L^*\right)$ is number of fibers of length $l$ making angle $\theta$ in the web are gripped at both ends in the jaws of span $L^*$ at extension $\varepsilon_y$ (Paradkar, 1987).

Total force exerted on the web is $P = \int_0^{\pi}\int_0^{l'} \alpha\left(\theta, l, \varepsilon_y, L^*\right).P_f(\varepsilon_{f,\theta}).\cos(\theta)\,dl.d\theta$

where, $l'$ is maximum fiber length (Paradkar, 1987).

The number of fibers gripped at both ends for completely oriented web, is given by

$$N_{L^*} = N\left(1-\frac{L^*}{l}\right)$$

where *N*- Total number of fibers in web cross section, $L^*$-Gage length and *l*-Fiber length.

When the curl factor, *c* and orientation angle are introduced into the model,

$$N_{L^*} = N\left(1-\frac{L^*}{l(1-c)\cos\theta}\right)$$

But in the case of unoriented web, fibers of length *l* cannot be gripped at both ends after a critical angle $\theta^*$. Thus only fibers lying between angles -$\theta^*$ and $\theta^*$ can be expected to bear load.

$$\theta^* = \cos^{-1}\left(L^*/l(1-c)\right)$$

Total number of fibers gripped at both ends for a given orientation is $2\sum_{\theta=0}^{\theta^*} N_{L^*}$.

Derivation for estimation of total number of fibers in a web is given. For calculating this, fiber web was divided into *n* number of strips and in each strip fibers were assumed to be oriented at a different but constant angle $\theta$.

Number of fibers in a strip is $= \frac{MW10^5}{nt}$

where, *M* is the mass of parent web in g, *W* is the width of web in cm and *t* is single fiber tex.

Using the mathematical models such as shown above, computer simulations were performed by many researchers for nonwovens (Britton, Sampson, Elliott, Graben, & Gettys, 1983; Britton, Sampson, & Gettys, 1984; Grindstaff & Hansen, 1986; Tianyi Liao & Adanur, 1999). These simulations were conducted by the finite element method. The basic procedure followed was that a fabric given a small amount of strain was in a static equilibrium. The restoration of such equilibrium was carried out by finding new co-ordinates for the elements. Then the net force acting on the fibers was calculated from fiber stress-strain curve. The cumulative of these forces gives the force acting on the fabric. Strain is increased incrementally in steps and corresponding forces are calculated. The computation gives the output such as values of stress, strain, Poisson's ratio, tenacity etc. These models differ from each other in terms of the assumptions made. Liao *et al* (Tianyi Liao & Adanur, 1999) were able to explain fiber deformation states, and buckling, elastic, plastic deformation and failure criterion with their model (Figure 2.16). They showed that not all fibers under strain behaved in the same way. Some fibers were buckled, some were in elastic strain region, while some others started to break. Fibers oriented parallel to the loading axis broke first.

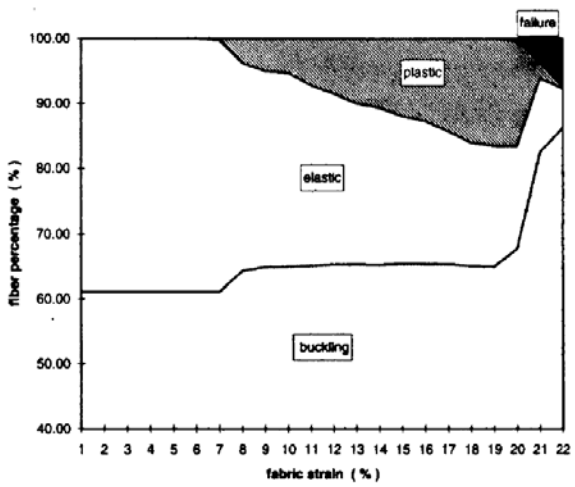


**Figure 2.16:** Fiber deformation states during fabric extension

By making use of numerical simulations and mathematical modeling, it is possible to analyze the fabric behavior and their properties. These models can be used not only to predict the properties of fabrics but also to find and understand the effects of fiber and fabric geometry parameters involved.

## 2.4 Fiber orientation:

Mechanical properties of nonwoven fabrics are determined by the properties of fabric constituents and structural arrangement of these components. Important aspect is fiber orientation. The contribution of fiber to strength of fabric depends on the orientation of that fiber. The orientation of the fibers in web can be expressed in the form of orientation angle distribution. This gives the number of fibers oriented in a given span of angle.

Hearle and Ozsanlav (Hearle & Ozsanlav, 1979a) have investigated the determination of fiber orientation and curl distribution. The distributions are relatively independent of factors

such as fiber type, linear density, fiber length, web thickness etc., but depend only on web forming processes. The authors suggested that orientation could be assessed from the direction phenomena aspects of dichroism, transmitted light intensity and birefringence, and from direct visual techniques. From the orientation distribution graph based on visual measurements, it was observed that relative frequency was a function of some power of the cosine of orientation angle.

$$y = a \pm b\cos^n\beta$$

where, $y$ is the relative frequency at an orientation angle $\beta$ , and $a$, $b$, and $n$ are constants. Parameter $b$ is positive when the maximum frequency occurs at $\beta = 0^0$ and negative when peak is at $90^0$. The total frequency is given by

$$N = \int_{-\pi/2}^{\pi/2} \left(a \pm b\cos^n\beta\right) d\beta = a\pi + b\pi \frac{n-1}{n}.\frac{n-3}{n-2}.....\frac{3}{4}.\frac{1}{2}$$

Orientation angle distribution for composite structures made of two web types is given by

$$y_{\text{comp}} = N_1\{\text{Distribution equation of web 1}\} + N_2\{\text{Distribution equation of web 2}\}$$

where, $N_1$ and $N_2$ are relative numbers of segments in each web type.

Work done by Hearle *et al.* (Hearle & Stevenson, 1963) on the anisotropy of nonwoven fabrics revealed that curl distribution varies with directional angle and the fabric structure. In general, a sharply peaked distribution of curl factors will result in high strength because large number of fibers with similar curl factors will be able to contribute equally to load bearing.

Curl factor distribution is also expressed by the power cosine rule. If $\theta = \frac{(c-1)}{(c_{\max}-1)}\frac{\pi}{2}$,

where $c_{\max}$ is the maximum curl factor and $c$ takes values from 1 to $c_{\max}$, then the relative frequency $y$ is given by:

$$y = a + b\cos^n \theta$$

Mathematical models like the one above are utilized in predicting the properties of textile materials.

## 2.5 Summary:

Studies made on the fundamentals of the electrospinning process, the parameters influencing the process, and effect of process variables on the structure and morphology of electrospun web are reviewed in this chapter. Process for producing aligned fibers in electrospinning and principles behind the process are examined. Limited work on testing mechanical properties of random electrospun web and single fiber are reviewed. Literature found on the mechanical properties of different polymers, and effect of solvents and processing variables are summarized. Work done on mathematical models to predict the tensile behavior of nonwoven fabrics is reviewed. Fiber network theory and Energy methods to predict the nonwoven fabric properties, results obtained and the comparison between the experimental and the theoretical values are also discussed.

Mechanical behavior is considered to be one of the main characteristics of a fibrous assembly. In electrospinning many factors affect the dimensions, the structure and presumably including the mechanical properties of the web. Literature is lacking in this field, i.e. on the effect of the processing factors on the structure of the electrospun web and on their mechanical properties. This study was undertaken to close a part of this gap.

# 3. MODELING OF THE STRUCTURE FOR TENSILE PROPERTIES

## 3.1 Introduction

Strength is a primary property of importance for most materials. Prediction of strength is important for determining the behavior of webs for different applications. Mathematical modeling allows one to know the effect of material and processing factors on the product properties. Strength of a non-woven web is determined by areal density, fiber orientation distribution, test specimen size, properties of individual fibers and the nature of interactions among fibers. The strength of a single fiber can be expected to vary with the processing conditions which would influence the molecular orientation in the fiber. Prior to strength prediction, it will be important to know the number of fibers supporting the load and contributing to it along the direction of the test. Based on the known structure of electrospun webs, a model for the mechanical properties of electrospun web is proposed with some assumptions. In an unbounded and unoriented sample used for tensile testing, fibers can be placed into three groups:

Gripped at both ends

Gripped at only one end

Not gripped at either end but loose

Another factor contributing to the strength of a material is the level of bonding or the magnitude of friction between the fibers at the cross-over points. Accordingly, the number of

cross-over points in a sample can possibly affect the mechanical properties. Based on some of these factors, a structural model is proposed to predict the strength and stress-strain properties of an unoriented electrospun web.

### 3.2 Assumptions:

Electrospun web is primarily assumed to have randomly oriented fibers. A web with such orientation has same number of fibers distributed at all angles. For the convenience of calculations, it is assumed that the web is made up of number of rectangular or circular layers (discs) superimposed on each other and each disc has fibers oriented parallel to each other with a constant spacing ($S$) between them (Figure 3.1).

Parameters required for modeling the web properties are

- Web thickness, $T$ (cm)
- Fiber diameter, $d$ (cm)
- Fiber density, $\delta_f$ (g/cc)
- Web areal density, (g/cm$^2$)
- Sample dimensions, (cm)
- Fiber stress-strain properties

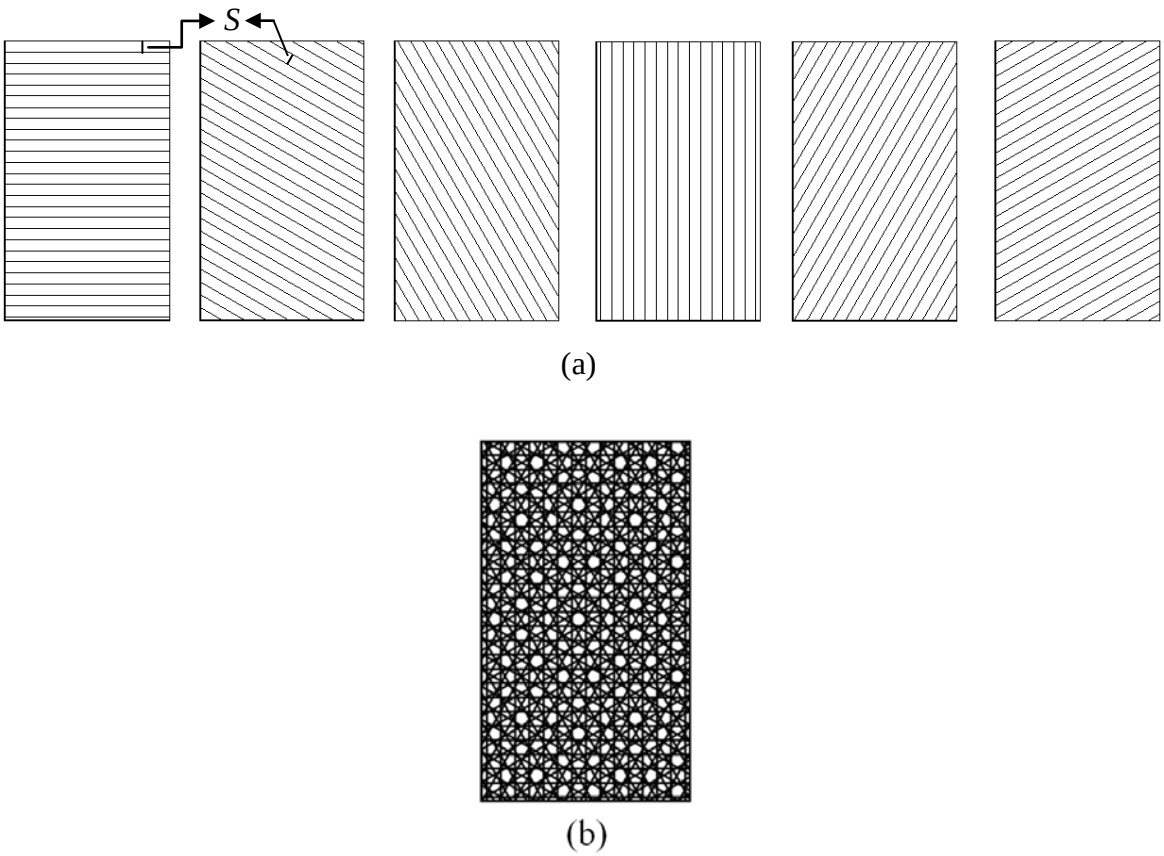


**Figure 3.1:** Schematic representation of the assumption made: web is constructed of overlapped layers: (a) Individual layers, (b) superimposed layers resulting in the final web

### 3.3 Modeling of the web structure:

By using some of the above mentioned parameters, one can evaluate the web structure.

As assumed, web is composed of number of layers, each with parallel fibers with constant spacing between the fibers. Number of discs can be obtained by dividing the thickness of the web ($T$) with the diameter of fiber ($d$).

Number of discs in a web ($n_d$):

$$n_d = T/d \tag{3.1}$$

Consider the specimen used for tensile test as shown in Figure 3.2.

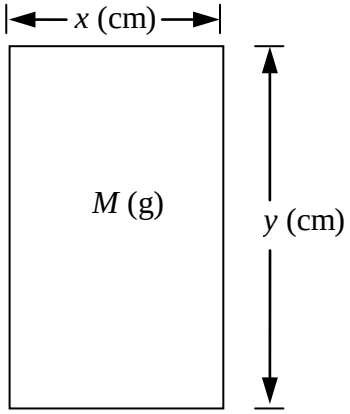


**Figure 3.2:** Specimen used for tensile test

Mass of a material is the product of volume and density.

$$Density\,(g/cc) = Mass/Area \bullet Length$$

From this formula, hypothetical total length of fiber ($L$) in a sample web of mass, $M$, is given by:

$$L = \frac{4M}{\pi d^2 \delta_f} \quad \text{or} \quad L = \frac{4M v_f}{\pi d^2} \tag{3.2}$$

where $M$ is the mass (g) of the sample of length $y$ (cm) and width $x$ (cm), $\delta_f$ is the density of fiber (g/cc) and $v_f$ is the specific volume of fiber (cc/g).

Length of fiber ($l$) in each disc is given by the ratio of total length ($L$) to the number of layers or discs:

$$l = \frac{L}{n_d} = \frac{4M\nu_f}{\pi d^2 n_d} = \frac{4M\nu_f}{\pi T d} \tag{3.3}$$

With a change in orientation angle in a disc, total length of fiber in a disc ($l$) may change somewhat but the graph (Figure 3.3) below show that $l$ is approximately the same for all discs of a sample, i.e. irrespective of the angle of orientation. In Figure 3.3, the hypothetical values shown are for a square sample of 10.8cm side with three different spacings, which were 0.32cm, 0.64cm and 1.28cm.

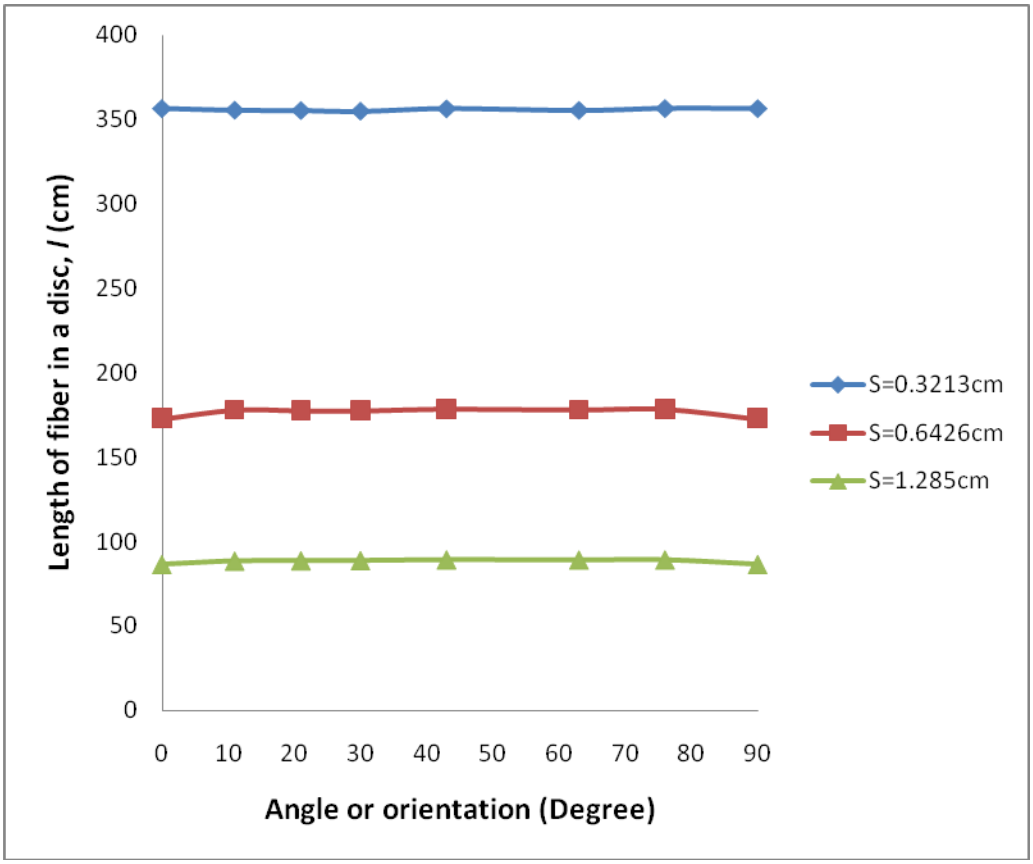


**Figure 3.3:** Graph showing, *l* is approximately same at all angles of orientation.

### *3.3.1 Determining spacing between fibers in a disc:*

As mentioned earlier, the perpendicular distance (*S*) between fibers in different discs of the same sample is constant.

A specimen of dimensions *x* and *y* cm as shown earlier in Figure 3.2 is considered. The total length of fibers in each disc making up the sample is the same. Consider the disc in which fibers are oriented length wise, i.e. at $0^0$.

Number of fibers ($n$) in the disc is:

$$n = \frac{\text{Total length of fiber in disc}}{\text{Length of the sample}} = \left[ l/y \right]$$

Spacing ($S$) between fibers is:

$$S = \frac{\text{Width of the sample}}{\text{Number of fibers in the disc}} = x/n = xy/l$$

$$S = \frac{xyT\pi d}{4M\nu_f} \tag{3.4}$$

Accordingly, by knowing the sample mass or weight, fiber diameter, fiber density, web thickness and sample dimensions, one can calculate the spacing ($S$) between fibers. The number of fibers in a disc and their contribution to the strength will, however, vary with the angle of orientation in the disc.

### *3.3.2 Number of fibers in a sample:*

The discs vary in terms of the angle of orientation of the fibers. We shall assume that the difference in the angle of orientation of fibers between successive discs is constant and is given by $\gamma$:

$$\gamma = \frac{\pi}{Number\ of\ discs} = \frac{\pi}{n_d} \tag{3.5}$$

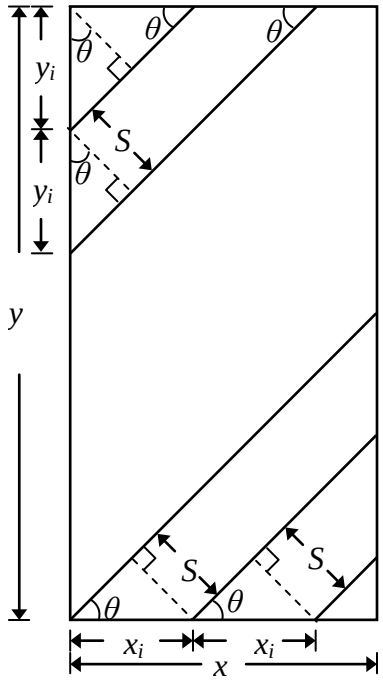


**Figure 3.4:** Fibers arranged in a disc

From Figure 3.4, $\cos\theta = \frac{S}{y_i}$ and $\sin\theta = \frac{S}{x_i}$ (3.6)

Number of fiber ends in length $y$ is the number of $y_i$ s in $y$.

Number of $y_i$ s $= \frac{y|\cos\theta|}{S}$ (3.7)

Similarly, number of $x_i$ s in width $x$ is $= \frac{x|\sin\theta|}{S}$ (3.8)

Combining the above two quantities gives the number of fiber segments in a disc.

Number of fiber segments in a single disc $= \dfrac{x|\sin\theta| + y|\cos\theta|}{S}$ (3.9)

As mentioned earlier, these fibers can be separated into three groups. The factor responsible for this separation is the angle $\theta$.

Case 1: $0 < \theta < \tan^{-1}\left(y/x\right)$, or

$$\pi - \tan^{-1}\left(y/x\right) < \theta < \pi$$

In this case, fibers will be either gripped at one end or not gripped at all.

Case 2: $\tan^{-1}\left(y/x\right) \le \theta \le \pi - \tan^{-1}\left(y/x\right)$

In this case, fibers will be either gripped at both ends or gripped at only one end. Loose fibers will not be a part of this group.

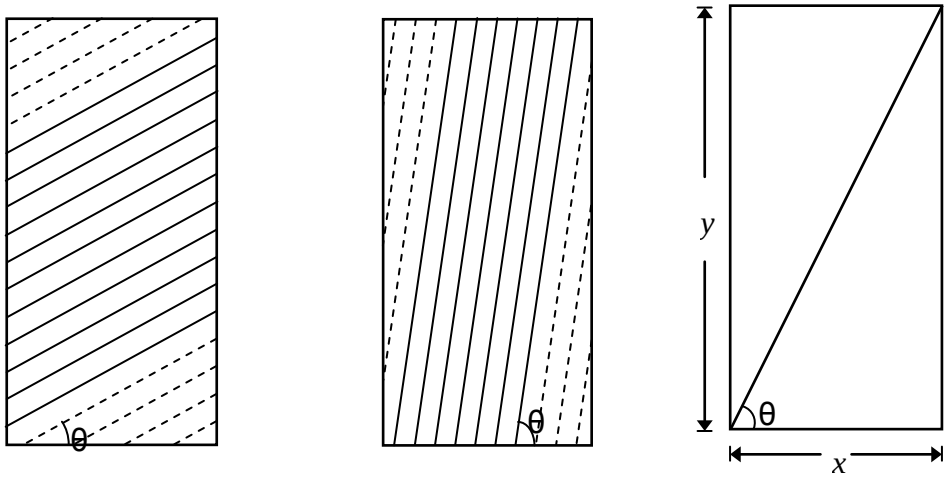


(A) (B) (C)

**Figure 3.5:** Schematic representation of (A) case 1, (B) case 2 and (C) transition point between two cases

Finding the number of fibers category-wise:

Case 1, Fibers gripped at only one end or not gripped at all:

The fibers in the jaws are gripped at only one end, as shown by those represented by dotted lines in Figure 3.5(A). From Equation 3.8, number $x_i$ s in width $x$ gives number of fibers gripped in a jaw. When two jaws are considered, then

$$\text{the total number of fibers gripped at any end} = \frac{2x|\sin\theta|}{S} \tag{3.10}$$

The remaining fibers are loose (solid lines in Figure 3.5(A)).

$$\text{Number of loose fibers} = \frac{x|\sin\theta| + y|\cos\theta|}{S} - \frac{2x|\sin\theta|}{S}$$

$$= \frac{y|\cos\theta| - x|\sin\theta|}{S} \tag{3.11}$$

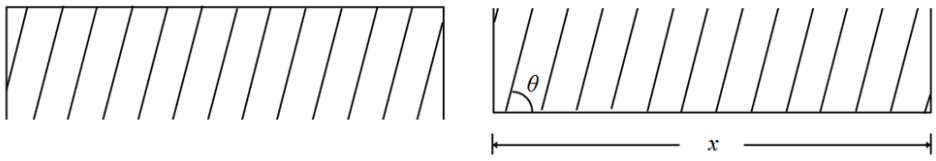


**Figure 3.6:** Fibers of a disc gripped at one or both ends by the jaws of a tensile testing machine

Case 2, Fibers gripped at one end or both ends:

$$\text{Number of fiber ends in jaws} = \frac{2x|\sin\theta|}{S}$$

In this case there are no loose fibers. Subtracting the total number of fibers in a disc from the number of fiber ends in jaws gives the number of fibers gripped at both ends (solid lines in Figure 3.5(B)).

$$\text{Number of fibers gripped at both ends} = \frac{2x|\sin\theta|}{S} - \frac{x|\sin\theta| + y|\cos\theta|}{S}$$

$$= \frac{x|\sin\theta| - y|\cos\theta|}{S} \tag{3.12}$$

The remaining are the number of fibers gripped at only one end, or

$$= \frac{x|\sin\theta| + y|\cos\theta|}{S} - \frac{x|\sin\theta| - y|\cos\theta|}{S}$$

$$= \frac{2y|\cos\theta|}{S} \tag{3.13}$$

For simplification of equations, two terms *a* and *b* are introduced, which are related to the critical angle (transition point), shown in Figure 3.5(C), between the cases 1 and 2. *a* and *b* are integers and have values as follows:

$$a = \frac{\tan^{-1}\left(y/x\right)}{\gamma} \qquad b = \frac{\pi - \tan^{-1}\left(y/x\right)}{\gamma} \tag{3.14}$$

*a* is the minimum angle required for the fibers to be gripped at both ends and *b* is the maximum angle at which fibers can be gripped at both ends.

Total number of fibers gripped at both ends in a sample $= \sum_{j=a}^{b} \frac{x|\sin j\gamma| - y|\cos j\gamma|}{S}$ (3.15)

Total number of loose fibers in a sample

$$= \sum_{j=1}^{a-1} \frac{y|\cos j\gamma| - x|\sin j\gamma|}{S} + \sum_{j=b+1}^{n_d} \frac{y|\cos j\gamma| - x|\sin j\gamma|}{S} \quad (3.16)$$

Total number of fibers gripped at only one end in a sample

$$= \sum_{j=1}^{a-1} \frac{2x|\sin j\gamma|}{S} + \sum_{j=a}^{b} \frac{2y|\cos j\gamma|}{S} + \sum_{j=b+1}^{n_d} \frac{2x|\sin j\gamma|}{S} \quad (3.17)$$

The above three equations give the number of fibers in a web category wise.

3.3.2.1 Calculations using hypothetical values:

Using Equations 3.15, 3.16 and 3.17, the number of fibers for each category in a hypothetical sample is calculated to show their validity.

For a given web with the following reasonable values:

Fiber diameter ($d$) = 210 nm,

Web thickness (T) = 175μm,

Fiber density ($1/\nu_f$) = 1.13g/cc,

Web areal density ($M/xy$) =1.81X10$^{-3}$ g/cm$^2$ and

Sample length ($y$) = 1.5cm

Sample width ($x$) = 1cm.

Substituting the above values in Equation 3.4, gives value of $S$, or space between fibers

$S$ = 1.798 µm

Number of discs, $n_d = T/d = 833$

Angle interval, $\gamma = 180/n_d = 0.216^0$

From Equation 3.14, $a$=261 and $b$=572.

This means that fibers in discs 1 to 260 and those in 573 to 833 were either loose or gripped at one end. Fibers in discs 261 to 572 have fibers gripped at either one end or both ends.

From the number 261 to 572 only, discs have some fibers gripped at both ends. For disc 261, number of fibers gripped at both ends $= \frac{x|\sin j\gamma| - y|\cos j\gamma|}{S}$ (from Equation 3.15)

$$= \frac{1|\sin(261*0.216)| - 1.5|\cos(261*0.216)|}{1.798*10^{-4}}$$

=15

Similarly number of fibers gripped at both ends was calculated for all discs (from 261 to 572). The summation of these types of fibers in all discs = 892820.

For disc 260 number of fibers not gripped at all (loose fibers) from Equation 3.16

$$= \frac{y\left|\cos j\gamma\right| - x\left|\sin j\gamma\right|}{S}$$

$$= \frac{1.5\left|\cos(260*0.216)\right| - 1\left|\sin(260*0.216)\right|}{1.798*10^{-4}} = 22$$

Similarly the number of loose fibers was calculated for discs 1 to 260 and 573 to 833 similarly. The total number of loose fibers in the whole sample is 2367376.

For disc 260, number of fibers gripped at one end only from Equation 3.17 is

$$= \frac{2x\left|\sin j\gamma\right|}{S}$$

$$= \frac{2*1\left|\sin(260*0.216)\right|}{1.798*10^{-4}} = 9240.$$

For all discs, from disc 1 to 833, number of fibers gripped at one end, calculated using Equation 3.17, are 4111844.

To find the effect of width on number of fibers for each category, similar calculations were conducted for different widths of sample. All parameters, other than the width, were kept constant. Table 3.1 shows the number of fibers of the three categories in a particular sample along with their fractions.

**Table 3.1:** Number of fibers of falling in three categories and their fractions for different widths of the sample.

| Width of sample (cm) | Number of fibers | | | | Fraction of fibers | | |
|---|---|---|---|---|---|---|---|
| | Both ends | Loose | One end | Total | Both ends | Loose | One end |
| 0.25 | 60980 | 3747294 | 1351796 | 5160070 | 0.01182 | 0.72621 | 0.26197 |
| 0.50 | 239224 | 3188288 | 2469896 | 5897408 | 0.04056 | 0.54063 | 0.41881 |
| 0.75 | 522058 | 2733874 | 3378780 | 6634712 | 0.07869 | 0.41206 | 0.50926 |
| 1 | 892820 | 2367376 | 4111844 | 7372040 | 0.12111 | 0.32113 | 0.55776 |
| 1.25 | 1334580 | 2071822 | 4703004 | 8109406 | 0.16457 | 0.25548 | 0.57994 |
| 1.5 | 1832270 | 1832252 | 5182200 | 8846722 | 0.20711 | 0.20711 | 0.58578 |
| 1.75 | 2373630 | 1636350 | 5574052 | 9584032 | 0.24767 | 0.17074 | 0.58160 |
| 2 | 2949078 | 1474504 | 5897792 | 10321374 | 0.28573 | 0.14286 | 0.57142 |
| 2.25 | 3551184 | 1339326 | 6168196 | 11058706 | 0.32112 | 0.12111 | 0.55777 |
| 2.5 | 4174428 | 1225198 | 6396448 | 11796074 | 0.35388 | 0.10386 | 0.54225 |

From the plots drawn between number of fibers and the width of sample shown in Figure 3.7, the following observations are made. The number of fibers gripped at both ends increases, the number of loose fibers decreases and the number of fibers gripped at one end increases with increase in sample width.

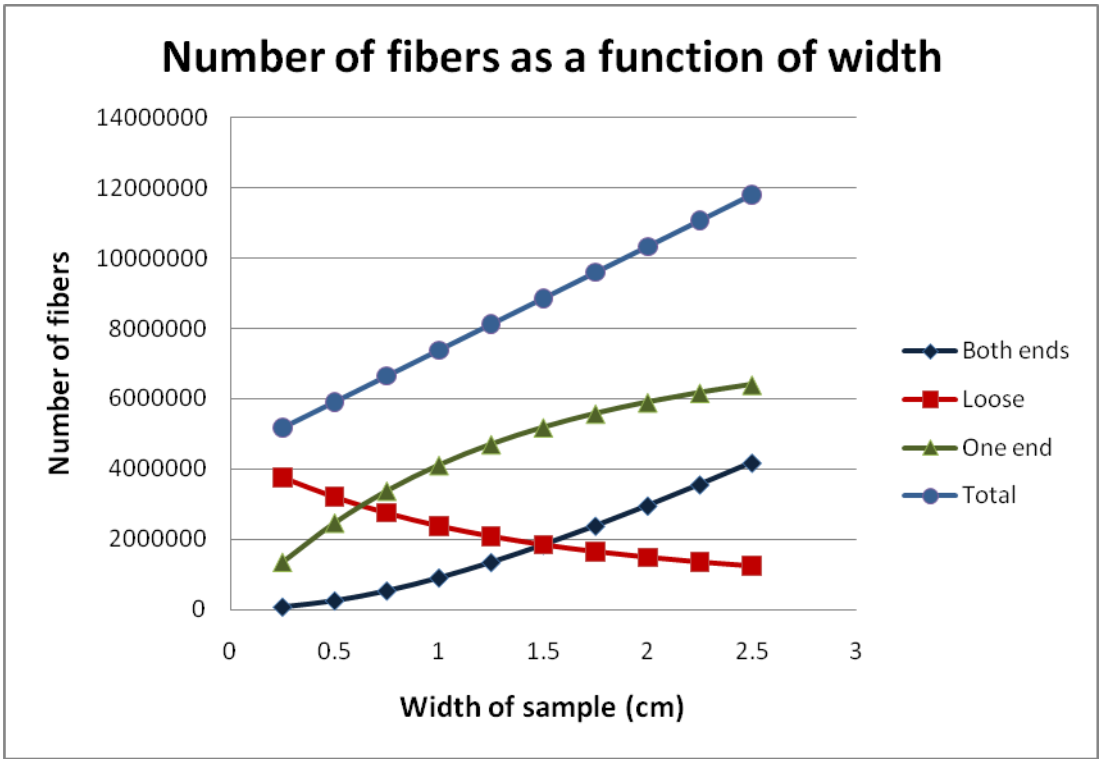


**Figure 3.7:** Plot drawn between the sample width and number of fibers.

When these values are observed as fraction of total number of fibers in a sample (Figure 3.8), and plotted against the width, somewhat similar trends, although with some change in rate, are observed. The major noteworthy observation is that the fraction of fibers gripped at one end goes through a maximum.

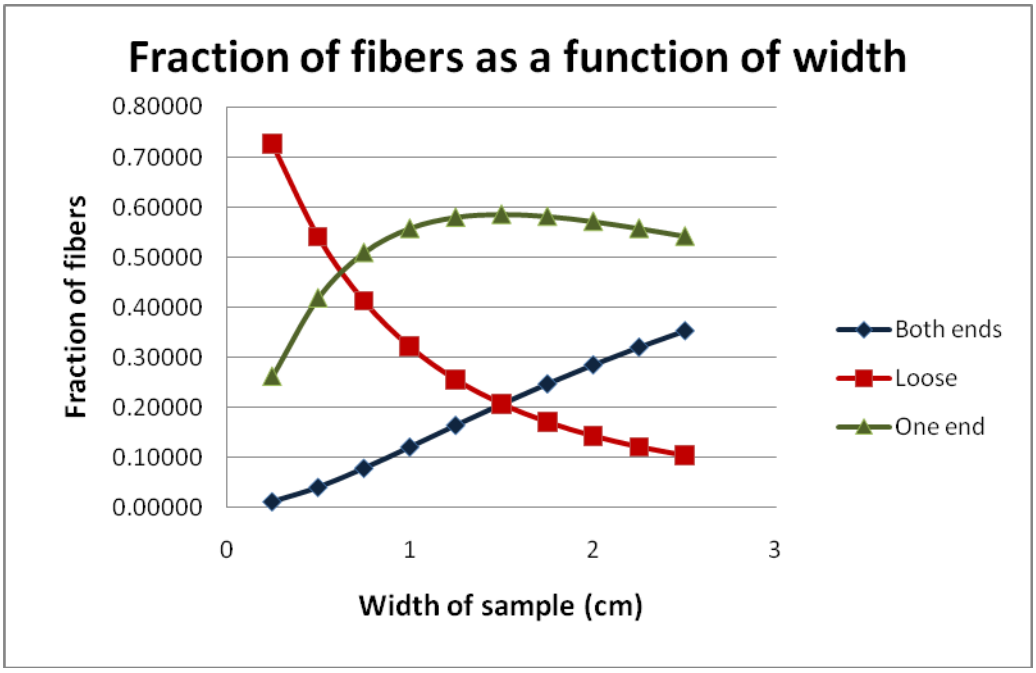


**Figure 3.8:** Plot between fraction of type of fibers and sample width.

### *3.3.3 Length of fibers in a disc:*

In a given disc, all fibers gripped at two ends have the same length as also do the fibers that are not gripped at all. However, this is not the case with fibers gripped at one end. The latter is clear from the illustration given in Figure 3.9.

Let $l_i$ be the length of the $i^{th}$ fiber. We know the total number of fibers in a disc, i.e. $n$, which equals the summation of loose fibers, fibers held at one end, and fibers gripped at both ends.

Let $i = n/2$

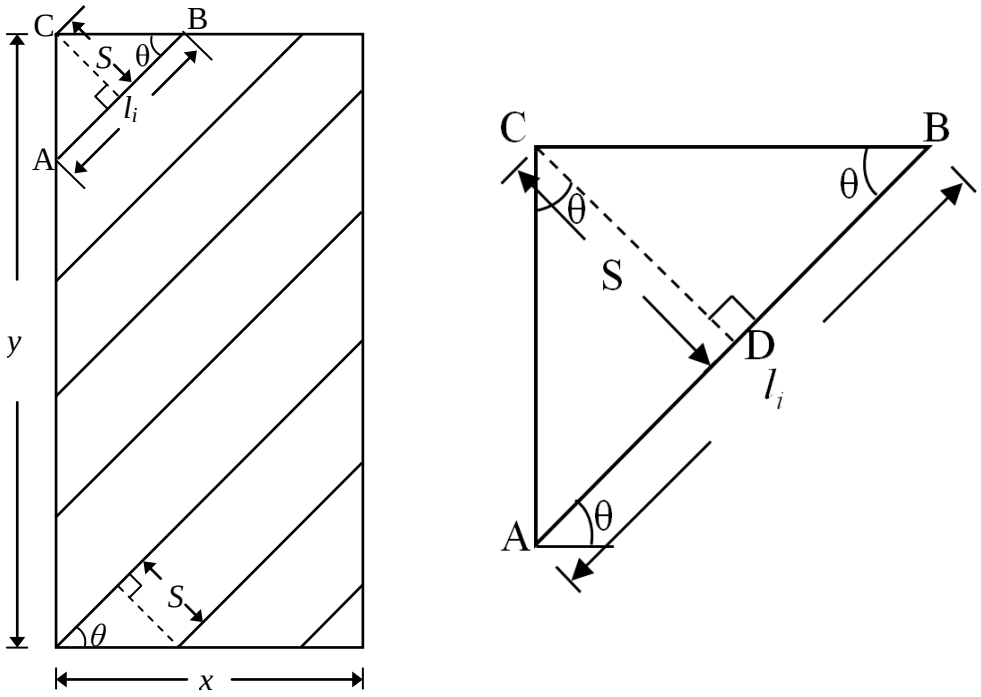


(a) (b)

**Figure 3.9:** Geometry of fibers gripped at one end: (a) general, (b) magnified section of the segment ABC.

In the Figure 3.9, in the segment ABC, AB=AD+DB

In the section ACD, $\tan\theta = \frac{\text{AD}}{S}$; or $\text{AD} = S \cdot \tan\theta$

In the section BCD, $\cot\theta = \frac{\text{DB}}{S}; \text{DB} = S \cdot \cot\theta$

Length of the fiber, $l = S\left(\tan\theta + \cot\theta\right)$

For the fiber adjacent to the previous one, CD=2$S$ and the length of fiber is $2S\left(\tan\theta+\cot\theta\right)$

Similarly, the length of $i^{\text{th}}$ fiber is $l_i = i\cdot S\left(\tan\theta+\cot\theta\right)$ (3.18)

This is only up to $i\cdot S < x\cdot\sin\theta$ or $i\cdot S < y\cdot\cos\theta$, whichever is less.

If $i\cdot S \geq x\cdot\sin\theta$, then $l_i = \dfrac{x}{\cos\theta}$, or

if, $i\cdot S \geq y\cdot\cos\theta$, then $l_i = \dfrac{y}{\sin\theta}$

As mentioned earlier, fibers in a disc can be categorized into 3 groups. Among these, the fibers gripped at both ends as well as those not gripped at all have the same lengths. Only the fibers gripped at one end have lengths that vary from fiber to fiber. In the latter case, the length increases with the distance from the corner.

3.3.3.1 Length of fibers gripped at both ends:

From the triangle shown in Figure 3.10,

$\sin\theta = \dfrac{y}{l_i}$, or

$$l_i = \frac{y}{\left|\sin\theta\right|} \tag{3.19}$$

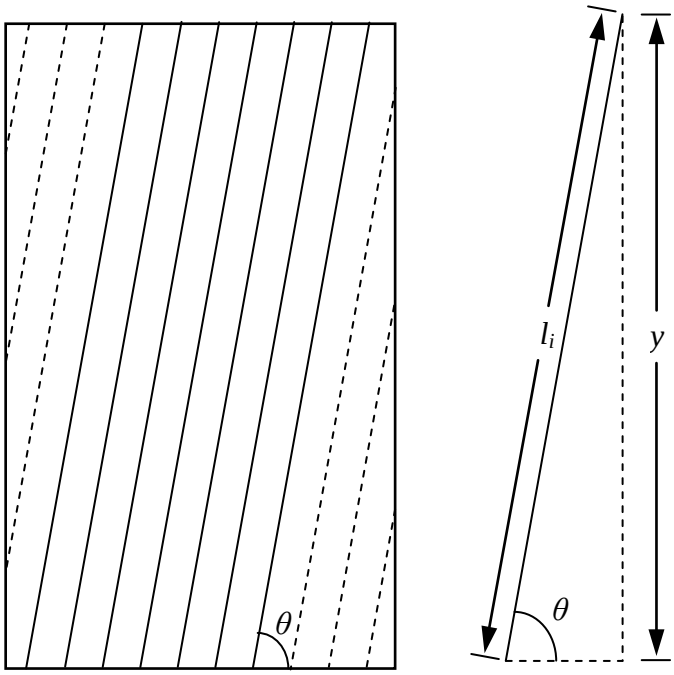


**Figure 3.10:** Geometry of fibers gripped at both ends

3.3.3.2 Length of loose fibers:

From the triangle shown in the Figure 3.11,

$\cos\theta = \frac{x}{l_i}$, or

$$l_i = \frac{x}{|\cos\theta|} \tag{3.20}$$

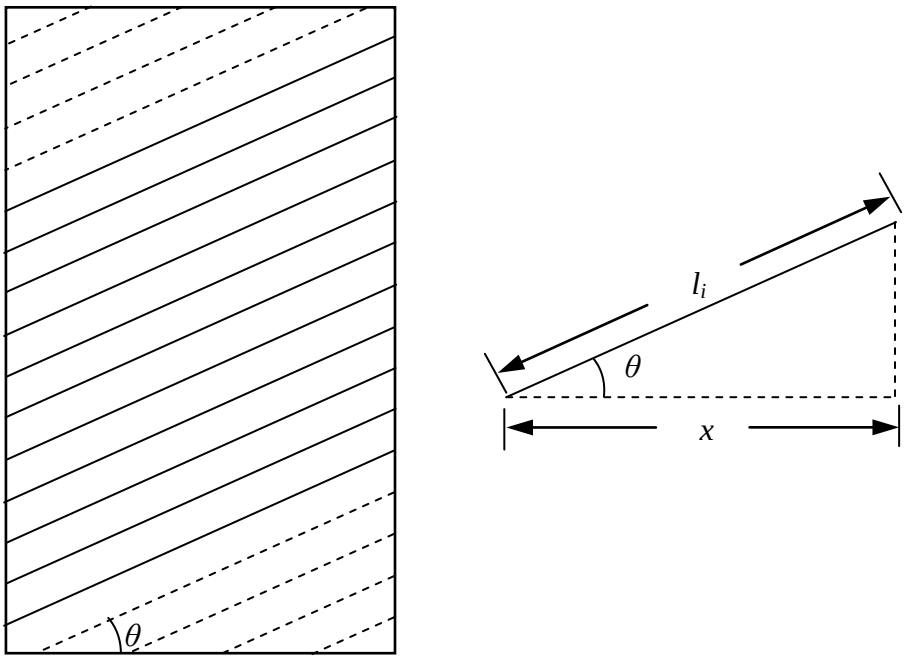


**Figure 3.11:** Geometry of loose fibers

3.3.3.3 Length of fibers gripped at only one end:

Length of fibers gripped at only one end changes as the fiber position changes with respect to the corner. The fiber length increases proportionately with increase in the distance from the corner.

The length of $i^{\text{th}}$ fiber is $l_i = i \cdot S \left| \tan\theta + \cot\theta \right|$ (Equation 3.18)

The lengths of the three types of fibers in a disc are given by Equations 3.18, 3.19 and 3.20 .

### *3.3.4 Number of cross-over points among the fibers in a specimen:*

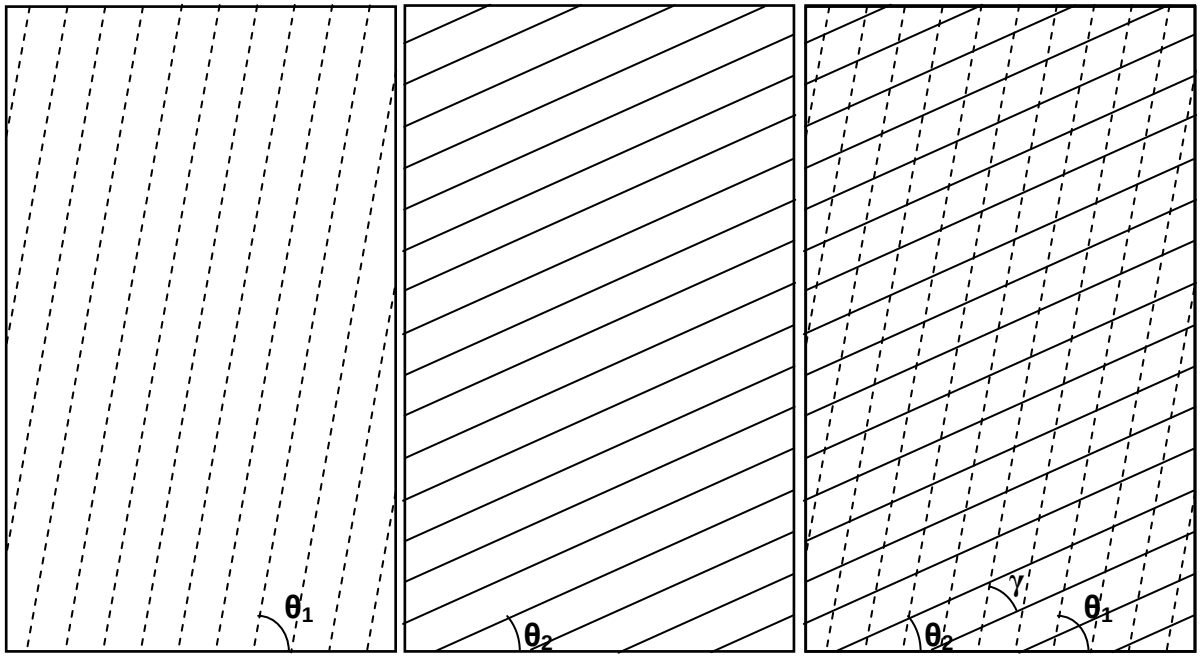


disc 1 disc 2 overlapped discs

(a)

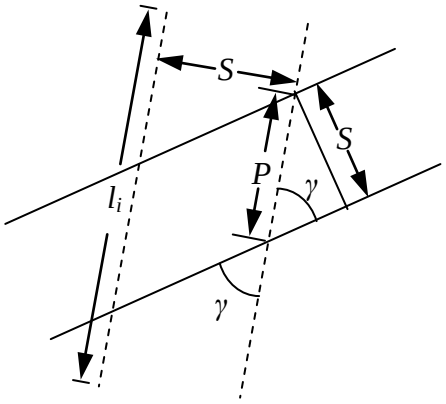


(b)

**Figure 3.12:** Schematic representation of the cross-over points generated by the overlapping of the fibers from two discs: (a) general figure, (b) expanded view of a small section.

Another factor relevant to the strength of a fabric is the number of cross-over points, whose contribution to the strength occurs due to bonding or friction between fibers. Unless an adhesive is used, one may assume that the fibers of a given layer will be bonded with those of the layer immediately above and below it. Number of cross-over points between two layers is estimated below.

Let the fibers in disc-1 make angle $\theta_1$ and those in disc-2 make angle $\theta_2$.

Angle interval $\theta_2 - \theta_1 = \gamma = \dfrac{180^0}{n_d}$ ($n_d$ is the number of discs)

The distance $P$ between the cross-over points of the fibers of discs 1 and 2 along the length of fibers of disc 1 (Figure 3.12) is

$$P = \frac{S}{\sin\gamma}$$

The number of cross-over points made by fibers of disc-1 with the $i^{th}$ fiber of disc-2 of length $l_i$ is

$$l_i / P = \frac{l_i \sin\gamma}{S} \tag{3.21}$$

Now considering fibers belonging to all three categories in discs 1 and 2, the total number of cross-over points between the fibers of the two discs will be given by the equation below:

$$n_{be}\left[\frac{y}{|\sin\theta|}\cdot\frac{\sin\gamma}{S}\right]+n_{lf}\left[\frac{x}{|\cos\theta|}\cdot\frac{\sin\gamma}{S}\right]+2\sum_{i=1}^{n_{oe}/2}\left[i\cdot S\left(|\tan\theta|+|\cot\theta|\right)\cdot\frac{\sin\gamma}{S}\right] \quad (3.22)$$

$$=n_{be}\left[\frac{y}{|\sin\theta|}\cdot\frac{\sin\gamma}{S}\right]+n_{lf}\left[\frac{x}{|\cos\theta|}\cdot\frac{\sin\gamma}{S}\right]+\frac{n_{oe}\left(n_{oe}+2\right)}{4}\left[\left(|\tan\theta|+|\cot\theta|\right)\cdot\sin\gamma\right] \quad (3.23)$$

where $n_{be}$, $n_{oe}$ and $n_{lf}$ represent the number of fibers that are gripped at both ends, one end and not at all, respectively.

3.3.4.1 Sample calculations using hypothetical values:

To calculate the number of cross-over points, the hypothetical values used are the same as used in Section 3.3.2.1 for calculating the number of fibers and their fractions.

In this example, there are 833 discs, of which discs 1 to 260 and 573 to 833 have fibers that are either gripped at one end or not gripped at all and discs 261 to 572 have fibers gripped at two ends or one end.

From Equation 3.23, number of cross-over points made by fibers gripped at both ends of disc number 261 with 262 disc is

$$n_{be}\left[\frac{y}{|\sin\theta|}\cdot\frac{\sin\gamma}{S}\right]=15\left[\frac{1.5}{|\sin(261*0.216)|}\cdot\frac{\sin 0.216}{1.79*10^{-4}}\right]=566$$

Calculations similar to the above were made for discs 261 to 572 and the summation of all cross-over points is 28965094.

From Equation 3.23, number of cross-over points made by the loose fibers of disc 260 with fibers of disc 261 is

$$n_{lf}\left[\frac{x}{|\cos\theta|}\cdot\frac{\sin\gamma}{S}\right]=22\left[\frac{1}{|\cos(261*0.216)|}\cdot\frac{\sin 0.216}{1.79*10^{-4}}\right]=829$$

Summation of all cross-over points for loose fibers from discs 1 to 260 and 573 to 832 is 54557146.

From same Equation 3.23, number of cross-over points made by fibers gripped at one end of disc 260 with those of the next disc is

$$\frac{n_{oe}\left(n_{oe}+2\right)}{4}\left[\left(|\tan\theta|+|\cot\theta|\right)\cdot\sin\gamma\right]$$

$$=\frac{9240\left(9240+2\right)}{4}\left[\left(|\tan(260*0.216)|+|\cot(260*0.216)|\right)\cdot\sin 0.216\right]=174130.$$

The total number of cross-over points made by fibers gripped at one end in the sample is 62047856.

To find the effect of sample width on the number of cross-over points, calculations were done for several different widths of sample. All other parameters were kept constant as done for the calculations in Section 3.3.2.1. Calculated numbers of cross-over points along with their fractions are listed in the Table below.

**Table 3.2:** Number of cross-over points falling in three categories and their fractions for different widths of the sample

| Width of sample (cm) | Number of cross-over points for fibers gripped at | | | | Fraction of cross-over points for fibers gripped at | | |
|---|---|---|---|---|---|---|---|
| | Both ends | No end | One end | Total | Both ends | No end | One end |
| 0.25 | 1922912 | 25580208 | 8886676 | 36389796 | 0.05284 | 0.70295 | 0.24421 |
| 0.50 | 7592872 | 40052640 | 25137576 | 72783088 | 0.10432 | 0.55030 | 0.34538 |
| 0.75 | 16733628 | 48911708 | 43530632 | 109175968 | 0.15327 | 0.44801 | 0.39872 |
| 1 | 28965094 | 54557146 | 62047856 | 145570096 | 0.19898 | 0.37478 | 0.42624 |
| 1.25 | 43876270 | 58277732 | 79811900 | 181965902 | 0.24112 | 0.32027 | 0.43861 |
| 1.5 | 61072308 | 60808790 | 96478724 | 218359822 | 0.27969 | 0.27848 | 0.44183 |
| 1.75 | 80205510 | 62579808 | 111968040 | 254753358 | 0.31484 | 0.24565 | 0.43952 |
| 2 | 100981774 | 63850834 | 126316064 | 291148672 | 0.34684 | 0.21931 | 0.43385 |
| 2.25 | 123151990 | 64782668 | 139609192 | 327543850 | 0.37599 | 0.19778 | 0.42623 |
| 2.5 | 146517750 | 65477572 | 151946192 | 363941514 | 0.40259 | 0.17991 | 0.41750 |

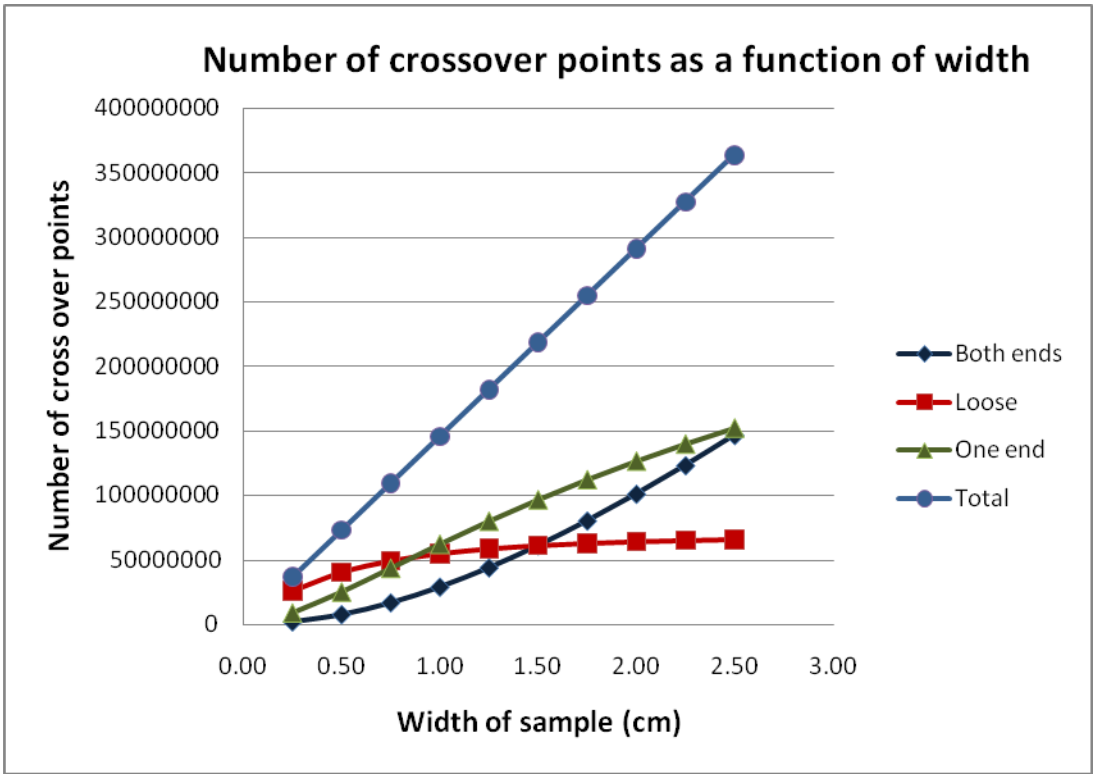


**Figure 3.13:** Graph between number of cross-over points and sample width for a fabric. (For fabric details refer Section 3.3.2.1)

As shown in Figure 3.13, the number of cross-over points made by the three category of fibers increase with increase in width. But the number of such points made by loose fibers increases with the width to some extent and then tends to reach a plateau. With the increase in width, the number of fibers gripped at one or both ends increases and number of cross-over points increases. But in the case of loose fibers, the number of fibers decreases with increase in sample width. The increased number of fibers in other category increases the number of cross-over points on these loose fibers. This mixed effect causes the plateau in the curve of loose fibers. In Figure 3.14, the graph drawn is between fraction of cross-over points

made by three categories and sample width. These fractions follow similar trends as noted for the number of fiber fractions in Section 3.3.2.1, indicating that the number of cross-over points is dependent on the number of fibers.

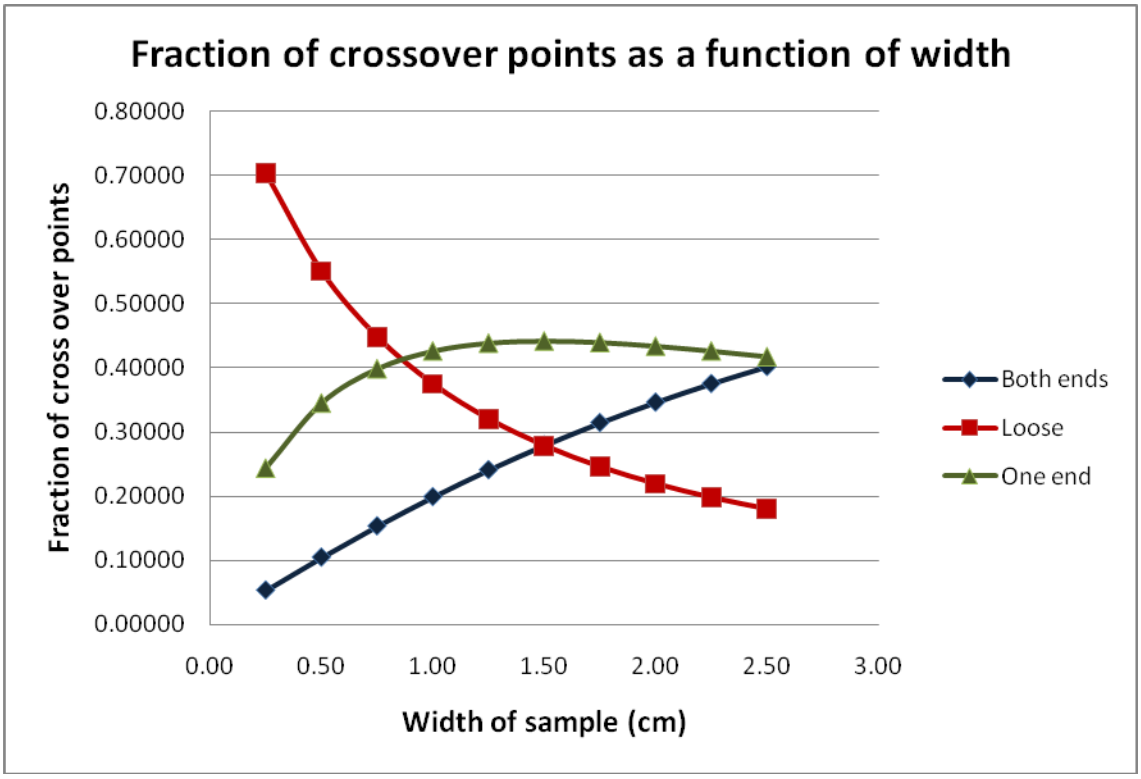


**Figure 3.14:** Graph between fraction of cross-over points made by a type of fiber and sample width for hypothetical values.

## 3.4 Modeling of the tensile properties of the electrospun web

### *3.4.1 Stress-strain properties of a fabric using the force method*

Fibers gripped at both ends are the ones that primarily contribute to the strength of the electrospun fabric, as mentioned earlier. The number of fibers gripped at both ends are maximum only when $\theta_j = 90^0$.

At this angle, fiber strain ($\varepsilon_j$) is equal to the fabric strain ($\varepsilon_i$), or the fiber elongation ($\Delta l$) equals the fabric elongation ($\Delta y$).

Accordingly, one can assume that the peak load in a fabric will be reached when the strain in the fabric equals the strain corresponding peak stress in the fibers ($\varepsilon_{jp}$).

Force method uses the following steps.

1. Finding individual fiber strains for a given fabric strain
2. Getting fiber force or stress for the fiber strain from fiber load - elongation curve
3. Resolving the forces in the fibers, in the direction parallel to the fabric strain axis
4. Adding all the forces to get the force on fabric

A. <u>Fiber elongation from fabric elongation:</u>

Referring to Figure 3.15, let OQ be a fiber of length *l* which makes an angle $\theta_j$ to the horizontal axis.

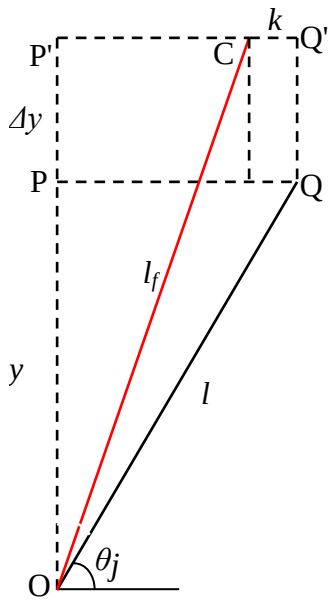


**Figure 3.15:** Deformation of fiber

Due to a fabric strain, $\varepsilon_i$, or deformation $\Delta y$, points P and Q moves to P′ and Q′, respectively.

$$\varepsilon_i = \frac{\mathrm{PP}'}{\mathrm{OP}} = \frac{\Delta y}{y}$$

The strain $\varepsilon_i$ deforms the fiber OQ to OC.

The lateral contraction = CQ′= *k*.

From the Pythagoras theorem, $\mathrm{OC}^2 = \mathrm{OP}'^2 + \mathrm{CP}'^2 = \mathrm{OP}'^2 + (\mathrm{PQ} - \mathrm{CQ}')^2$ (3.24)

$$\mathrm{OC}^2 = (y + \Delta y)^2 + (y\cot\theta_j - k)^2 = (y + \Delta y)^2 + (y\cot\theta_j - \Delta y \nu_{LT}\cot\theta_j)^2 \quad (3.25)$$

when $\nu_{LT}$ is the Poisson's ratio of the fabric.

Fiber elongation $\Delta l = \mathrm{OC} - l = \left[ (y + \Delta y)^2 + \cot^2 \theta_j (y - \Delta y \nu_{LT})^2 \right]^{1/2} - y / \sin \theta_j$ (3.26)

$$\Delta l = \frac{\left[ (y + \Delta y)^2 \sin^2 \theta_j + (y - \Delta y \nu_{LT})^2 \cos^2 \theta_j \right]^{1/2} - y}{\sin \theta_j} \tag{3.27}$$

B. Force on fiber:

Force $F(\Delta l)$ on fiber at elongation $\Delta l$ can be read from the fiber load - elongation curve.

This force acts on fiber in the direction of fiber axis which is at angle $\theta_j$ to the fabric axis.

Force $F(\Delta l)$ of the fiber along fabric axis is given by:

$F(\Delta l) \sin \theta_j$ (3.28)

In the previously mentioned three categories of fibers, only fibers gripped at both ends contribute directly to the strength of fabric. The remaining fibers may contribute through friction or adhesive bonding made with other fibers. If we ignore the contribution to strength by bonding or friction at cross-over points, then force acting on a disc is equal to summation of forces acting on fibers gripped at both ends.

Force in a fabric disc

= Number of fibers gripped at bothends * Force on a fiber resolved along the fabric axis

$$= \frac{x|\sin j\gamma| - y|\cos j\gamma|}{S} \cdot F(\Delta l) \cdot \sin\theta_j \tag{3.29}$$

Force developed in the fabric due to the elongation $\Delta y$ in the fabric is given by the summation of forces on all discs.

$$\text{Total force on fabric} = \sum_{j=a}^{b} \frac{x|\sin j\gamma| - y|\cos j\gamma|}{S} \cdot F(\Delta l) \cdot \sin j\gamma \tag{3.30}$$

As explained earlier, peak load on fabric is expected when the elongation of fabric equals to the peak elongation in the fiber ($\Delta l_p$).

$$\text{Peak load in fabric} = \sum_{j=a}^{b} \frac{x|\sin j\gamma| - y|\cos j\gamma|}{S} \cdot F(\Delta l_p) \cdot \sin j\gamma \tag{3.31}$$

$$\text{In Equation 3.31, } \Delta l = \frac{\left[(y + \Delta l_p)^2 \sin^2\theta_j + (y - \Delta l_p \nu_{LT})^2 \cos^2\theta_j\right]^{1/2} - y}{\sin\theta_j} \tag{3.32}$$

Equation 3.30 gives the force in a fabric developed when it is given an elongation of $\Delta l$. By varying $\Delta l$ from 0 to the peak elongation of the fiber, the load-elongation curve of the fabric can be generated. This can be converted into the stress-strain curve by normalizing the values of the force by dividing it with linear density and elongation by dividing it with the test length. Or by knowing the peak load and corresponding elongation of the fiber, one can

compute the peak load or stress of the fabric. The assumption involved in developing the model is that no bonding exists at the cross-over points. Although an adhesive is not involved, some bonding does exist between fibers as they lay over each other during the electrospinning process. This bonding, howsoever small, can be expected to allow even loose and one end gripped fibers to contribute to the strength of the fabric. Accordingly, the model presented can only be considered as the first step towards characterizing the mechanical behavior of electrospun webs. Similarly, one can use the structural model and the energy method proposed by Hearle and Newton and compute the tensile properties of the web. An attempt using this method was made but is included in the Appendix A of the thesis.

# 4. MATERIALS & METHODS

The materials and methods were selected to vary structure of the electrospun web and its areal density and examine their effects on web mechanical properties. The primary objective was to be able to measure the mechanical properties of webs and examine the effects of some of the web construction factors on them. A second but equally important objective was to attempt to model and predict these properties. Twenty-seven different samples were prepared. They varied in terms of the polymer concentration used, the diameter of the electrospun fiber produced, and the areal density of the web obtained. Four specimens were prepared for each set of conditions, making the number of different samples electrospun to be 108. The prediction of properties using mathematical model required tensile behavior of single nanofibers. For this oriented bundles of fibers were produced. Four such bundles, produced under different conditions, each with six repetitions were prepared for measuring and evaluating the single fiber mechanical properties. Details about the materials used, variables studied and the methods followed are discussed in this chapter.

## 4.1 Polymer and solvent

The polymer used was Polyethylene oxide (PEO) with a repeat unit as $-CH_2-O-CH_2-$. PEO was chosen because of its easy availability, non-toxicity and rapid solubility in various types of solvents, including water, Dimethyl formamide, ethanol and chloroform. (Ojha, 2007) PEO is biocompatible and has been used frequently in biomaterial applications, including scaffolds for tissue engineering and prosthesis. Diameter of fiber was one of the

variables of interest as it could be expected to influence the mechanical properties. The polymer has been shown to lead to fibers in the diameter range of 50nm to 5μm through electrospinning. Such versatile nature of PEO was another reason for choosing this polymer for the current study. Polyethylene Oxide of average molecular weight ($M_v$) 400,000 purchased from Sigma-Aldrich, USA, was used. The solvent used was de-ionized water.

## 4.2 Polymer solution preparation

To prepare polymer solution of PEO in water, calculated amount of polymer was weighed using the Mettler Toledo AG245 weighing balance and put in a glass vial. Required amount of solvent was added with a pipette (Eppendorf) to the vial to get a particular concentration of the solution. A magnetic stirrer bar was dropped into the vial and the vial was sealed with paraffin film. It was then placed on a magnetic stirrer for several hours using a stirring speed of 200 rpm.

## 4.3 Electrospinning

### *4.3.1 Set-up for the regular electrospun web*

The polymer solution prepared above was transferred to a plastic syringe obtained from Becton Dickinson & Co., NJ, to which was attached a metal capillary needle of 7 mm length, 0.6mm inner and 0.9mm outer diameter (Reusable Type 304 Stainless steel, McMaster-Carr, Atlanta, GA). This syringe was actuated for dispensing of polymer solution at desired speeds by a syringe pump obtained from New Era Pump Systems, Inc., Wantagh, NY. An aluminum circular plate of 15cm diameter was used as the collector for the fibers (Figure 4.1). Distance

between the collector plate and the tip of the needle was varied as needed. Height of the jack on which the pump-syringe was placed was adjusted in such a way that the needle tip pointed at the centre of the collector plate. The collector plate and needle capillary were connected to a high voltage power supply (ES 40P-5W, Gamma High Voltage Research, Ormond Beach, FL). The magnitude of the power used could be controlled with an analog voltage adjustment device. A video camera with a monocular lens was set up and focused on the needle tip in order to view the jet as it formed at the needle and its behavior.

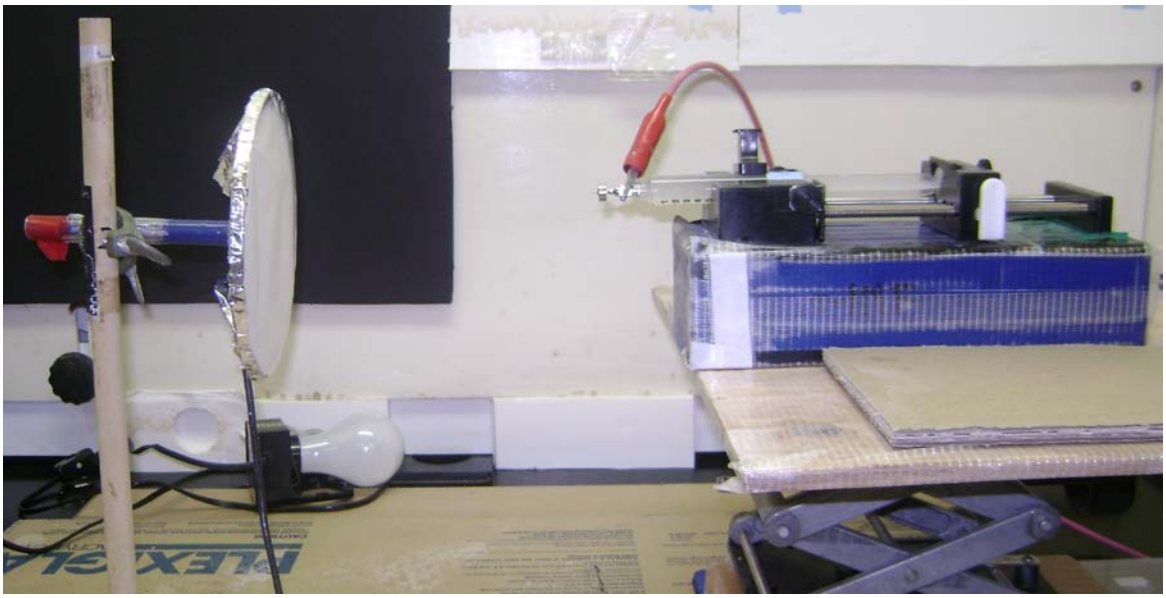

**Figure 4.1:** Image of electrospinning set-up for producing random nanofiber web

### *4.3.2 Set-up for a bundle of oriented nanofibers*

For predicting tensile properties using a structured model, it was necessary that we had the stress-strain curve of a single electrospun fiber. The fibers being so minute, the only recourse was to electrospin bundle of oriented fibers, measure its tensile properties and

deduce the properties of a single fiber from it. For producing such a bundle, two parallel aluminum plates were used in place of the round collector plate in the above setup (Figure 4.2). The distance between the parallel plates could be adjusted with screws. Height of the needle was adjusted with the jack such that the needle tip was pointed at the midpoint between the plates.

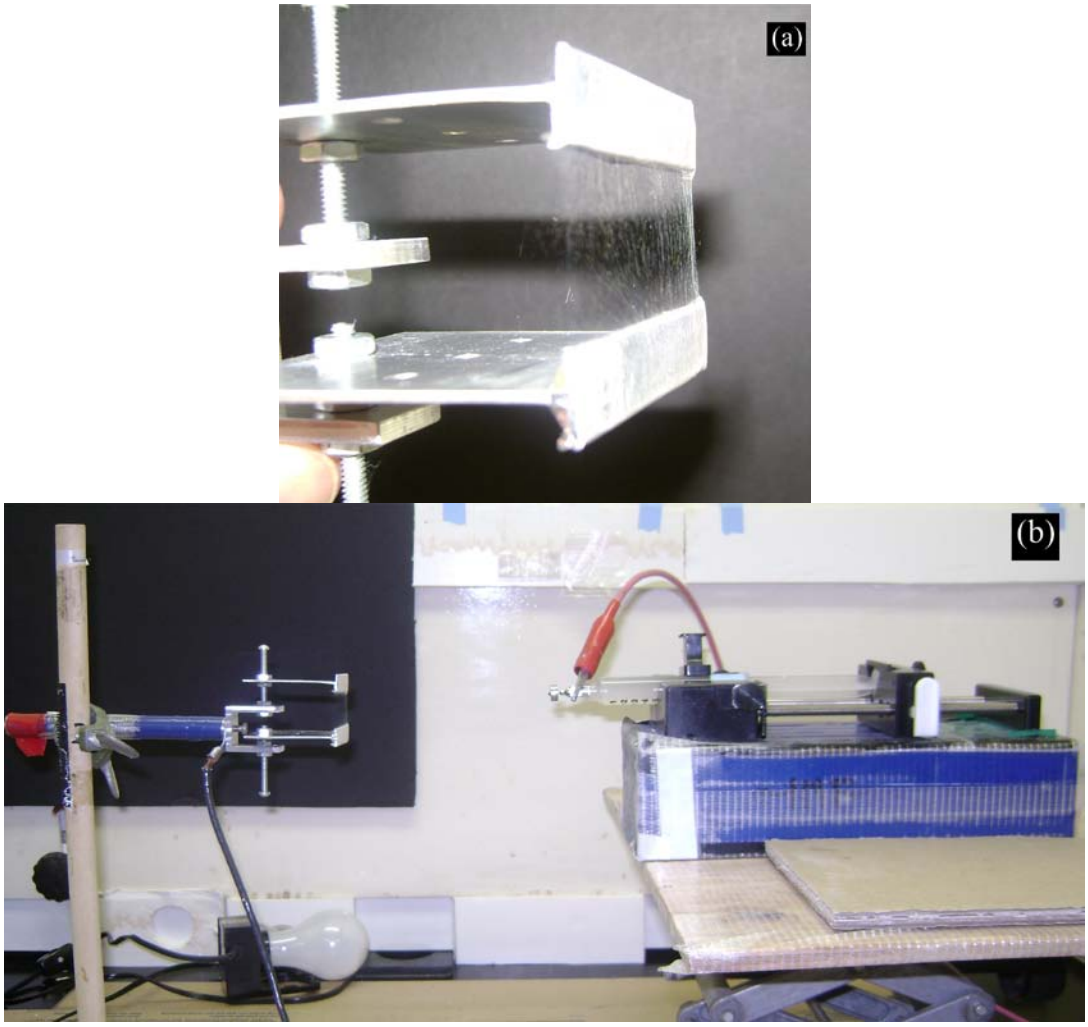


**Figure 4.2:** (a) Image of parallel collectors with oriented web, (b) electrospinning set-up for producing aligned fibers

### *4.3.3 Spinning process*

The collector plate was covered with an aluminum foil on which the fibers were to be deposited. The syringe pump with the solution in the syringe was turned on. The speed of the pump was set at 300µl/hr. As the solution started to come out of the needle, the power supply was turned on and the voltage gradually increased until a jet of the polymer solution erupted from the tip of the needle. The voltage was adjusted to stabilize the Taylor cone. After spinning the fiber for the desired length of time, power supply was turned off and the deposited material taken out for evaluation and testing.

## 4.4 Process variables

The primary variable used was polymer concentration. Polymer concentration affected the fiber diameter as well as the orientation of molecules, the latter due to the change in voltage that was necessary when polymer concentration was changed. Number of fibers gripped in jaws also has effect on mechanical properties of web. This number could be changed with the change in the dimensions of the sample in tensile tester or the time of collection of web. Experimental work was done to find the effect of concentration, production time and sample dimensions on the mechanical properties of electrospun nanofiber web. Work was also conducted to study the mechanical properties of single fibers, and the effect of concentration and distance between collector plate and needle on these properties.

### *4.4.1 Concentration of PEO*

Three different concentrations, namely 8%, 10% and 12.5%, of PEO polymer in solution with de-ionized water as the solvent were used. The voltage between the collector and needle was changed as needed to stabilize the Taylor cone associated with the jet. Similarly, the distance between the needle tip and the collector plate was adjusted to obtain a uniform collection of the sample. The spinning variables used are as listed in Table 4.1. For 12.5% concentration of PEO, voltage needed to stabilize the Taylor cone was 17kV, but at 15cm distance solvent was not evaporated completely and fusing of fibers was observed. To get uniform fibers with 12.5% PEO, distance was increased to 18cm.

**Table 4.1:** Details of voltage and distance used for production

| % Concentration | Voltage (kV) | Distance (cm) |
|---|---|---|
| 8 | 9.5 | 15 |
| 10 | 11.5 | 15 |
| 12.5 | 17 | 18 |

### *4.4.2 Production time*

It was thought that some dimensional parameters that were known to affect mechanical properties should be varied to examine their effects on the properties measured as well as on the properties predicted. This, in addition to the fiber diameter (Section 4.4.1), was considered to be the areal density. There was no direct way to control the areal density of the

web other than by collecting the webs at different time periods. Webs were collected for 4, 5 and 6hours for a given concentration of polymer.

### *4.4.3 Sample dimensions*

In tensile tests, the dimensions of the test sample could be expected to affect the properties measured. This is because the dimensions of an unoriented or partially oriented web could be expected to influence the fraction of fibers gripped at both ends. It was decided to keep the length of the test specimen constant at 15 mm but vary the width over three levels; 10, 15 and 20 mm.

### *4.4.4 Summary of variables for regular or unoriented web properties*

The above mentioned 3 variables, namely concentration of polymer solution, collection time and sample width, were considered for finding their effects on mechanical properties. Flow chart in Figure 4.3 illustrates the variables. Overall 27 different samples were considered for testing. For each set of conditions four specimens were prepared.

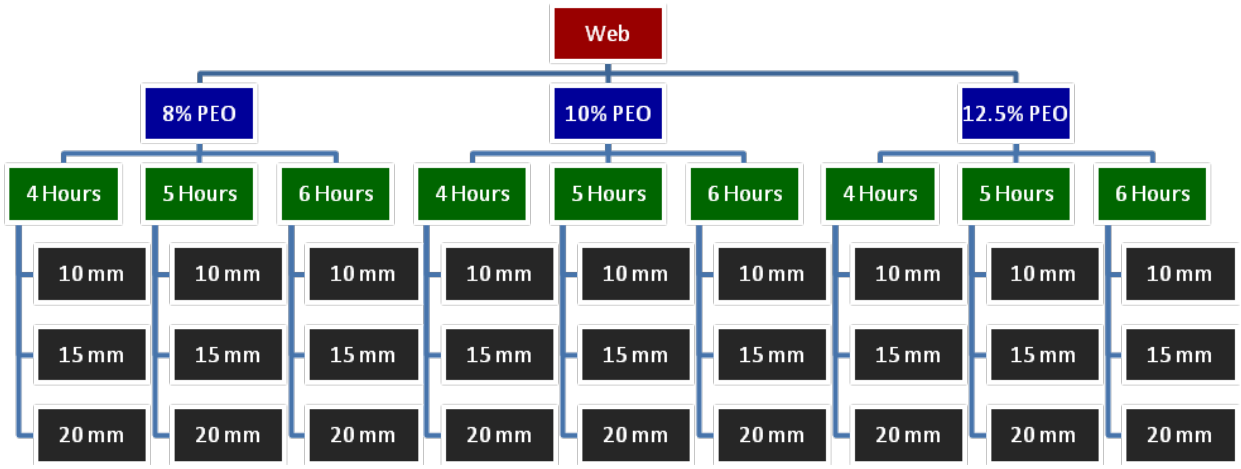


**Figure 4.3:** Flowchart of types of samples studied for web

Time of collection was expected to change the linear density of web proportionately. On the measured stress-strain properties of web, time of collection was not expected to have any effect, but in the way the model is constructed, the time of collection affected the thickness of the web and with it the number of layers and the calculated value of the force. Therefore, for the measured values, the time factor could be ignored. This essentially meant that the results pertaining to different time periods could be lumped together. Accordingly nine different samples (3 concentrations and for each 3 widths) with repetition of 12 specimens for each sample were considered. However for the computation of theoretical values and validation of the model, 27 different samples with repetition of 4 specimens per sample were considered.

### *4.4.5 Variables for single fiber properties*

In order to produce oriented bundle of parallel fibers of the same set of diameters as obtained on the random web, different combinations of concentrations, distances between the collector and needle, and voltages were needed. The required diameters as that of the fibers

in the web were accomplished at reduced distances for a given concentration. It was thought that, in addition to obtaining single fibers of comparable dimensions and observing their tensile properties for use in the model, studying the effect of concentration and the spinning distance on these properties of single fiber would be valuable. For this pursuit, 4 combinations of conditions were selected, as listed in Table 4.2.

**Table 4.2:** Details of voltage and distance used for aligned bundle production

| Type | % Concentration | Distance (cm) | Voltage (kV) |
|---|---|---|---|
| 1 | 8 | 15 | 9.5 |
| 2 | 8 | 10 | 9.5 |
| 3 | 10 | 15 | 11.5 |
| 4 | 10 | 10 | 11.5 |

Using this process, bundles consisting of parallel fibers were collected. It was observed that after certain time of collection, fibers were not collecting parallel to each other which may be due to deposition of charges. So the collection time was limited to 25 seconds for each spinning (after this, the fibers collected were not aligned). Fibers deposited on collector were transferred to a cardboard frame, but the bundle was too thin and delicate for performing tensile tests. So, the number of collections of parallel bundles for placing on a cardboard for tensile tests had to be increased to 45 times. Overall, four different types of samples (two concentrations, each with two distances and voltages) with 6 specimens for

each sample were prepared and tested. The flow chart in Figure 4.4 shows the types of samples considered for oriented fiber analysis.

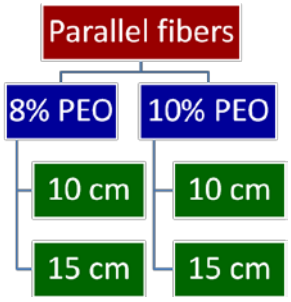


**Figure 4.4:** Flowchart of types of samples studied for aligned fiber properties

## 4.5 Characterization

### *4.5.1 Morphology, orientation*

Scanning Electron Microscopy was used for determining the fiber morphology and orientation of electrospun web. Specimen of small sizes were carefully cut and mounted onto the stubs with a conductive carbon tape. The stubs were sputter coated with Gold-Palladium alloy (60-40). Since ionized gas molecules tended to melt the PEO fibers, low current of 10milliamp was used for 90 seconds for coating the samples. The samples were then viewed under SEM (Hitachi S-3200 or JEOL 6400F) with a working distance of 10mm at 5kV for high resolution. Images were captured at 1000x to 10000X depending on the objective. Lower magnification was used for examining the morphology and web thickness, and higher magnification was used for measuring fiber diameters. Image analysis was conducted to determine the orientation distribution of the webs.

In the case of the oriented webs, the fibers were expected to be parallel with each other and oriented along the bundle axis. But the number of fibers in a sample was needed to be estimated. For this, an optical microscope (Nikon Eclipse 50iPOL with ELWD objective) of 500X resolution was used. Fibers collected between the parallel plates were transferred to a cardboard frame with a double-sided cellophane tape, then placed on the microscope slide and observed. The number of fibers collected in 25 seconds on collector plate was counted and used in calculations.

### *4.5.2 Fiber diameter*

For measurement of fiber diameter, images were acquired at 10000x magnification. The "Revolution", which is the image analysis software, was used to measure the diameter of fibers. Scale given on the magnification bar was utilized to measure the diameter of a fiber when a line was drawn perpendicular to its axis and the length assessed digitally. A number of readings (150) of diameter were taken and averaged to get the average value for the web.

### *4.5.3 Thickness of the web*

The expected thickness of nanofiber web for the run times given earlier was 150µm - 800µm. Measuring the thickness of a highly delicate web was complex because when a web was cut with a blade, the edge tended to compress irrespective of how sharp the blade was. To avoid this, freeze-fracturing technique was adopted. Web was immersed in liquid nitrogen, allowed to freeze, and then sliced with a sharp razor blade while still in liquid nitrogen. The sliced sample was taken out and kept in room atmosphere for one minute. A

piece of copper tape was attached on the inclined edge of the SEM stub, shown in Figure 4.5. The sample was adhered to the tape in such a way that the cut edge faced up. The sample was observed under SEM and images were acquired. Using the "Revolution" software, thickness of the sample was measured at several places and averaged.

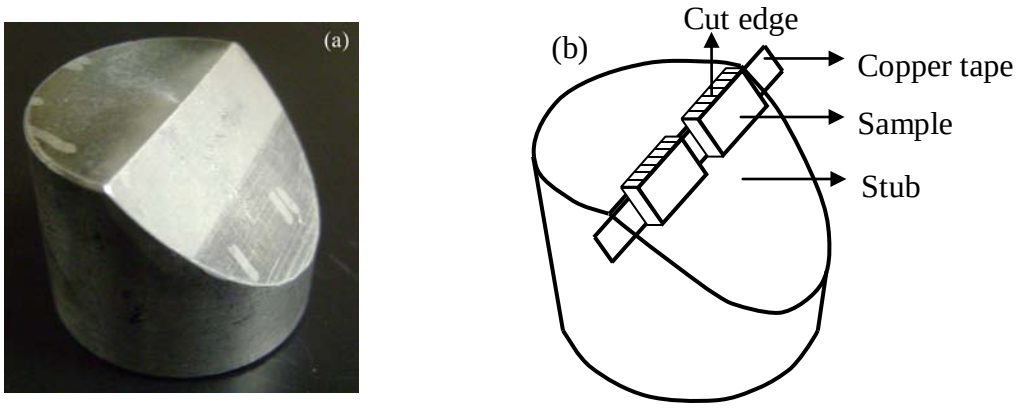


**Figure 4.5:** (a) Inclined stub used for measuring thickness of web (b) Schematic image of sample mounted on the stub

### *4.5.4 Crystallinity and structure from X-ray diffraction:*

X-ray diffraction analysis was conducted to investigate internal molecular structure and crystallinity of polymeric fibers. Cu Kα radiation from Omni Scientific Instruments, Inc. of Biloxi was used to perform X-ray diffraction measurements. Reflection scans were collected for $2\theta$ diffraction angles varying from $5^0$ to $49.9^0$ in steps of $0.1^0$, with a count time of 5 seconds. These reflection spectra are generated from the crystal dimensions. Transmission patterns were collected from the samples that were mounted horizontally at a distance of 7.5cm to the Polaroid Type 57 film. These patterns give details about the orientation of crystals.

## 4.6 Tensile tests

### *4.6.1 Web tensile testing*

#### 4.6.1.1 Sample preparation

Nanofiber webs were kept in a desiccator after they were produced. These webs were taken, marked for the required width and the 35mm length, and then cut with a razor blade. These samples, which had aluminum foil at the back that helped them avoid prestretching and mishandling, were weighed on a sensitive balance. The samples were fixed to a cardboard frame, shown in Figure 4.6, which had double sided tape above and below the window. The window had dimensions of 15mm length and 25mm width. After carefully attaching the sample to the frame, aluminum foil was removed, weighed and this value was subtracted from the initial weight to get the sample weight. The latter was used to determine the areal density. Another frame was then attached to the back side of the sample to sandwich the sample. The specimen so prepared was taken for the tensile testing on an Instron tester.

**Figure 4.6:** Image of a cardboard frame used in tensile testing

4.6.1.2 Testing:

Instron 5544 machine was used for tensile testing of the unoriented web samples using a 100N load cell. Crosshead speed used was 10mm/min. A sample prepared as described earlier was aligned and mounted in the upper clamp, the gauge length adjusted to 15mm, then the other end of the sample was mounted in the lower clamp. The edges of the frame were cut with a pair of sharp scissors. The load was set to zero. Then the machine was started and the sample stretched at the rate of 10mm/min until the sample ruptured. The load-elongation data was stored digitally.

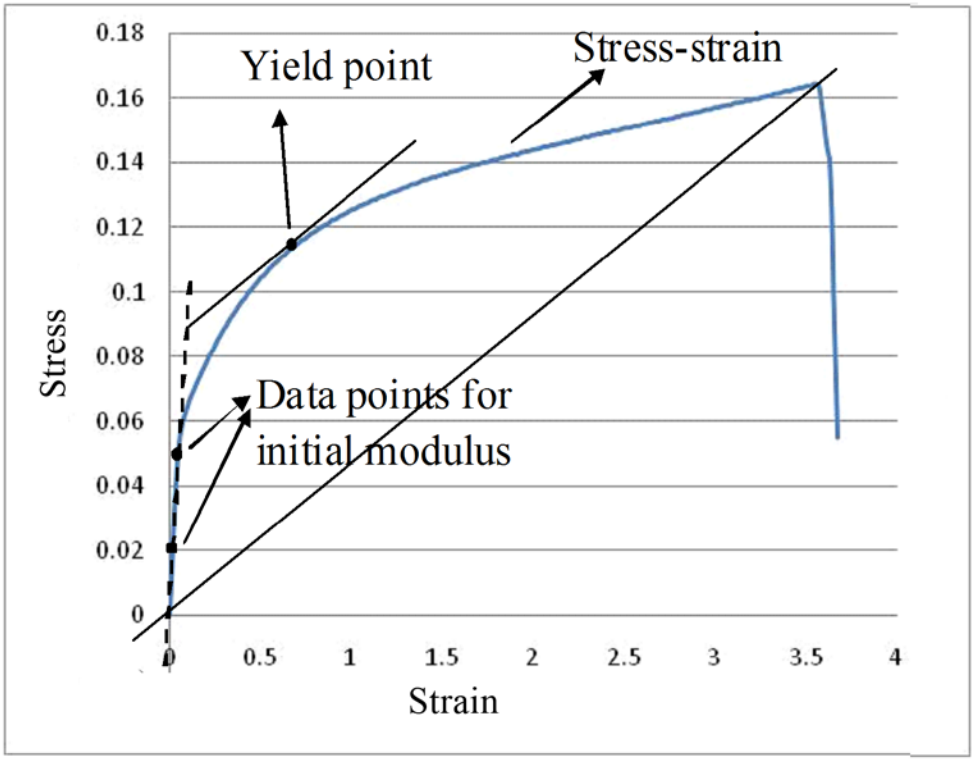


**Figure 4.7:** Schematic diagram of initial modulus and yield points from a stress-strain curve

From the data stress-strain curve, peak stress, strain corresponding the peak stress, initial modulus and yield point were obtained. Initial modulus is the slope of stress-strain curve of a specimen at the origin (Figure 4.7). This was calculated from the data points of curve at the initial stage. Yield point is the point at which tangent to the stress-strain curve is parallel to the line joining the origin and the peak point. A line tangent to the stress-strain curve and parallel to the line joining origin and peak point was drawn. Coordinates of yield point, the data point at which tangent line was touching the curve, was obtained.

### *4.6.2 Tensile testing of aligned fiber bundles:*

Aligned fibers produced as explained in the Section 4.4.5 were collected on cardboard frames. MTS Q-test 5 machine with 50gm load cell was used for testing. Gauge length was set at 15mm and cross-head speed used was 10mm/min. The frame with fibers in it was mounted in the clamps, edges were cut with a pair of scissors and then the test started. The data of load-elongation recorded digitally was evaluated for the tensile properties as done for the web above.

# 5. RESULTS & DISCUSSION

## 5.1 Introduction

A number of experiments were conducted to understand the effect of process parameters on the properties of electrospun materials. PEO polymer was chosen for this study because it could be electrospun in a wide range of diameters and because it required simple solvent, i.e., deionized water. Primary objective of this research was to characterize and model the tensile properties of electrospun webs. Little has been published in the literature on these properties and this study is an attempt to fill a part of the gap. The major variables of the study that we thought would affect the mechanical properties are polymer concentration, which would affect the diameter of the fiber, and the width of the test sample. Because the web is assumed to have randomly oriented fibers, one would expect that width of sample used in tensile test would govern the number of fibers gripped at both ends; this should directly affect the strength. The effects of these variables were examined on the peak stress, the strain corresponding the peak stress, the modulus, the yield stress and the yield strain values of the web.

The goal in this study was not only to find the effect of these parameters but also to model and predict the tensile properties of the electrospun webs. For this an effective modeling of the structure in terms of the number of fibers gripped in jaws and contributing directly to the strength was essential. The structure of the web was modeled that facilitated the calculation and understanding of the tensile properties. Prediction of the mechanical

properties of a web also required the stress-strain properties of the fibers making up the web. But these fibers are nano-dimensional, not viewable with naked eye and are delicate to handle. The single fiber properties were, therefore, needed to be deduced from the tests on oriented bundles. The latter were produced, as mentioned in Section 4.3.2, by collecting fibers on parallel strips separated with a gap.

To be able to use the properties measured on single fibers for prediction of the properties of web, it was thought that the fibers in the oriented bundle should have the same diameter as that of the fibers in the random web. This required a mini experiment to be conducted in which, for each of the concentrations of the polymer solution used, the flight time, i.e. the distance between needle tip and collector, was varied and its effect on fiber diameter determined. The distance that provided the same diameter as the fiber in the web was identified. The effects of the two variables, i.e. the concentration and the distance between needle and collector, on the tensile properties of the single fiber were also evaluated.

The properties of single fiber obtained were plugged in the model for the web and properties of web were predicted. Predicted and measured values are compared.

The above gives an overall introduction to the experiments conducted. The sequence in which the results would be discussed is as follows:

1. The effect of the concentration of the polymer in solution on the fiber diameter and areal density.

2. The effects of the polymer concentration and the sample width on the web tensile properties.

3. The results obtained from the tests on single fiber bundles; i.e. the effect of concentration and collection distance on fiber diameter and fiber tensile properties.

4. Comparison of the tensile properties of the web predicted by the model with the properties measured experimentally.

## 5.2 Web dimensional properties

### *5.2.1 Diameter of fibers*

Three concentrations of PEO polymer were used to obtain fibers of different diameters in electrospun web. In order to get stable Taylor cone and uniform fibers, it was necessary to adjust the voltage and distance between the needle and collector plate. The webs obtained were subjected to SEM analysis for fiber diameter and orientation distribution. The values of fiber diameter were obtained from image analysis of SEM micrographs. Examples of webs obtained from different concentrations are shown in Figure 5.1. The results related to fiber diameters and standard deviations associated with them are given in Table 5.1.

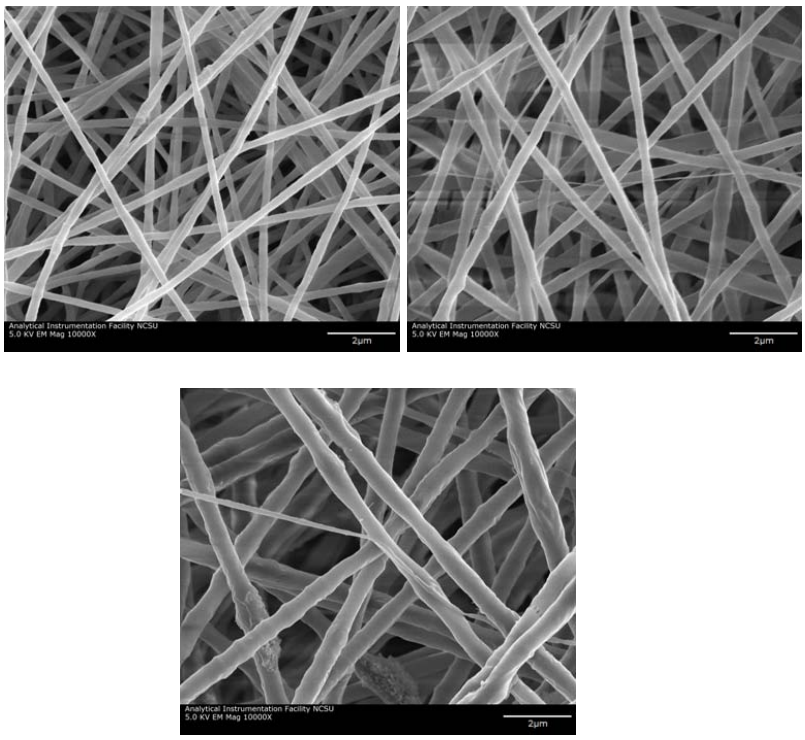


**Figure 5.1:** 8% PEO, 10% PEO and 12.5% PEO SEM images at 10000X.

**Table 5.1:** Fiber diameters obtained with the required voltage and distances for 3 polymer concentrations

| % Concentration | Diameter (nm) | Voltage (KV) | Distance (cm) |
|---|---|---|---|
| 8 | 210±24.5 | 9.5 | 15 |
| 10 | 325±37.4 | 11.5 | 15 |
| 12.5 | 550±44.4 | 17 | 18 |

The histograms given in Figure 5.2 show the distribution of fiber diameters, which reflect approximately normal distribution. The diameters lying in the range 200-600nm indicate that the system used produced fibers in the nano range, required for many important applications,

including tissue engineering. The standard deviation being low, indicate high reproducibility of results. Results in Table 5.1 and Figure 5.1 and Figure 5.3 show that with increase in concentration fiber diameter increased. The change in diameter is not linear, and this is because of a complex inter-relationship that exists between concentration, distance and voltage.

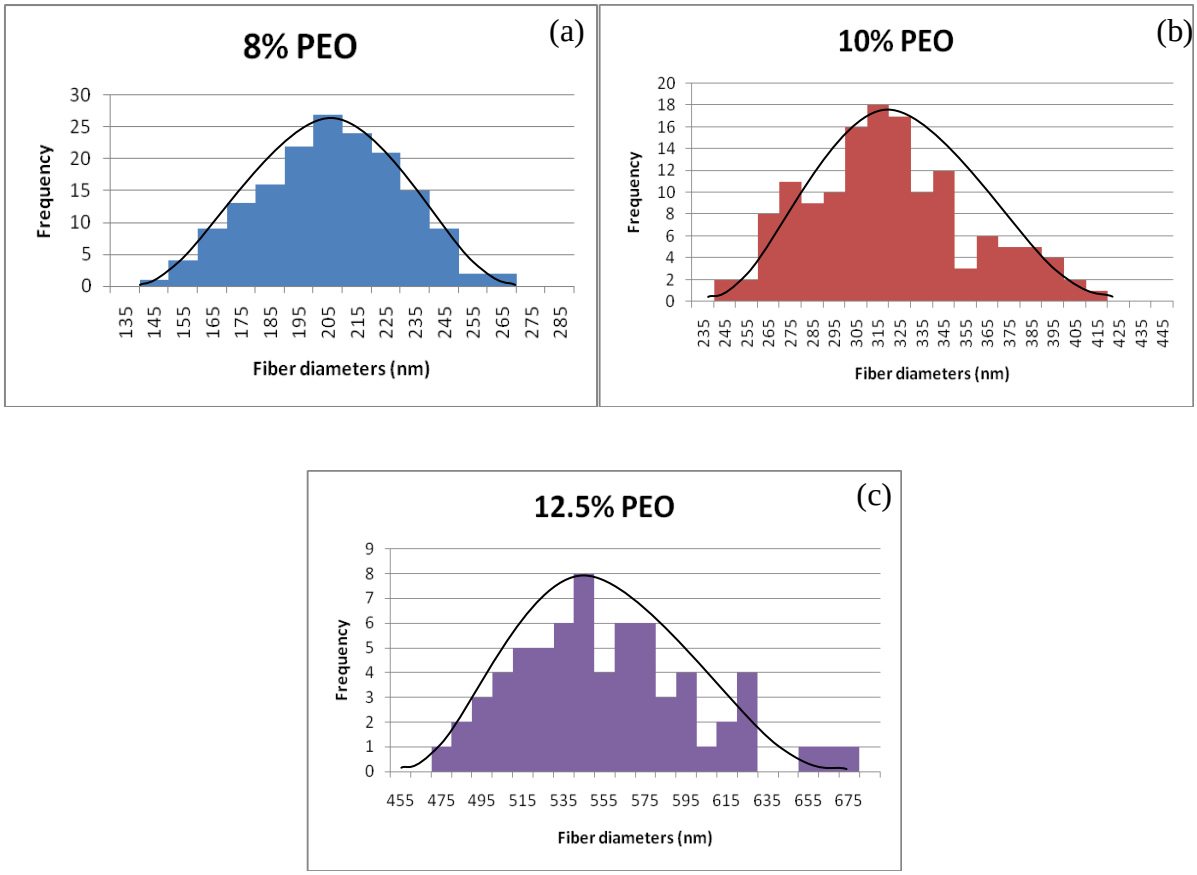


**Figure 5.2:** Histograms of fiber diameter distribution for (a) 8% PEO, (b) 10% PEO and (c) 12.5% PEO

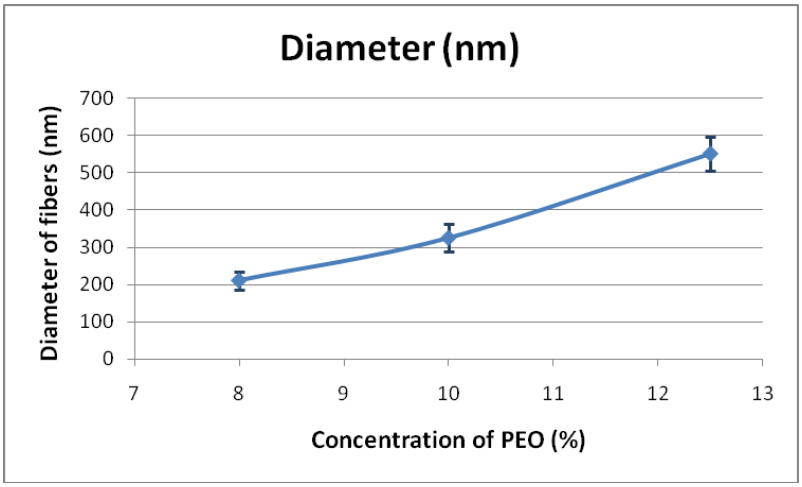


**Figure 5.3:** Graph between fiber diameter and polymer concentration

With an increase in the concentration of polymer in solution, the number of entanglements between the polymer chains increases. This causes an increase in viscosity. As discussed in the experimental Section 4.4.1, when the concentration or viscosity is increased, voltage also must be increased to get a stable Taylor cone. The increase in concentration led to an increase in diameter which to some extent is due to increase in voltage. Assuming the distance between the needle tip and collector plate to be the same, an increase in voltage could be expected to lead to an increase in acceleration and decrease in flight time. This would result in a decrease in stretching of extruded polymer and increase in fiber diameter. It is noted that the increase in voltage for change in concentration from 10% to 12.5% PEO is 5.5KV; this is more than twice the increase in voltage when the concentration increased from 8% to 10% PEO. This explains why the diameter obtained at 12.5% concentration is greater

than one would expect if the effect of voltage was negligible and that of concentration was linear.

Regression analysis (Quadratic regression) was also conducted to develop a predictive model for fiber diameter. The terms included were concentration, concentration$^2$. The output of analysis (Table 5.2) shows that first degree of concentration is the only significant term in predicting peak stress.

**Table 5.2:** Statistical model to predict the fiber diameter

| Parameter | Estimate | Standard error | t- value | Pr > F |
|---|---|---|---|---|
| Intercept | 344.3254890 | 73.93818826 | 4.66 | <.0001 |
| Conc | -75.6431976 | 14.97586576 | -5.05 | <.0001 |
| Conc$^2$ | 7.3718897 | 0.73966670 | 9.97 | <.0001 |

Equation to predict the fiber diameter from concentration of polymer with the $R^2$ value 0.93 is given below.

Fiber diameter = 344.33 - 75.64*Conc+7.37*Conc$^2$

### *5.2.2 Thickness and areal density of the web*

The thickness of the web is required as an input parameter in the model to calculate the number of layers which the web is made up of. It was expected that with change in the concentration of polymer, the thickness and areal density of the web will also change.

Thickness was assessed from the SEM analysis of the cross-sections of the webs as explained in Section 4.5.3. An example of SEM image of a cross-sectioned web is given in Figure 5.4.

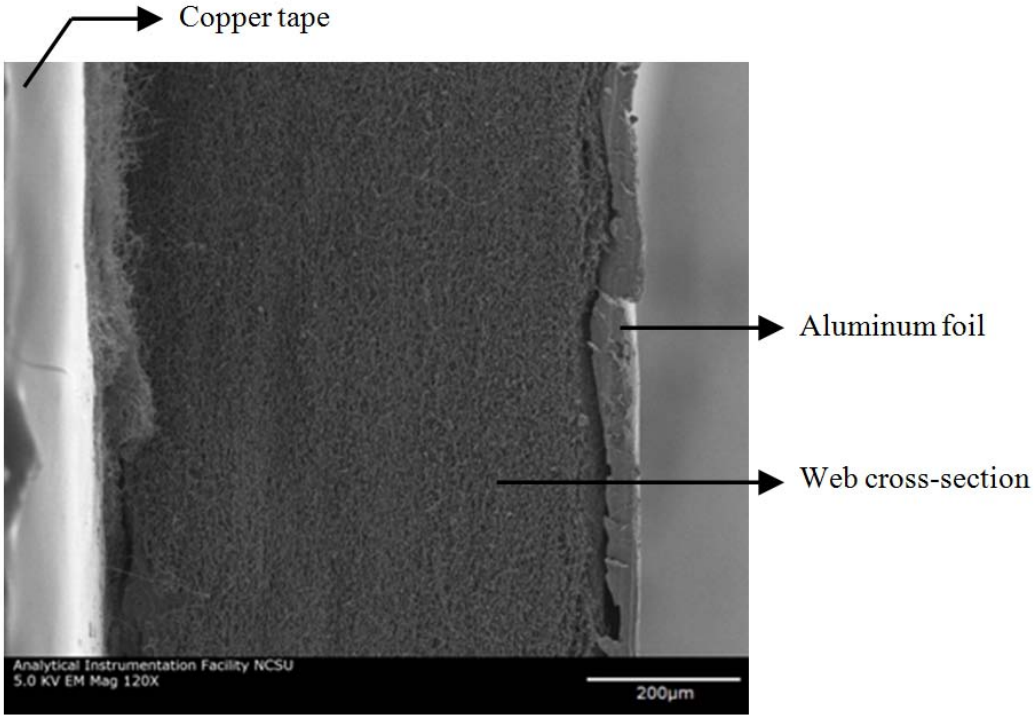


**Figure 5.4:** SEM image of web cross-section acquired to measure the thickness of web

The values of areal density and thickness are plotted against polymer concentration in Figure 5.5. The results show that web thickness and areal density increased with increase in polymer concentration. The change is non-linear which is due to the reasons given earlier (Section 5.2.1). The changes in web thickness and areal density are proportional to each other.

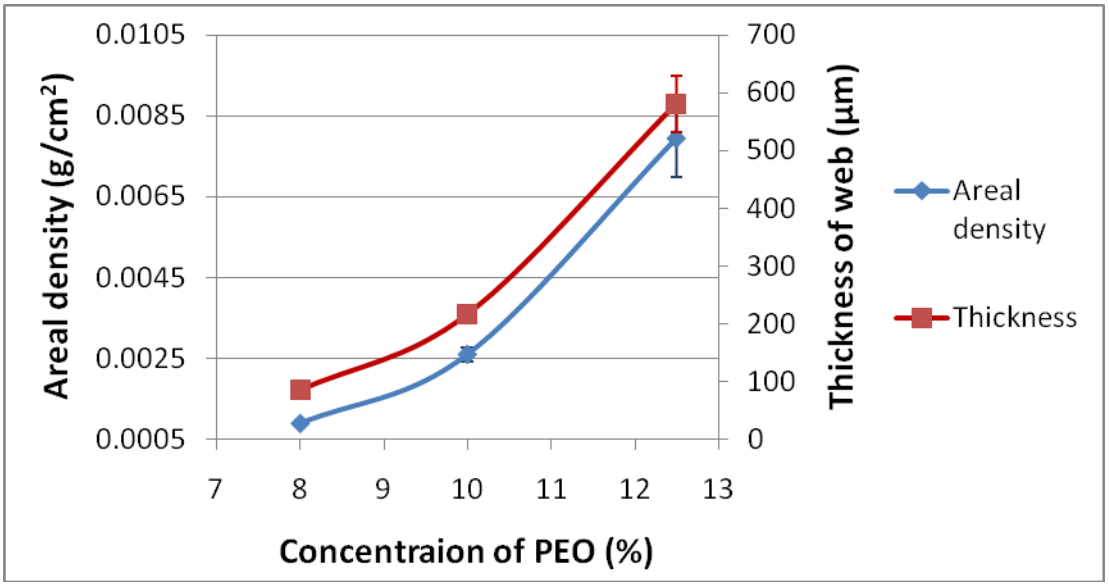


**Figure 5.5:** Plot showing change in areal density and thickness with polymer concentration

With an increase in polymer concentration fiber diameter increases as explained in the previous Section 5.2.1. As the concentration of polymer increases, greater mass of polymer deposits on the collector in a given time and leads to an increase in the areal density of web. With the increase in concentration, jet instability decreases while it is travelling towards the collector and results in the decrease of area of spread of fibers. The web collected in the smaller area also causes an increase in the web areal density as well as the thickness. This explains a non-linear change in thickness and areal density with increase in polymer concentration.

## 5.3 Web mechanical properties

### *5.3.1 Peak stress*

Peak loads of web specimens were obtained from the digital data collected on the Instron machine. Peak stress, given by the ratio of the peak load to the linear density, was used to compare the strength properties of the samples. Averages and standard deviations based on values of tests on 12 different specimens for each set of conditions, the latter involving three different concentrations and three test widths are given in Table 5.3. The results in the table as well as those plotted in Figure 5.6 show that peak stress decreases with increase in concentration. The change is non-linear, i.e. the decrease in peak stress is relatively greater when concentration increases from 10 to 12.5% than when it increases from 8 to 10%.

**Table 5.3:** Averages and standard deviations of 12 specimen's peak stresses for 9 different samples.

| Width (cm) | Peak Stress (cN/Den) | | |
|---|---|---|---|
| | 8% PEO | 10% PEO | 12.5% PEO |
| 1 | 0.144±0.015 | 0.135±0.021 | 0.123±0.012 |
| 1.5 | 0.141±0.023 | 0.142±0.025 | 0.122±0.011 |
| 2 | 0.142±0.020 | 0.133±0.017 | 0.112±0.008 |

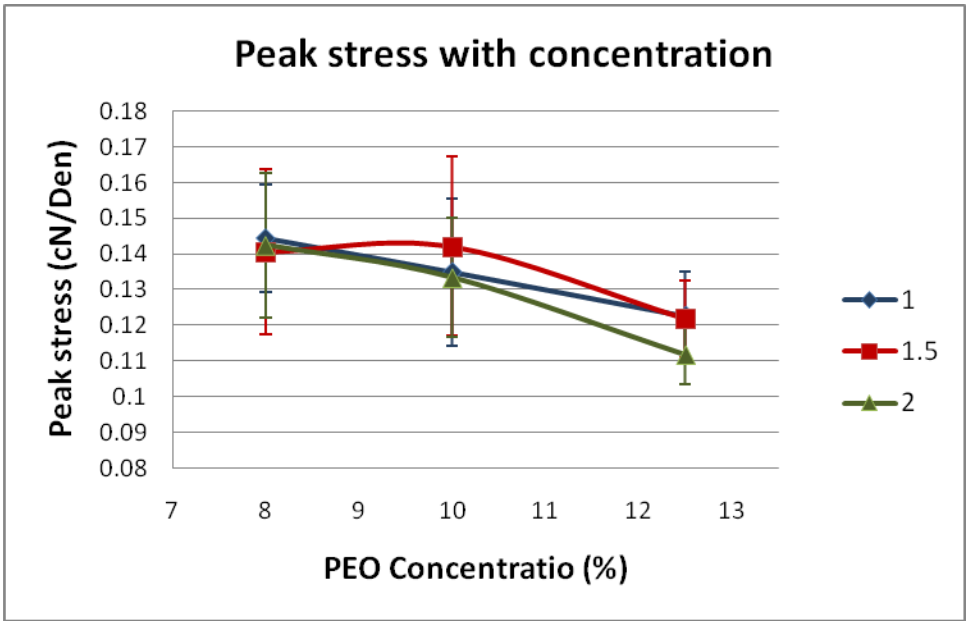


**Figure 5.6:** Plot between peak stress and polymer concentration.

To erupt a polymer jet from the needle, the voltage has to be increased when the concentration is increased. The increased voltage makes the jet accelerate faster and deposit on collector in shorter time. A reduction in flight time impairs the ability of the polymer jet to stretch and orient. A decrease in molecular orientation, expected with increase in polymer concentration could cause a reduction in the strength of the material.

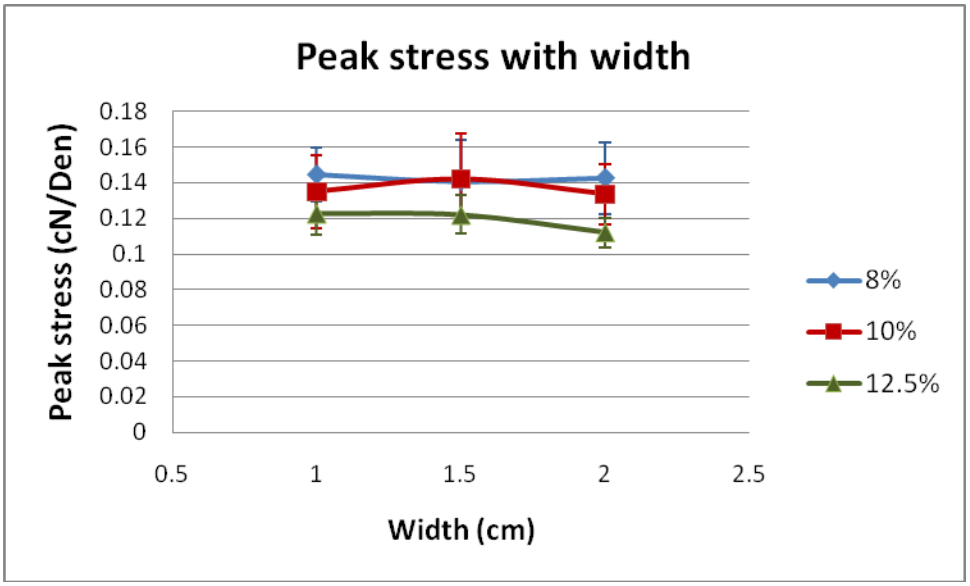


**Figure 5.7:** Graph between peak stress and width of test sample

The graph (Figure 5.7) plotted between the peak stress and the width of sample show that width has little or no effect on the peak stress. An increase in width of sample increases the number of fibers contributing to the strength as well as the linear density of the sample. Accordingly, no effect of the width on peak stress of a fabric strip could be expected.

While stretching of web during tensile test, necking at the center of web was observed as shown in Figure 5.8. This type of behavior is common in regular fabrics, in which width has no effect on the fabric stress. Thus the effect of width on peak stress of sample is not expected to be significant.

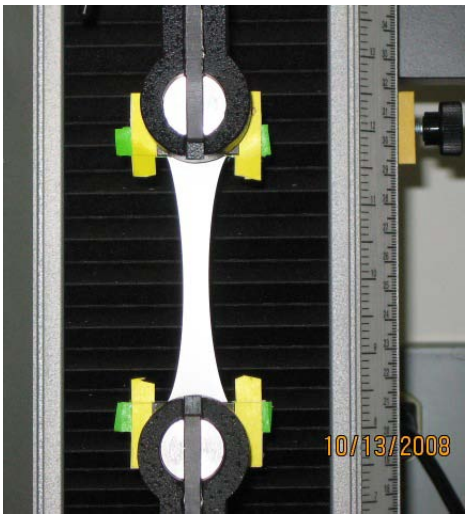


**Figure 5.8:** Necking of web while conducting tensile test

Statistical analysis of variance was conducted using SAS® to confirm the effects of concentration and sample width on peak stress. The results are shown in the Table 5.4, which show that only concentration had a significant effect.

**Table 5.4:** ANOVA table to find the effect of concentration and width on peak stress

| Parameter | F- value | Pr > F |
|---|---|---|
| Concentration | 17.71 | <.0001 |
| Width | 1.06 | 0.3486 |

Regression analysis (Quadratic regression) was also conducted to develop a predictive model for web peak stress. The terms included were concentration, concentration$^2$, web width and concentration*web width. The output of analysis (Table 5.5) shows that first degree of concentration is the only significant term in predicting peak stress.

**Table 5.5:** Statistical model to predict the peak stress

| Parameter | Estimate | Standard error | t- value | Pr > F |
|---|---|---|---|---|
| Intercept | 0.18696996 | 0.0095546 | 19.57 | <.0001 |
| Concentration | -0.0053388 | 0.00092476 | -5.77 | <.0001 |

Equation to predict the peak stress from concentration of polymer with the $R^2$ value 0.24 is given below.

Peak stress = 0.1869 - 0.0053*Concentration

### *5.3.2 Strain corresponding the peak stress*

Strain at peak stress gives the details of material's stretchability before its failure, which is an important mechanical property of a material. Average values of strain and corresponding values of standard deviation are given in Table 5.6 for the nine samples. The results plotted in Figure 5.9 show that strain increases with increase in concentration.

**Table 5.6:** Values of strain corresponding peak stress

| Width (cm) | Strain corresponding to Peak stress | | |
|---|---|---|---|
| | 8% PEO | 10% PEO | 12.5% PEO |
| 1 | 3.66±0.88 | 4.36±0.86 | 4.95±1.28 |
| 1.5 | 3.62±0.96 | 5.00±0.78 | 5.64±1.69 |
| 2 | 3.70±0.54 | 4.88±1.08 | 4.39±1.00 |

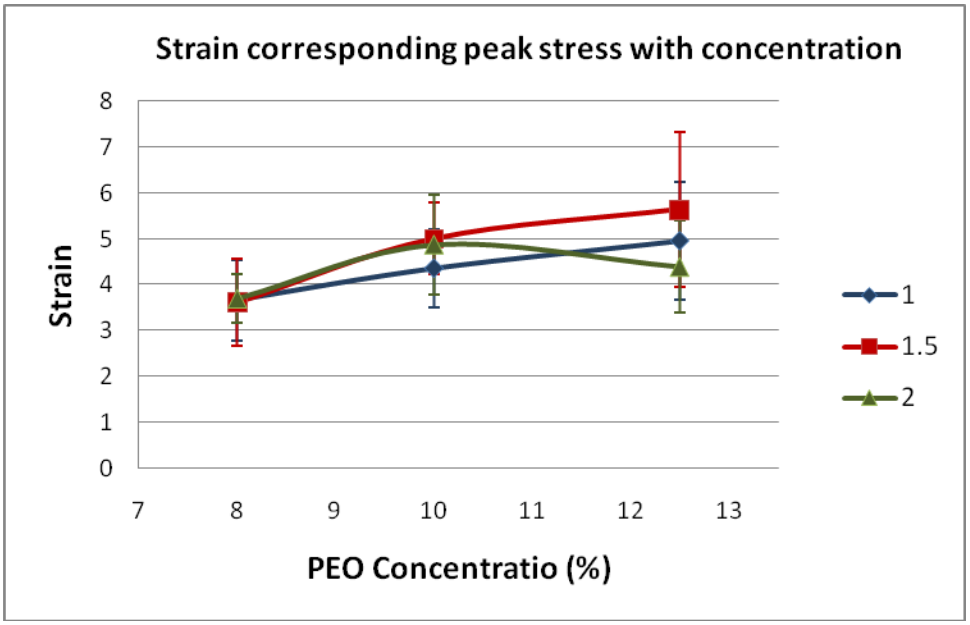


**Figure 5.9:** Graph between strain corresponding peak stress and polymer concentration

For a given fiber material, the factors that lead to an increase in peak stress also lead to a decrease in peak strain. Accordingly, peak strain increased on account of an increase in disorientation of molecular chains with increase in polymer concentration.

As noted earlier on the effect of test width on peak stress, the effect of test width on peak strain is little or none (Figure 5.10).

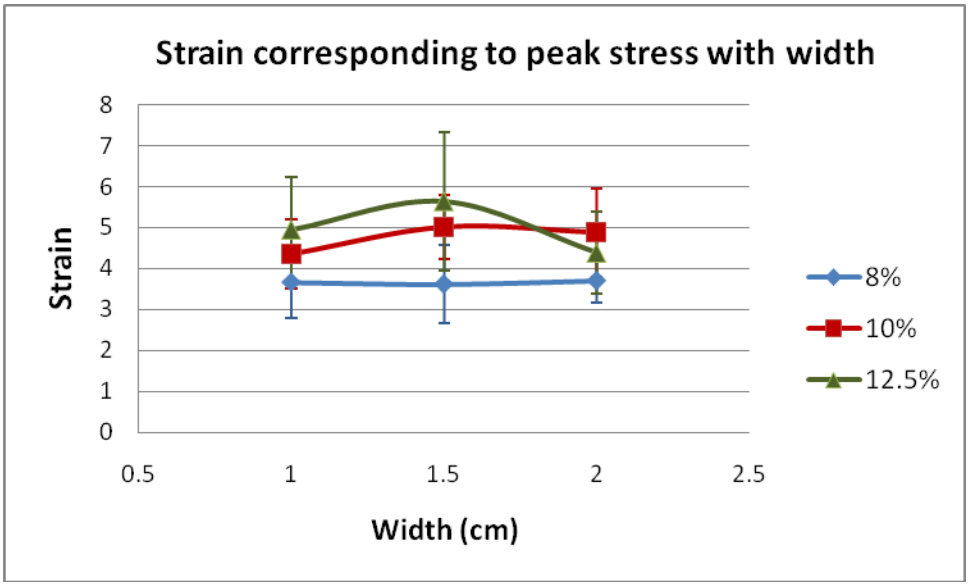


**Figure 5.10:** Plot between the strain and test width of specimen

The effect of concentration and test specimen width on peak strain discussed above are confirmed from the results of the statistical analysis (ANOVA) given in the Table 5.7:.

**Table 5.7:** ANOVA output for the strain corresponding peak stress

| Parameter | F- value | Pr > F |
|---|---|---|
| Concentration | 15.81 | <.0001 |
| width | 1.95 | 0.147 |

### *5.3.3 Initial modulus*

Initial modulus is the slope of stress-strain curve at the origin and is a measure of resistance to extension at small deformations. It is reciprocal of compliance, which is

considered an important characteristic for biomaterial prostheses. Average values of initial modulus of twelve specimens for each concentration and test width are listed in Table 5.8 along with the values of standard deviation. The results plotted in Figure 5.11 show that initial modulus value decreases with increase in concentration of polymer. Test width again has no effect.

**Table 5.8:** Values of initial modulus for 9 samples

| Width (cm) | Modulus (cN/Den) | | |
|---|---|---|---|
| | 8% PEO | 10% PEO | 12.5% PEO |
| 1 | 0.848±0.056 | 0.648±0.055 | 0.592±0.072 |
| 1.5 | 0.850±0.047 | 0.660±0.047 | 0.578±0.040 |
| 2 | 0.848±0.058 | 0.654±0.051 | 0.536±0.064 |

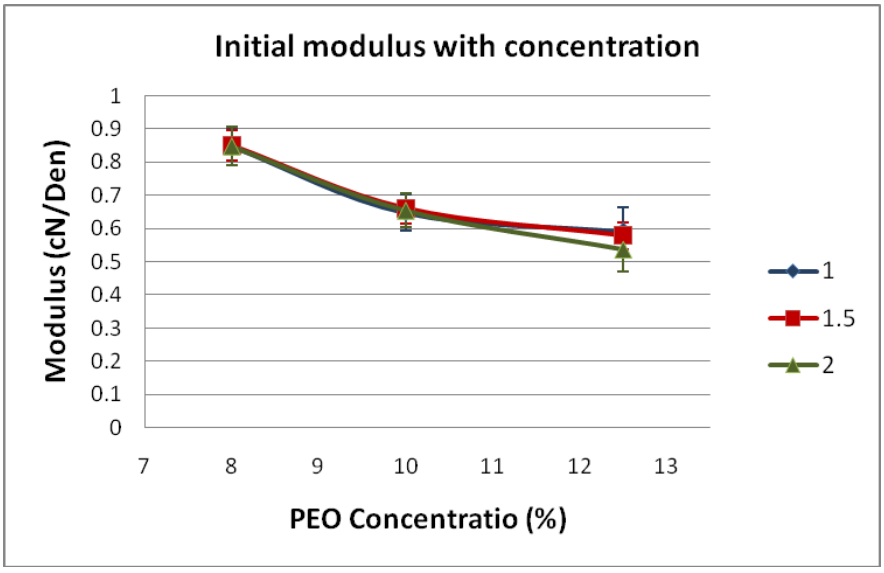


**Figure 5.11:** Plot of initial modulus against polymer concentration for three test widths.

The decrease in initial modulus is expected to be due to an increase in the disorientation of molecules with increase in concentration.

Statistical analysis conducted on the data (Table 5.9) confirm the above results.

**Table 5.9:** ANOVA output for initial modulus

| Parameter | F- value | Pr > F |
|---|---|---|
| conc | 240.83 | <.0001 |
| width | 1.08 | 0.3434 |

Regression analysis was conducted to develop a predictive model for initial modulus. Results are given in Table 5.10.

**Table 5.10:** Regression analysis for initial modulus of electrospun web

| Parameter | Estimate | Standard error | t- value | Pr > F |
|---|---|---|---|---|
| Intercept | 2.7501436 | 0.23482149 | 11.71 | <.0001 |
| Conc | -0.3499248 | 0.04685582 | -7.47 | <.0001 |
| $Conc^2$ | 0.01403331 | 0.00227217 | 6.18 | <.0001 |

The best fit model found with the $R^2$ value of 0.82 is as follows:

$$Modulus = 2.75 - 0.35*Conc + 0.014*Conc^2$$

### *5.3.4 Yield point*

Yield point is the point at which a tangent to the curve is parallel to the line joining the origin and the breaking point (Morton & Hearle). The material usually behaves elastic up to the yield point, and then starts to experience permanent deformation once past this point. The values of yield stress and yield strain were obtained. The averages along with the standard deviation values for the nine conditions are given in Table 5.11.

**Table 5.11:** Values of yield stress and yield strain for each of three concentrations and three widths.

| Width (cm) | Yield Stress (cN/Den) | | | Yield Strain | | |
|---|---|---|---|---|---|---|
| | 8% PEO | 10% PEO | 12.5% PEO | 8% PEO | 10% PEO | 12.5% PEO |
| 1 | 0.104±0.009 | 0.093±0.013 | 0.094±0.011 | 0.58±0.13 | 0.77±0.16 | 0.98±0.29 |
| 1.5 | 0.103±0.016 | 0.101±0.015 | 0.094±0.008 | 0.53±0.12 | 0.76±0.14 | 1.05±0.29 |
| 2 | 0.104±0.013 | 0.095±0.011 | 0.083±0.006 | 0.52±0.08 | 0.79±0.11 | 0.72±0.18 |

Although there is scatter in values, the results plotted in Figure 5.12 and Figure 5.13, show, in general, that yield stress decreases and yield strain increases with increase in concentration. These trends are as expected and support those observed for change in other tensile properties discussed earlier. The effect of test width is irregular and insignificant as seen from the plots given in Figure 5.14 and Figure 5.15.

Statistical analysis (ANOVA) was also conducted for the values of yield stress and strain. The results given in Table 5.12 show that concentration had a very strong effect and width had either non-significant or weak effect.

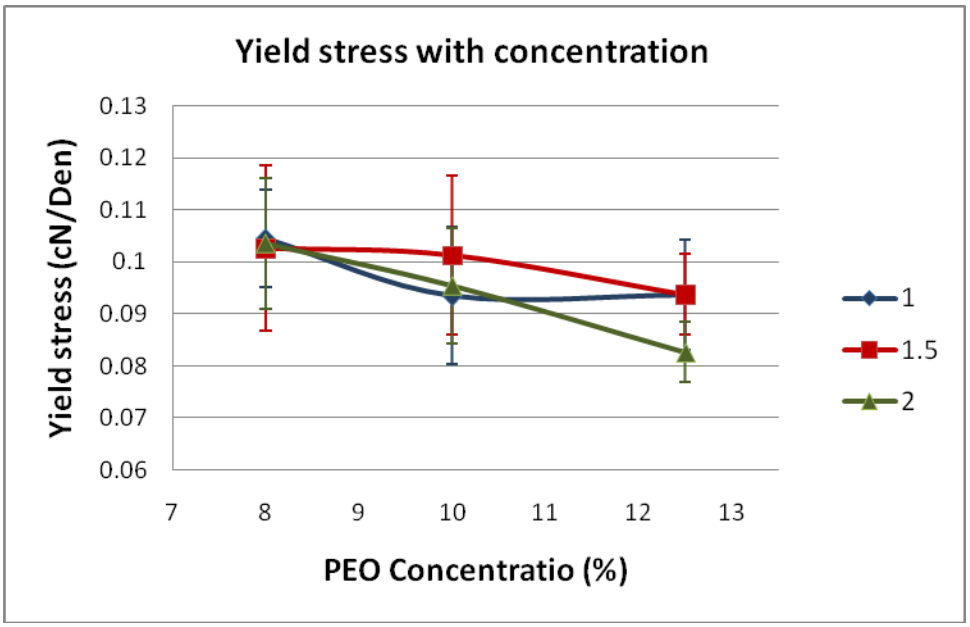


**Figure 5.12:** Graph between yield stress and polymer concentration

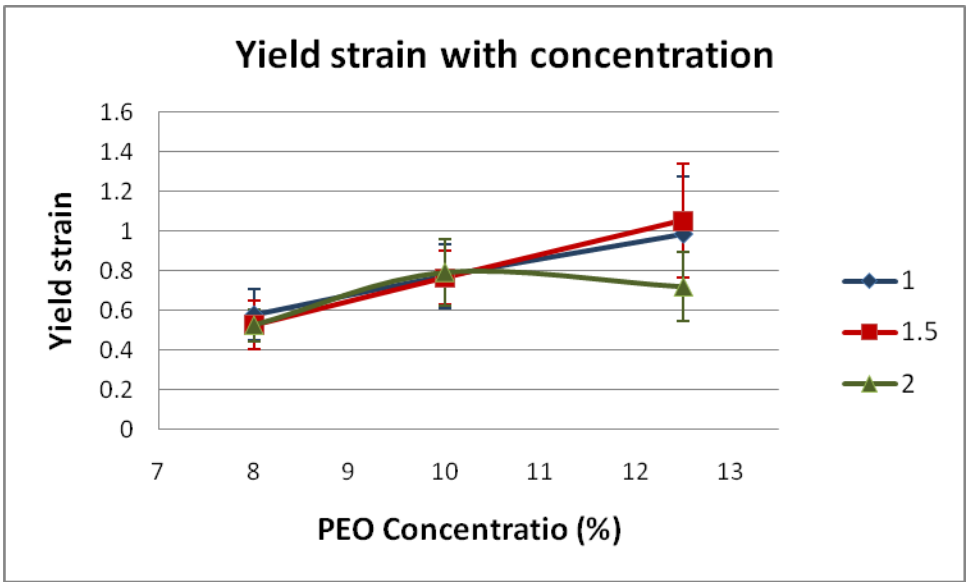


**Figure 5.13:** Graph between yield strain and polymer concentration

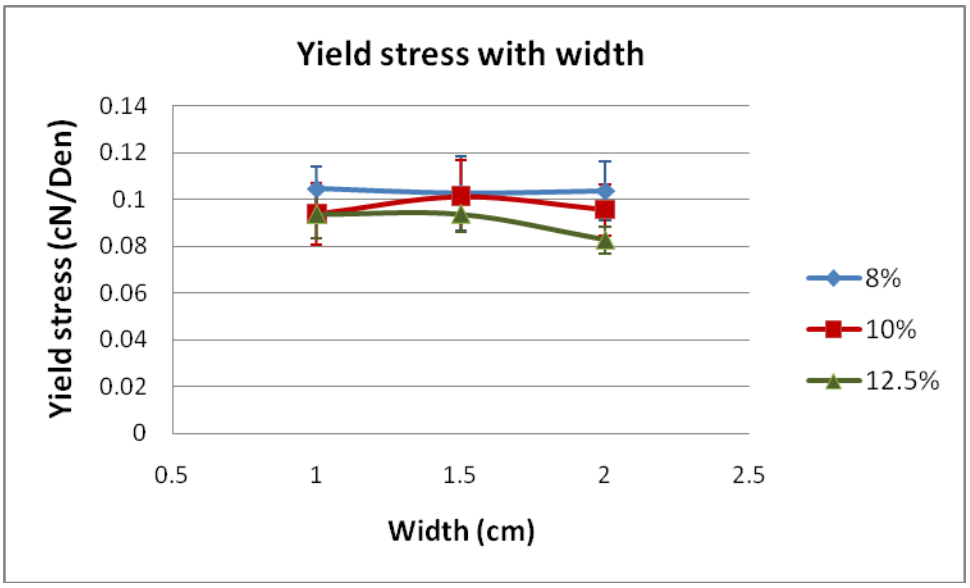


**Figure 5.14:** Graph between yield stress and test width of specimen

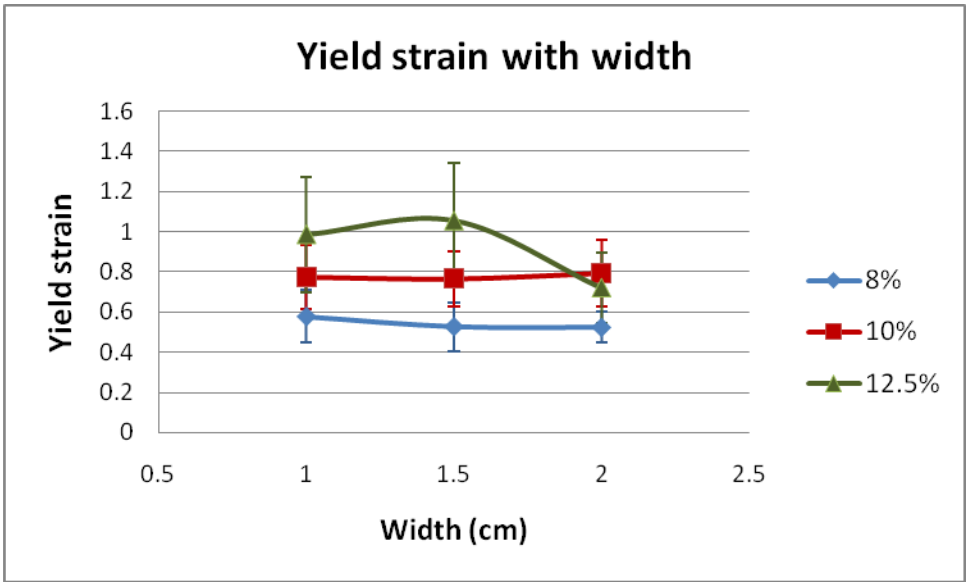


**Figure 5.15:** Graph between yield strain and test width

**Table 5.12:** ANOVA output for yield stress and strain.

| Parameter | Yield stress | | Yield strain | |
|---|---|---|---|---|
| | F- value | Pr > F | F- value | Pr > F |
| Concentration | 11.78 | <.0001 | 34.19 | <.0001 |
| width | 1.86 | 0.1607 | 3.3 | 0.0407 |

## 5.4 Single fiber properties

Using two strip collectors separated with a gap, aligned fibers were collected to study single fiber mechanical properties. In pursuit of getting aligned fibers of same diameter as that of fibers in the unoriented web, the effect of distance between collector plate and needle on fiber diameter had to be determined. From this, the distance giving roughly the required diameter was identified. This exercise was also undertaken to understand the effect of distance and polymer concentration on tensile properties of single fibers. As mentioned in Chapter 4, for each of four combinations of concentration and distance (Table 4.2), oriented bundle were collected for 25 seconds. 45 such bundles were combined together to get the required size of sample for tensile tests. After conducting tensile tests on these samples, loads were divided by the number of fibers to get single fiber properties.

### *5.4.1 Fiber diameter*

The values of fiber diameters obtained for 8% and 10% PEO concentrations and for 10cm and 15cm collection distances are given in Table 5.13. With 12.5% PEO concentration, fiber diameter of 550nm could not be achieve at different combinations of voltage and distances.

Fibers were noted to be fused at smaller distance and thinner fibers were collected at longer distance.

It is observed from the table and SEM images of fibers (Figure 5.16) that fiber diameter increased with an increase in concentration and decreased with an increase in distance.

**Table 5.13:** Values of fiber diameters obtained with parallel plate set-up.

| Type | % Concentration | Distance (cm) | Voltage (KV) | Diameter (nm) | Denier ($X10^{-6}$) |
|---|---|---|---|---|---|
| 1 | 8 | 15 | 9.5 | 150 | 179.72 |
| 2 | 8 | 10 | 9.5 | 205 | 335.67 |
| 3 | 10 | 15 | 11.5 | 258 | 531.68 |
| 4 | 10 | 10 | 11.5 | 320 | 817.92 |

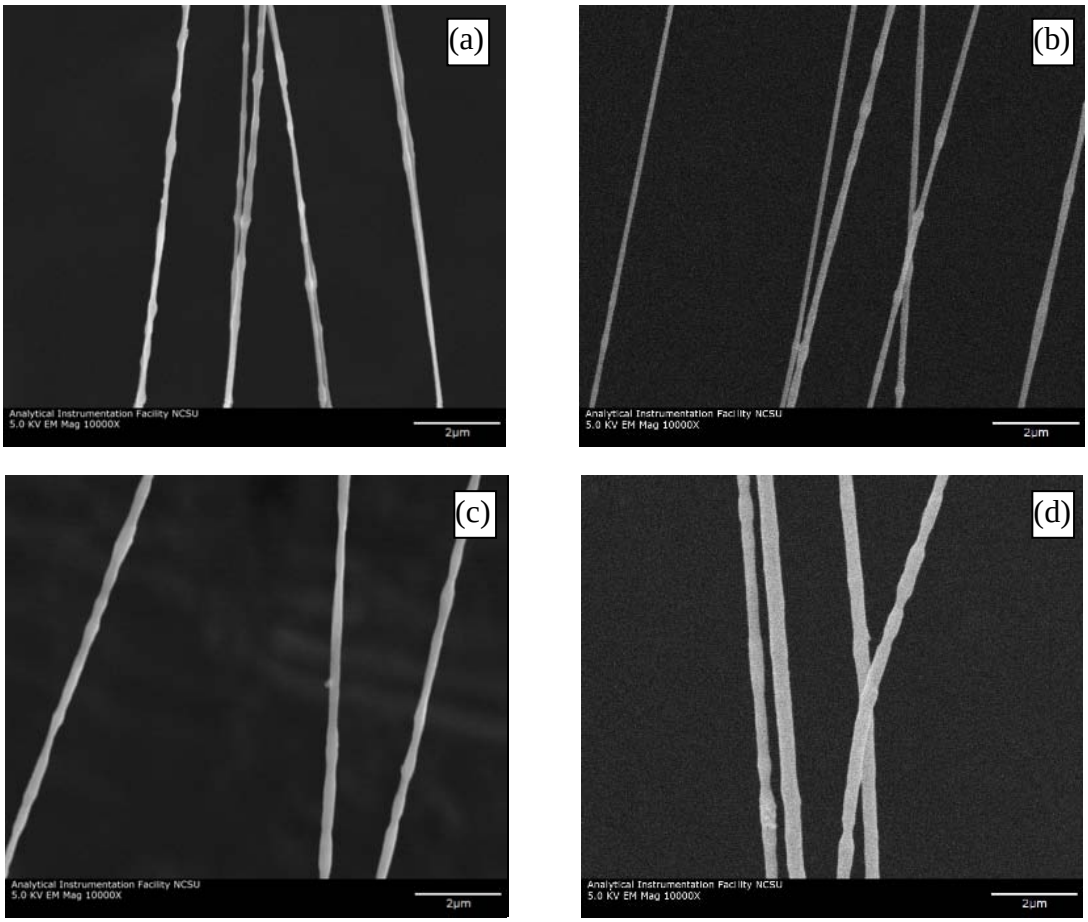


**Figure 5.16:** SEM images at 10000X of fibers produced with (a) 8% PEO and 15cm distance, (b) 8% 10cm, (c) 10% 15cm and (d) 10% 10cm

As explained earlier, when concentration is increased, the voltage also had to be increased to get a stable Taylor cone. This causes the jet to accelerate to travel faster towards the collector plate which gives less flight time for the polymer extrudate. Reduced flight time of jet gives a decrease in the draw ratio and an increase in the fiber diameter. But when the distance is increased for the same concentration and voltage, jet gets more flight time and

allows additional stretching. This explains the decrease in fiber diameter with increase in distance from 10cm to 15cm.

### *5.4.2 Effect of concentration and distance on tensile properties of single fibers*

The values of peak load, i.e. the maximum load a fiber can withstand, peak stress, strain corresponding peak stress and initial modulus of single fibers are listed in the Table 5.14. The results plotted in Figure 5.17 between peak load and concentration of polymer show that peak load increases with an increase in concentration. As explained in Section 5.2.1, concentration increase makes polymer solution more viscous, which needs more voltage to erupt a jet. Voltage increase causes increase in the fiber diameter. Thicker fibers carry more loads than thinner fibers. Because of this reason peak load of fibers increases with an increase in polymer concentration.

**Table 5.14:** Values of tensile properties for four samples

| **Concentration** | **8% PEO** | | **10% PEO** | |
|---|---|---|---|---|
| **Distance (cm)** | **15** | **10** | **15** | **10** |
| Denier ($X10^{-6}$) | 179.72 | 335.67 | 531.68 | 817.92 |
| Peak load X $10^{-5}$(gf) | 14.68±0.94 | 15.92±1.30 | 27.89±6.03 | 31.18±7.13 |
| Peak stress (gf/den) | 0.82±0.05 | 0.47±0.04 | 0.52±0.11 | 0.38±0.09 |
| Strain corresponding peak stress | 0.39±0.11 | 0.51±0.03 | 0.54±0.15 | 0.37±0.04 |
| Initial modulus (gf/den) | 7.57±1.11 | 4.59±0.56 | 5.00±0.88 | 3.57±0.57 |

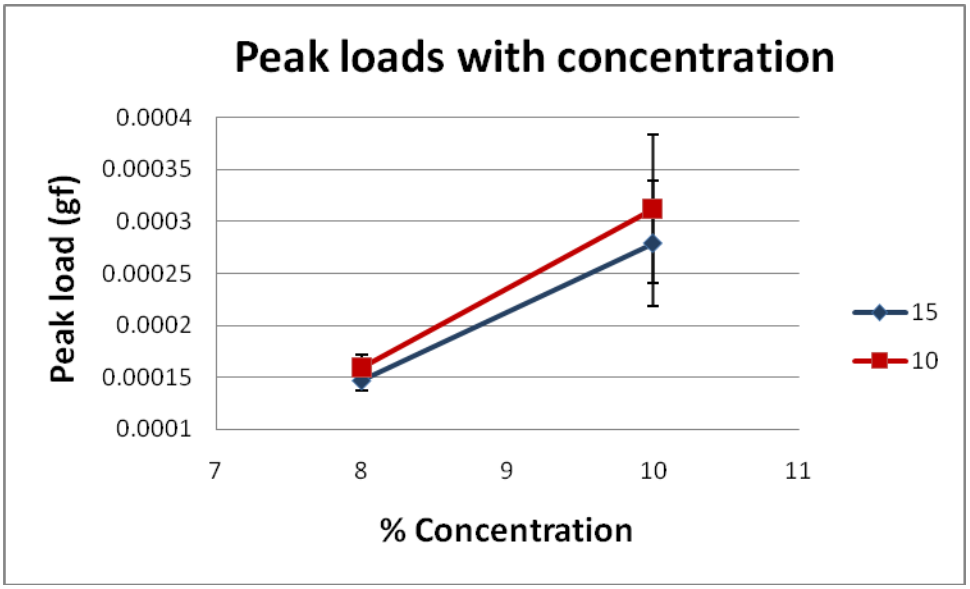


**Figure 5.17:** Plot showing the effect of polymer concentration on peak load

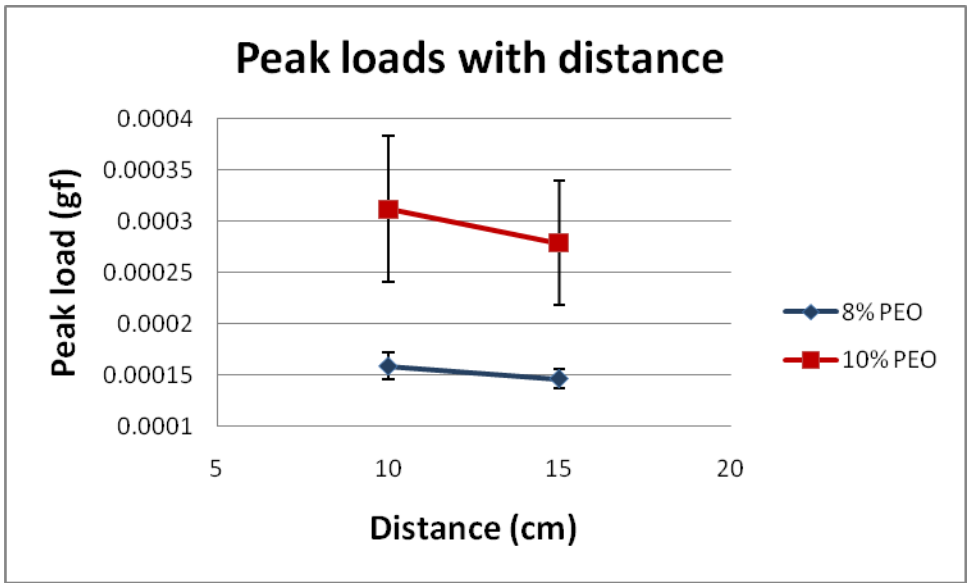


**Figure 5.18:** Plot between peak load and distance between needle and collector.

But with an increase in distance, peak loads decrease some but not much (Figure 5.18). As explained in Section 5.4.1, fiber diameter decreases with increased distance. Thinner fibers have less capability of bearing a load. Because of less fiber diameter, these fibers have lower peak load values. Fibers produced from increased flight time have more oriented polymer chains than fibers produced with 10cm distance because of increase in draw ratio. Orientation of molecules increases fiber strength. Because of these dual effects, there is a relatively small effect of distance on peak load.

Peak loads cannot be used to compare fibers of different diameters. Use of stresses, which are independent of dimensions, is an effective way to compare the material properties. Peak stress is calculated by dividing peak load with the linear density of the fiber. Observation for the effect of concentration on the fiber peak stress (Figure 5.19) reveals that peak stress decreases with an increase in concentration from 8% to 10% PEO.

With the concentration of polymer solution, voltage needs to be increased, which causes the polymer jet to accelerate faster. This accelerated speed gives less flight time for the jet and decrease in draw ratio. Less drawn fibers have more disoriented polymer chains. Disorientation of molecules decreases the fiber strength and resistance to deformation. Due to these reasons, fibers electrospun from higher concentration of polymer solution could be expected to show lower peak stress and lower initial modulus (Figure 5.20) than those spun from low concentration polymer solution. Strain corresponding peak stress is expected to increase with an increase in disorientation of chains from 8% to 10% PEO. This is observed

for the 15cm collection distance but not the 10cm collection distance (Figure 5.21). One of the reasons may be the variability in strain values which was high.

In the load-elongation curve of the aligned fibers (Figure 5.22), it can be observed that at peak load, elongation was not concentrated at single point. Over the wide range of elongation, variation in load value is very small near the peak load value. Due to this reason the peak strain value could not be precisely measured and, therefore, had greater variability.

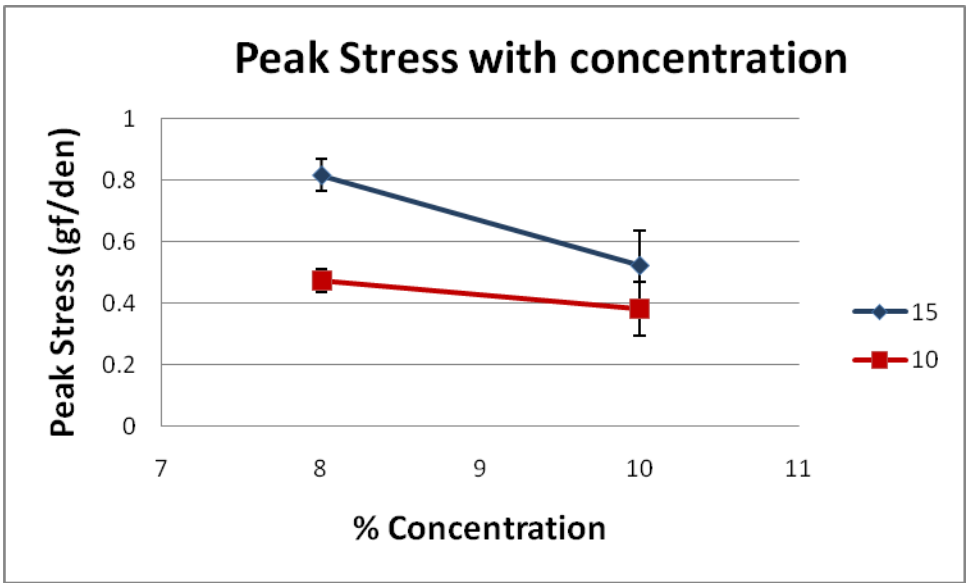


**Figure 5.19:** Peak stress vs. concentration of polymer

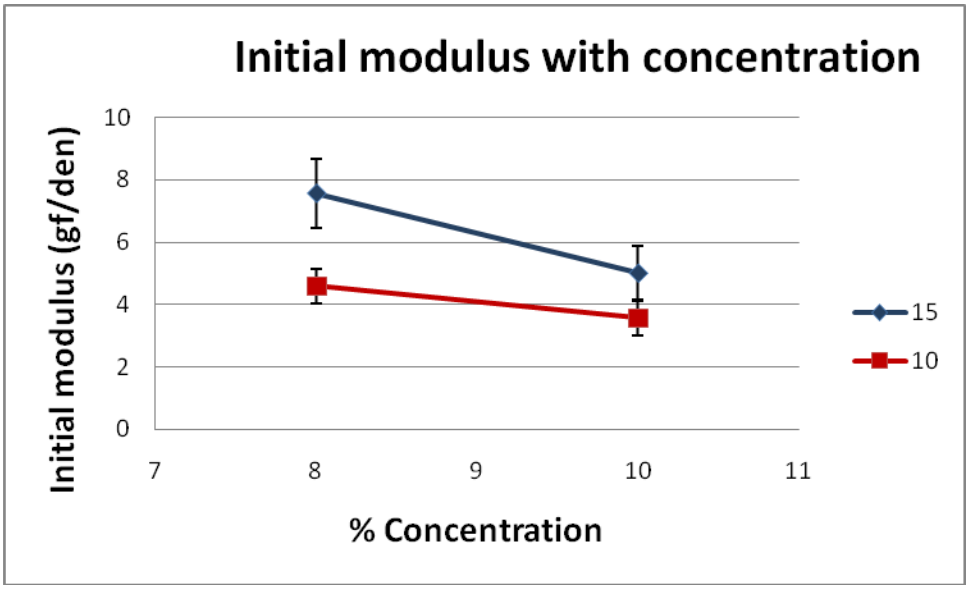


**Figure 5.20:** Initial modulus of single fiber vs. polymer concentration

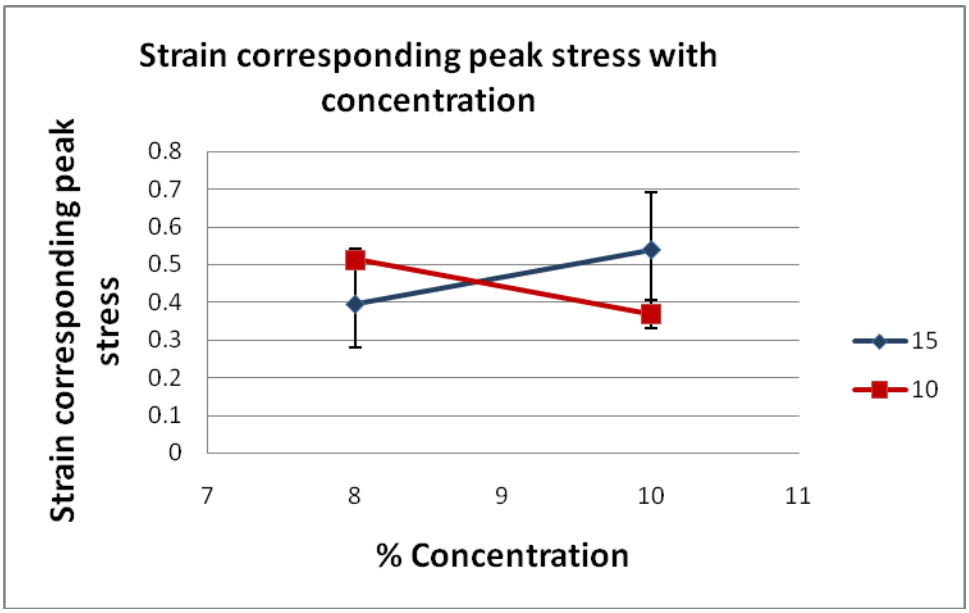


**Figure 5.21:** Plot between strain corresponding peak stress and polymer concentration

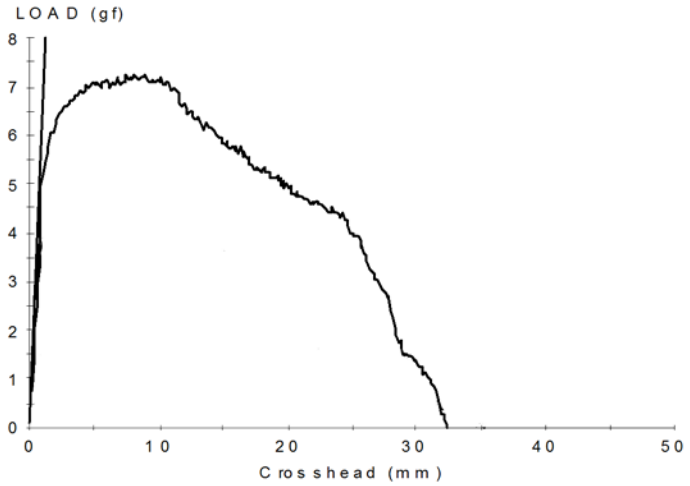


**Figure 5.22:** Load-elongation curve of bundle of aligned fibers for 10% PEO with 15 cm distance.

The results plotted (Figure 5.23) between peak stress and the distances between the needle and the collector plate show increase in peak stress with an increase in distance from 10cm to 15cm. When the distance is increased for the same concentration and voltage applied, flight time increases. Increased flight time allows the polymer jet to get higher draw ratio and improves the orientation of polymer chains. With the increased orientation of molecules, the fibers develop higher stress values. Due to this reason fibers spun with 15cm distance show higher initial modulus than 10cm distance (Figure 5.24). Increased orientation of polymer molecules expected to decrease the strain values. But in the results plotted in Figure 5.25 between spinning distance and strain corresponding peak load, relation is not definitive. This may due to the reason explained earlier in this section for the effect of concentration on strain.

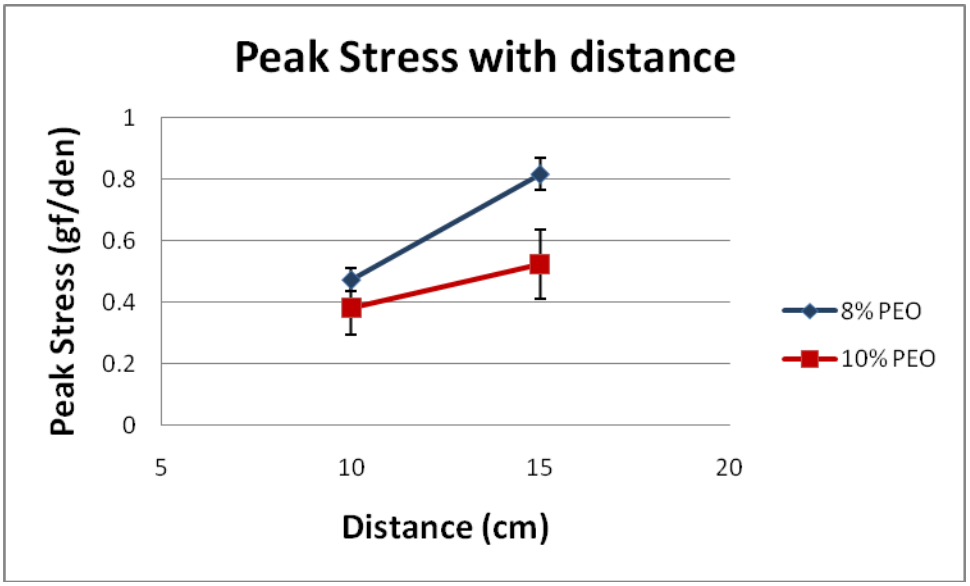


**Figure 5.23:** Plot showing the effect of spinning distance on peak stress.

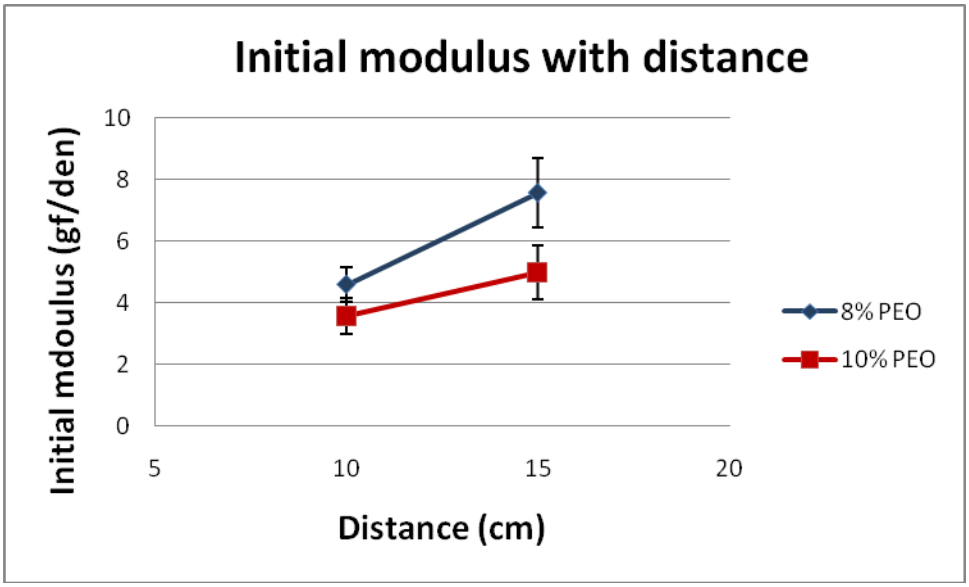


**Figure 5.24:** Plot between initial modulus of single fiber and the spinning distance

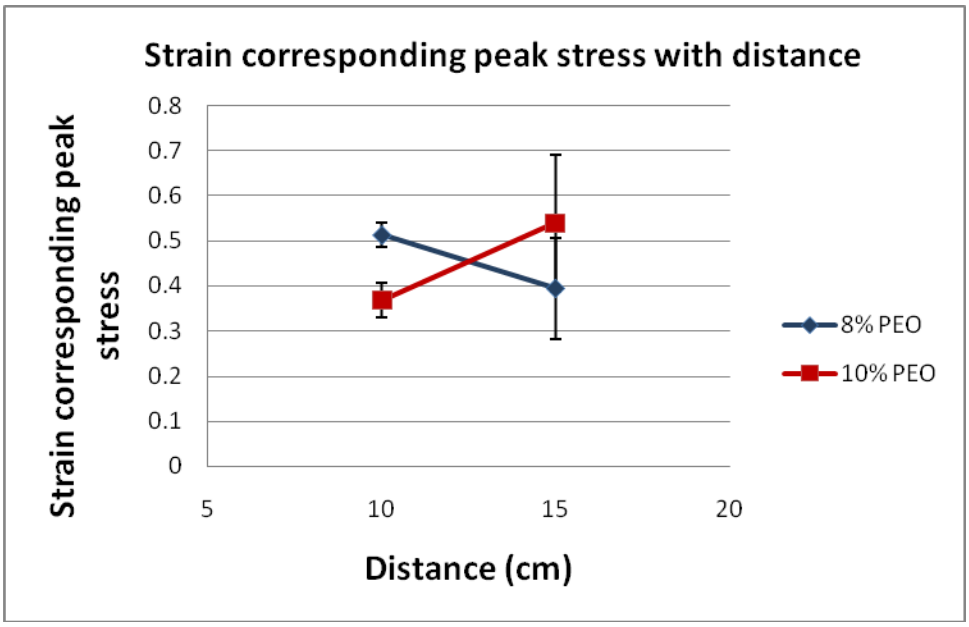


**Figure 5.25:** Plot showing the effect of distance between the needle and collector plate on strain

## 5.5 Prediction of the peak stress of the electrospun web by the structural model

Mathematical models were introduced in Chapter 3 to predict the tensile properties of electrospun web. The structural model is used to (1) calculate the number of layers in web, (2) angle subtended with the test direction and number of fibers supporting load, (3) the magnitude of the load supported, (4) the factor of this along test direction, (5) estimation of total load, and (6) determine the peak stress value. Space does not allow including full details in this section but data lending to calculations given in this section is included in Table 5.15

of the thesis. Using the "Force method", the following equations were derived to measure the peak load of electrospun web.

$$\text{Peak load of fabric} = \sum_{j=a}^{b} \frac{x\left|\sin j\gamma\right| - y\left|\cos j\gamma\right|}{S} \cdot F\left(\Delta l\right) \cdot \sin j\gamma$$

$$\text{when } \Delta l = \frac{\left[(y + \Delta l_p)^2 \sin^2\theta_j + (y - \Delta l_p \nu_{LT})^2 \cos^2\theta_j\right]^{1/2} - y}{\sin\theta_j}$$

where $x$ is sample width,

$y$ is sample length,

$S$ is spacing between fibers in a disc ,

$\gamma$ is angle interval between successive discs,

$F\left(\Delta l\right)$ is force on fiber at elongation $\Delta l$ ,

$\Delta l_p$ is elongation in fiber corresponding the peak load,

$\theta_j \left(= j\gamma\right)$ is angle of fiber orientation in a disc,

$\nu_{LT}$ is Poisson's ratio of fabric (assumed as zero in calculations),

$$a = \frac{\tan^{-1}\left(y/x\right)}{\gamma} \text{ and } \quad b = \frac{\pi - \tan^{-1}\left(y/x\right)}{\gamma}$$

Parameters required to calculate the peak load of fabric are,

Fiber load-elongation data,

Fiber elongation at peak load, $\Delta l_p$ (cm)

Fiber diameter, $d$ (cm)

Fiber density, $\delta_f$ (g/cc)

Web thickness, $T$ (cm)

Web areal density, (g/cm$^2$)

Sample dimensions, $x$ and $y$ (cm)

The above parameters obtained from the characterization of electrospun web and aligned fiber bundle, and tensile test conducted on the web specimen were substituted in the equations for individual web specimen. Microsoft Excel was used to calculate the peak loads of webs. These predicted values of peak load and peak stress are listed for individual specimen with their parameters and measured peak load in Table 5.15. To account for the difference between measured and the calculated values, a correction factor $K$ is introduced.

$$K = \frac{\text{Measured Peak Stress}}{\text{Predicted Peak Stress}}$$

The force method lends to the prediction of peak load and from it the peak stress. These predictions were made for the samples spun with 8 and 10% PEO concentrations. With 12.5% PEO concentration, fiber diameter in aligned fiber bundles could not be achieved as explained earlier. Calculations for 12.5% PEO were therefore had to be omitted. Tensile testing data of single fibers produced from 8 and 10% PEO with 10cm distance between needle and collector plate were used as an input for predicting the peak stresses of web. For the 8 and 10% PEO, the calculations were performed for each of the three different specimen widths (1, 1.5 and 2cm) and for each of the three different collection times (4, 5 and 6hours) of web. These were compared with the measured values. The results are given in Table 5.15.

**Table 5.15:** Values of peak loads predicted and measured for individual specimen with the parameters used for calculations

| Concentration % | Run time (hr) | Width (cm) | Areal density ($gm/cm^2$) | Thickness (µm) | Calculated peak load (N) | Calculated peak stress (cN/den) | Measured peak load (N) | Measured peak stress (cN/Den) | K=Measured/calculated |
|---|---|---|---|---|---|---|---|---|---|
| 8 | 4hr | 1 | 0.00081 | 78.53 | 0.678 | 0.092452 | 1.207 | 0.164765 | 1.7822 |
| 8 | 4hr | 1 | 0.00071 | 68.88 | 0.594 | 0.092436 | 1.158 | 0.180155 | 1.9490 |
| 8 | 4hr | 1 | 0.00087 | 84.04 | 0.725 | 0.092400 | 1.037 | 0.132218 | 1.4309 |
| 8 | 4hr | 1 | 0.00083 | 79.90 | 0.689 | 0.092439 | 1.144 | 0.153434 | 1.6598 |
| 8 | 5hr | 1 | 0.00110 | 107.67 | 0.915 | 0.092403 | 1.382 | 0.139566 | 1.5104 |
| 8 | 5hr | 1 | 0.00099 | 96.48 | 0.820 | 0.092453 | 1.226 | 0.138151 | 1.4943 |
| 8 | 5hr | 1 | 0.00134 | 131.44 | 1.117 | 0.092455 | 1.590 | 0.131529 | 1.4226 |
| 8 | 5hr | 1 | 0.00113 | 110.46 | 0.939 | 0.092436 | 1.352 | 0.133149 | 1.4404 |

Table 5.15 Continued

| | | | | | | | | | |
|---|---|---|---|---|---|---|---|---|---|
| 8 | 6hr | 1 | 0.00173 | 187.50 | 1.438 | 0.092453 | 2.059 | 0.132344 | 1.4315 |
| 8 | 6hr | 1 | 0.00157 | 170.45 | 1.307 | 0.092416 | 1.913 | 0.135258 | 1.4636 |
| 8 | 6hr | 1 | 0.00121 | 131.72 | 1.010 | 0.092407 | 1.571 | 0.14374 | 1.5555 |
| 8 | 6hr | 1 | 0.00110 | 119.32 | 0.915 | 0.092409 | 1.460 | 0.147473 | 1.5959 |
| 8 | 4hr | 1.5 | 0.00079 | 76.23 | 1.315 | 0.123252 | 1.851 | 0.173413 | 1.4070 |
| 8 | 4hr | 1.5 | 0.00084 | 80.82 | 1.395 | 0.123292 | 2.013 | 0.177939 | 1.4432 |
| 8 | 4hr | 1.5 | 0.00096 | 92.76 | 1.600 | 0.123187 | 1.999 | 0.153923 | 1.2495 |
| 8 | 4hr | 1.5 | 0.00083 | 79.90 | 1.379 | 0.123257 | 1.478 | 0.132115 | 1.0719 |
| 8 | 5hr | 1.5 | 0.00119 | 116.52 | 1.981 | 0.123281 | 2.226 | 0.138535 | 1.1237 |
| 8 | 5hr | 1.5 | 0.00102 | 99.74 | 1.696 | 0.123261 | 2.014 | 0.146413 | 1.1878 |
| 8 | 5hr | 1.5 | 0.00123 | 120.25 | 2.044 | 0.123227 | 2.264 | 0.136501 | 1.1077 |
| 8 | 5hr | 1.5 | 0.00131 | 128.64 | 2.187 | 0.123241 | 2.260 | 0.12737 | 1.0335 |
| 8 | 6hr | 1.5 | 0.00121 | 131.20 | 2.013 | 0.123304 | 1.440 | 0.088203 | 0.7153 |
| 8 | 6hr | 1.5 | 0.00152 | 165.29 | 2.535 | 0.123237 | 2.674 | 0.129978 | 1.0547 |
| 8 | 6hr | 1.5 | 0.00118 | 128.10 | 1.965 | 0.123252 | 2.282 | 0.143141 | 1.1614 |
| 8 | 6hr | 1.5 | 0.00117 | 127.07 | 1.949 | 0.123238 | 2.217 | 0.140203 | 1.1377 |
| 8 | 4hr | 2 | 0.00069 | 66.13 | 1.795 | 0.145454 | 2.183 | 0.176896 | 1.2162 |
| 8 | 4hr | 2 | 0.00080 | 77.15 | 2.095 | 0.145458 | 2.747 | 0.190788 | 1.3116 |
| 8 | 4hr | 2 | 0.00084 | 80.59 | 2.189 | 0.145493 | 2.012 | 0.133774 | 0.9194 |

Table 5.15 Continued

| | | | | | | | | | |
|---|---|---|---|---|---|---|---|---|---|
| 8 | 4hr | 2 | 0.00091 | 87.48 | 2.374 | 0.145383 | 2.236 | 0.136928 | 0.9418 |
| 8 | 5hr | 2 | 0.00101 | 99.26 | 2.653 | 0.145361 | 2.440 | 0.133667 | 0.9196 |
| 8 | 5hr | 2 | 0.00109 | 106.84 | 2.858 | 0.145479 | 2.840 | 0.144559 | 0.9937 |
| 8 | 5hr | 2 | 0.00115 | 112.56 | 3.010 | 0.145410 | 2.900 | 0.140096 | 0.9635 |
| 8 | 5hr | 2 | 0.00106 | 103.47 | 2.766 | 0.145345 | 2.363 | 0.124192 | 0.8545 |
| 8 | 6hr | 2 | 0.00145 | 157.28 | 3.795 | 0.145415 | 3.279 | 0.12565 | 0.8641 |
| 8 | 6hr | 2 | 0.00149 | 161.16 | 3.889 | 0.145426 | 3.606 | 0.134854 | 0.9273 |
| 8 | 6hr | 2 | 0.00104 | 112.35 | 2.711 | 0.145419 | 2.557 | 0.137161 | 0.9432 |
| 8 | 6hr | 2 | 0.00104 | 113.12 | 2.729 | 0.145364 | 2.532 | 0.134903 | 0.9280 |
| 10 | 4hr | 1 | 0.00214 | 179.21 | 1.278 | 0.066253 | 2.735 | 0.141818 | 2.1406 |
| 10 | 4hr | 1 | 0.00251 | 210.28 | 1.500 | 0.066303 | 2.732 | 0.120718 | 1.8207 |
| 10 | 4hr | 1 | 0.00286 | 238.95 | 1.704 | 0.066279 | 4.163 | 0.161896 | 2.4426 |
| 10 | 4hr | 1 | 0.00260 | 217.45 | 1.551 | 0.066296 | 4.124 | 0.176222 | 2.6581 |
| 10 | 5hr | 1 | 0.00300 | 282.07 | 1.790 | 0.066309 | 3.992 | 0.147842 | 2.2296 |
| 10 | 5hr | 1 | 0.00289 | 271.33 | 1.722 | 0.066314 | 3.013 | 0.115997 | 1.7492 |
| 10 | 5hr | 1 | 0.00334 | 314.31 | 1.994 | 0.066294 | 3.558 | 0.118274 | 1.7841 |
| 10 | 5hr | 1 | 0.00280 | 263.27 | 1.671 | 0.066300 | 2.715 | 0.107734 | 1.6249 |
| 10 | 6hr | 1 | 0.00314 | 287.03 | 1.875 | 0.066290 | 4.032 | 0.142539 | 2.1502 |
| 10 | 6hr | 1 | 0.00303 | 276.59 | 1.807 | 0.066298 | 3.809 | 0.139755 | 2.1080 |

Table 5.15 Continued

| | | | | | | | | | |
|---|---|---|---|---|---|---|---|---|---|
| 10 | 6hr | 1 | 0.00414 | 378.36 | 2.472 | 0.066293 | 4.330 | 0.116126 | 1.7517 |
| 10 | 6hr | 1 | 0.00431 | 394.01 | 2.574 | 0.066284 | 5.045 | 0.129927 | 1.9602 |
| 10 | 4hr | 1.5 | 0.00210 | 175.23 | 2.503 | 0.088479 | 4.077 | 0.144142 | 1.6291 |
| 10 | 4hr | 1.5 | 0.00227 | 189.57 | 2.707 | 0.088466 | 3.953 | 0.129187 | 1.4603 |
| 10 | 4hr | 1.5 | 0.00208 | 173.64 | 2.480 | 0.088470 | 5.094 | 0.18175 | 2.0544 |
| 10 | 4hr | 1.5 | 0.00230 | 192.75 | 2.754 | 0.088496 | 5.866 | 0.188536 | 2.1304 |
| 10 | 5hr | 1.5 | 0.00278 | 261.48 | 3.325 | 0.088560 | 5.721 | 0.152373 | 1.7206 |
| 10 | 5hr | 1.5 | 0.00293 | 275.80 | 3.507 | 0.088550 | 4.840 | 0.122211 | 1.3801 |
| 10 | 5hr | 1.5 | 0.00314 | 295.51 | 3.754 | 0.088486 | 5.268 | 0.124159 | 1.4031 |
| 10 | 5hr | 1.5 | 0.00278 | 261.48 | 3.325 | 0.088560 | 4.362 | 0.116178 | 1.3119 |
| 10 | 6hr | 1.5 | 0.00381 | 347.91 | 4.554 | 0.088551 | 5.669 | 0.110227 | 1.2448 |
| 10 | 6hr | 1.5 | 0.00339 | 309.64 | 4.052 | 0.088534 | 7.310 | 0.159699 | 1.8038 |
| 10 | 6hr | 1.5 | 0.00303 | 276.59 | 3.619 | 0.088505 | 6.029 | 0.147451 | 1.6660 |
| 10 | 6hr | 1.5 | 0.00429 | 391.40 | 5.120 | 0.088488 | 7.465 | 0.129019 | 1.4580 |
| 10 | 4hr | 2 | 0.00223 | 186.38 | 4.187 | 0.104383 | 5.232 | 0.130418 | 1.2494 |
| 10 | 4hr | 2 | 0.00256 | 213.86 | 4.808 | 0.104467 | 6.447 | 0.140066 | 1.3408 |
| 10 | 4hr | 2 | 0.00307 | 256.87 | 5.773 | 0.104425 | 8.711 | 0.157568 | 1.5089 |
| 10 | 4hr | 2 | 0.00259 | 216.25 | 4.860 | 0.104411 | 7.904 | 0.169825 | 1.6265 |
| 10 | 5hr | 2 | 0.00311 | 292.82 | 5.856 | 0.104473 | 7.978 | 0.14232 | 1.3623 |

Table 5.15 Continued

| | | | | | | | | | |
|---|---|---|---|---|---|---|---|---|---|
| 10 | 5hr | 2 | 0.00270 | 253.87 | 5.077 | 0.104455 | 5.738 | 0.118056 | 1.1302 |
| 10 | 5hr | 2 | 0.00311 | 292.82 | 5.856 | 0.104473 | 6.481 | 0.115614 | 1.1066 |
| 10 | 5hr | 2 | 0.00271 | 255.21 | 5.102 | 0.104436 | 5.714 | 0.116943 | 1.1198 |
| 10 | 6hr | 2 | 0.00344 | 314.43 | 6.471 | 0.104422 | 8.167 | 0.131794 | 1.2621 |
| 10 | 6hr | 2 | 0.00353 | 322.69 | 6.645 | 0.104485 | 8.163 | 0.128357 | 1.2285 |
| 10 | 6hr | 2 | 0.00454 | 414.89 | 8.546 | 0.104507 | 9.953 | 0.121722 | 1.1647 |
| 10 | 6hr | 2 | 0.00399 | 364.00 | 7.495 | 0.104473 | 9.199 | 0.128225 | 1.2274 |

Using the above calculated values of peak stress, further analysis was made to find the effects of process parameters on the stress value.

### *5.5.1 Effect of variables on the values of predicted peak stress:*

Predicted peak stresses calculated above are plotted in Figure 5.26 to observe the effect of collection time on it. Time of collection shows no effect on the predicted values of peak stress. Because for a given width of test specimen and concentration, the fraction of number of fibers gripped at both ends remains constant but only areal density increases with an increase in time of collection. Since areal density is not expected to be an effective factor when stress is computed, the time of collection should not have any effect on the predicted value of peak stress. Accordingly, the time factor has been removed from further analysis of data in this section.

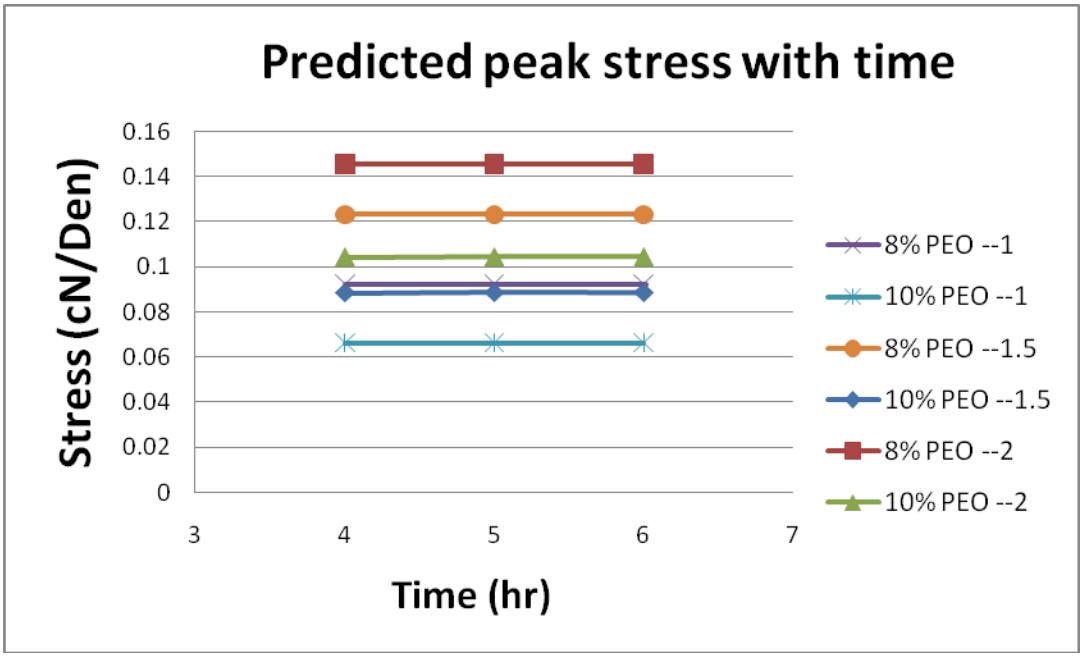


**Figure 5.26:** Plot between the predicted values of peak stress and time of collection

Graph in Figure 5.27 shows the relation between the predicted peak stress and width of test specimen. Predicted peak stress increases with an increase in the width from 1cm to 2cm. This is because, with the increase in width of the sample, the number of fibers gripped at both ends along with their proportion in total number of fibers increases (Section 3.3.2.1). The fibers gripped at both ends directly contribute to the strength of the material. This causes increase in peak stress with an increase in the width of specimen.

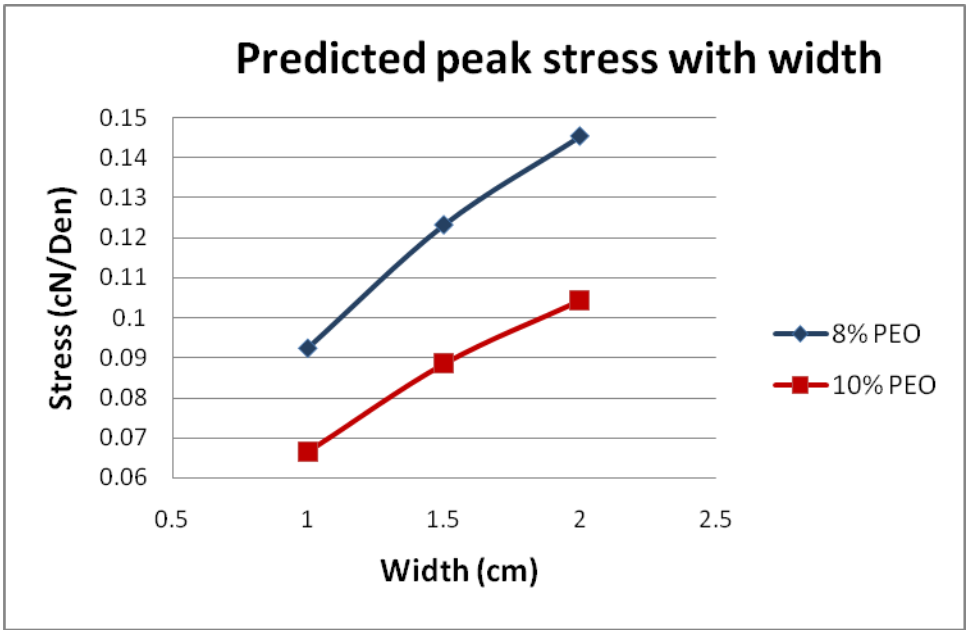


**Figure 5.27:** Plot between predicted peak stress and test specimen width

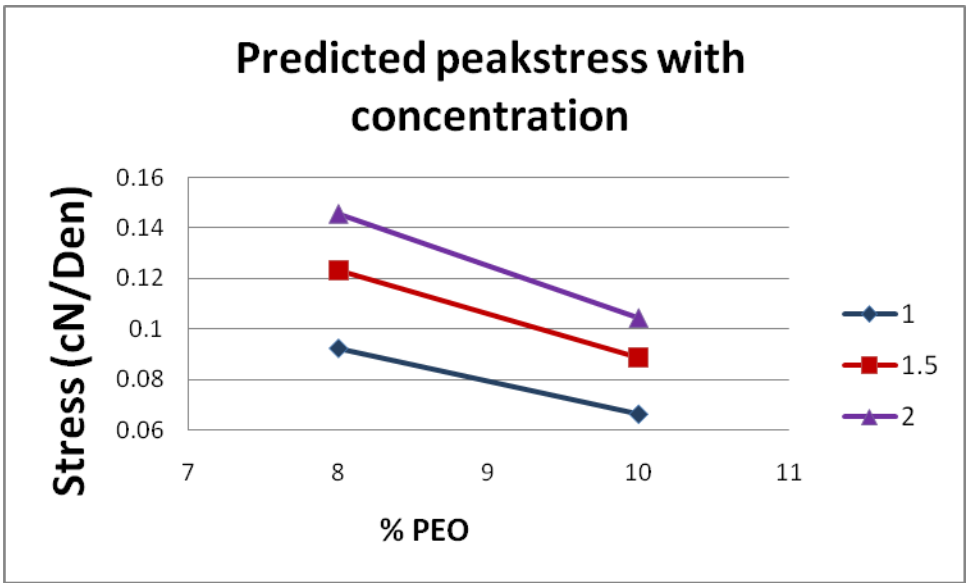


**Figure 5.28:** Graph between predicted peak stress and polymer concentration

Predicted values for the web peak stress plotted in Figure 5.28 against polymer concentration shows decrease in peak stress with an increase in concentration from 8 to 10%. Stress-strain values (Section 5.4.2) of single fiber obtained from tensile test on aligned bundles is used as the input value for prediction. Fiber stress values decreased with an increase in concentration. This causes the decrease in the value of predicted stress with an increase in the concentration of polymer.

### *5.5.2 Effect of variables on the value of the correction factor:*

Values of average Correction factor (*K*) and standard deviation for each sample are listed in Table 5.16. *K* values are greater than or equal to one for all cases, which means that the values of the measured peak stress are greater than the values of the predicted peak stress. Smaller values of predicted peak stress can be attributed to the omission of frictional force at the cross-over points of fibers. *K* value decreases with an increase in the width of specimen and moves toward 1 (Figure 5.29) which means predicted value and measured values are getting closer. With an increase in the sample width, the fraction of fibers gripped at both ends increases. This causes the value of the predicted peak stress to increase. Friction between the fibers at the cross-over points was ignored in this model. In smaller width specimen, the fraction of number of fibers gripped at both ends is relatively smaller as noted in Section 3.3.2.1. With the increase in width, the number of fibers along with the fraction of fibers gripped at both ends increases and fraction of other fibers decreases. The contribution of friction to the strength of material by the fibers gripped at one end or not at all decreases.

This explains increase in predicted value of stress with the increase in width. Therefore, this will be the expected behavior for the predicted value of stress.

The actual fabric, however, has some bonding at the cross-over points. This is evident from the behavior noted in Figure 5.8, which shows necking as the fabric strip is extended. This means that fabric acts like a film in which width should not have an effect on the stress. With the measured value being higher than the predicted but the latter increasing with increase in width allows it to come closer to the former. At this point, it is assumed that it is a coincident that the two values become nearly equal when the width is increased to 2 cm. Further research will be necessary to fully understand the behavior. It is suggested that the bonding at the cross-over points be incorporated in the model and its effect on the predicted value of tensile properties be determined.

One more reason might be the increase in the weak link effect of fibers gripped at both ends might cause the reduction in the measured value of peak stress when the width is increased. This explains the approach of $K$ value to 1 when the width of specimen is increased.

**Table 5.16:** Values of correction factor (*K*) for the samples.

| Concentration % | Width (cm) | K values | |
|---|---|---|---|
| | | Averages | Std dev |
| 8 | 1 | 1.561342 | 0.163574 |
| 8 | 1.5 | 1.141119 | 0.186562 |
| 8 | 2 | 0.981906 | 0.138491 |
| 10 | 1 | 2.034996 | 0.311392 |
| 10 | 1.5 | 1.605214 | 0.283602 |
| 10 | 2 | 1.277264 | 0.159821 |

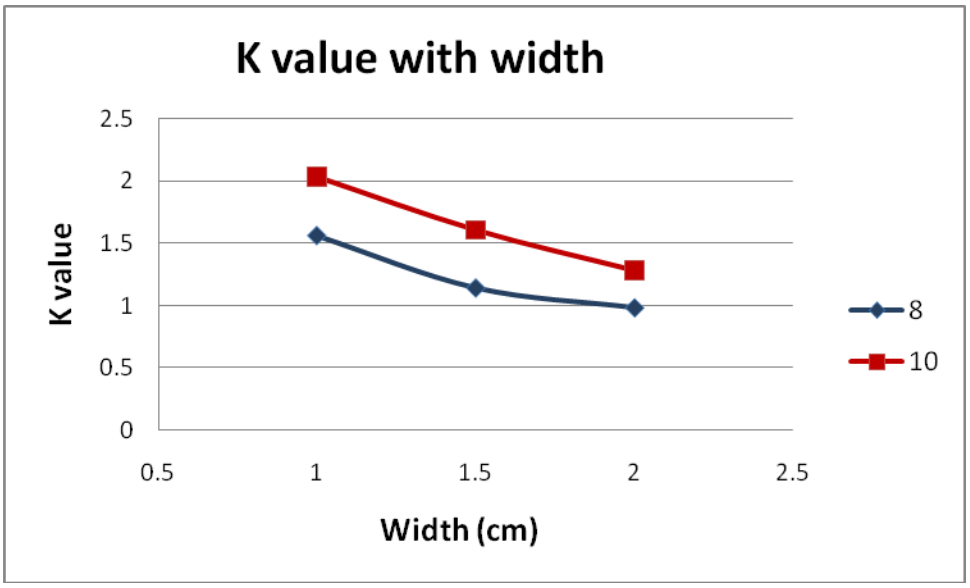


**Figure 5.29:** Plot between *K* value and the width of test specimen

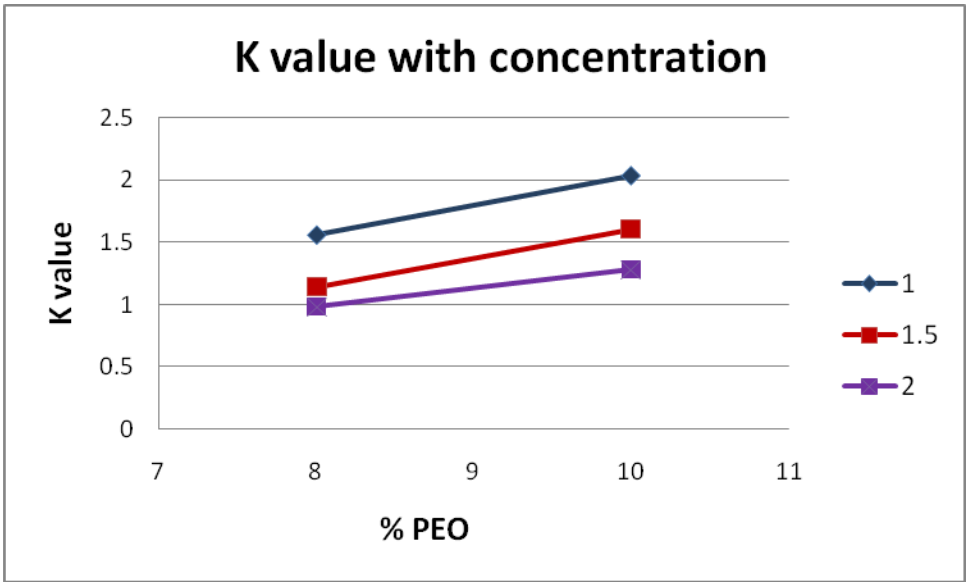


**Figure 5.30:** Graph between *K* value and concentration of PEO

Plot (Figure 5.30) between the *K* value and the concentratoin of the polymer solution shows increase in the former with an increase in the concentration. Increase in concentration causes a decrease in the number of fibers for the same areal density of web because of increase in fiber diameter. As the number of fibers decrease, the impact of the omission of the contribution made by the friction factor increases and this causes an increase in the departure of the predicted value from the measured value. This results in increase in *K* value with an increase in the concentration of polymer solution.

Analysis of variance to find the effect of concentration and width on *K* value was conducted and the results are given in Table 5.17. The results show that the effect of concentration and width on the *K* value are significant.

**Table 5.17:** ANOVA output to find the effect on *K* value.

| Parameter | F- value | Pr > F |
|---|---|---|
| Concentration | 63.8 | <.0001 |
| Width | 57.65 | <.0001 |

Regression analysis was conducted to develop a predictive model for *K* value. The output of analysis listed in Table 5.18 shows that concentration and specimen width are significant in predicting the value of K with $R^2$ value 0.71.

**Table 5.18:** Regression analysis of K value

| Parameter | Estimate | Error | t value | Pr > F |
|---|---|---|---|---|
| Intercept | 0.58685543 | 0.2546295 | 2.3 | 0.0242 |
| conc | 0.20551795 | 0.026056 | 7.89 | <.0001 |
| width | -0.6685846 | 0.0638238 | -10.48 | <.0001 |

Equation to predict the *K* value is as follows:

$$K = 0.59 + 0.21*\text{conc} - 0.67*\text{width}$$

From the results given in this section it can concluded that the model is useful in predicting the strength of material within about a factor of 2 of the measured value. This represents excellent progress. However, the model proposed for the tensile properties should be considered as an initial step towards mechanical characterization of the electrospun web.

Further modifications like including bonding or friction effects at the cross-over points and weak link effects should be made that could enhance the predictability of the model.

# 6. SUMMARY& CONCLUSIONS:

## 6.1 Summary:

The goal of this work was to be able to characterize the structure and understand, and model the tensile properties of electrospun nanofiber webs. To achieve the goal, primary objectives were set to (1) produce uniform and reproducible electrospun webs and analyze the web structure and fiber morphology, (2) find the effect of fiber diameter and sample dimensions on the mechanical properties of web, and (3) model the structure and tensile behavior of these webs to predict the mechanical properties. Since the prediction of web tensile behavior requires stress-strain properties of single nanofibers, a second objective was to produce aligned fibers with parallel plates as collector and obtain single fiber tensile properties. In this process, a mini experiment was also conducted in which the effects of polymer concentration and spinning distance on the mechanical properties of single fibers were examined.

Initial studies were aimed at producing uniform nanofiber webs of different diameters. For this, three concentrations, 8, 10 and 12.5% of PEO polymer were selected and water was used as the solvent. Stable Taylor cone, which was necessary to get uniform fibers in the web on round collector plate, was formed at 9.5 kV and 15cm distance between needle and collector for 8% PEO. For 10 and 12.5% PEO polymer concentrations, stable Taylor cone was formed at 11.5 kV and 15cm distance and 17 kV and 18cm distance, respectively. With these conditions, fiber diameters of 210nm, 325nm and 550nm were achieved, respectively

for the 8, 10 and 12.5% PEO polymer concentrations. Increased voltage, which was required to erupt a jet from increased viscosity due to the increase in polymer concentration, reduced the flight time for polymer extrudate, caused reduction in draw ratio and resulted in increased fiber diameter.

Effect of polymer concentration on thickness and areal density of web were also observed. For example, web thickness was increased from 85.4μm to 580.7μm and areal density from 8.9g/$m^2$ to 79.3 g/$m^2$ when the concentration changed from 8 to 12.5% PEO. When the polymer concentration increased, increase in the fiber diameter caused more mass of fiber to deposit on the collector. This resulted in increase in the areal density and thickness of web.

The effect of polymer concentration on peak stress, strain corresponding the peak stress, initial modulus, and yield point of webs was studied. Results showed that peak stress, initial modulus and yield stress values decreased, and strain corresponding peak stress and yield strain values increased with increase in polymer concentration of the solution. Peak stress value decreased from 0.142±0.020 to 0.112±0.008 cN/Den for 2cm width of specimen when the concentration was increased from 8 to 12.5% PEO. Similarly, the initial modulus value decreased from 0.85±0.06 to 0.54±0.06 cN/Den and the yield stress value decreased from 0.104±0.013 to 0.083±0.006 cN/Den for 2cm specimen width when the concentration was increased from 8 to 12.5% PEO. For the same change in concentration, strain corresponding peak load increased from 3.62±0.96 to 5.64±1.69 and yield strain increased from 0.53±0.12 to 1.05±0.29. With increase in polymer concentration, the voltage had to be increased. This

made the polymer jet to accelerate faster, which gave less flight time for drawing the jet, and resulted in decrease in stress and initial modulus values, and increase in strain values.

Width of the test specimen was studied to find its effect on the predicted tensile properties of the web. Increase in the stress and modulus values was expected with the increase in the width because with increase in width, fraction of number of fibers gripped at both ends increased. But in the actual results on test specimens no significant effect of width on any of the tensile properties was observed. This clearly indicated that in the actual web obtained by the electrospinning fibers, the fibers had some bonding at the cross-over points which caused the web to act as a regular fabric. Width of web should not have any effect on tensile properties in such structures. In contrast, the structure considered for modeling has no bonding at the cross-over points. In this case, the width directly affects the fraction of total fibers gripped in the jaws and therefore influences the mechanical properties.

To get single fiber stress-strain behavior, aligned nanofibers were collected on collector strips separated with gap. Fiber diameters that matched with the fibers in electrospun webs were obtained at reduced distance between needle and collector for a particular concentration. For 8% PEO, fibers of 205nm in diameter were obtained at 9.5kV and 10cm distance whereas for 10% PEO, 320nm diameter fibers were obtained at 11.5kV and 10cm distance. From the results, it is again observed that with increase in concentration, fiber diameter increased.

In the process of obtaining required fiber diameter in aligned fiber bundles, different combinations of voltage and distance were experimented with. This allowed to examine the effect of distance between needle and collector on fiber diameter. It was observed that with the decrease in distance, fiber diameter increased. Reduced flight time due to decrease in distance gave the jet smaller draw ratio and resulted in larger diameter fibers.

Effect of polymer concentration and spinning distance on tensile properties of single nanofibers were also investigated. These two factors were found to significant effect on peak stress and initial modulus values. For example, peak stress value decreased from 0.47 to 0.38gf/Den and initial modulus value decreased from 4.59 to 3.57gf/Den when the concentration was changed from 8 to 10% for the 10cm distance between the needle and the collector. High voltage required for more concentrated polymer solution accelerated the jet and gave less flight time for travel. This caused decrease in the fiber draw ratio and resulted in increased disoriented polymer chains. Fibers with disoriented molecules in high concentrated polymer solution could be expected to have low peak stress and initial modulus values.

Peak stress value increased from 0.47 to 0.82gf/Den for 8% PEO and from 0.38 to 0.52gf/Den for 10%PEO when distance between needle and collector increased from 10 to 15cm. Similarly, initial modulus value increased from 4.59 to 7.57gf/Den for 8% PEO and from 3.57 to 5.0gf/Den for 10% PEO. Increase in spinning distance increased the flight time of polymer jet which gave the extrudate increased draw ratio. Oriented molecular chains due to increased draw ratio led to increase in the fiber strength.

Analysis of web structure for fiber orientation under SEM showed that fibers were randomly arranged. Assuming no fusing or bonding between the fibers at the cross-over points the structure of the web was modeled that proved useful in calculating the number of fibers gripped between jaws of a tensile tester and their angular orientations. This facilitated modeling and predicting the tensile properties of the electrospun web. Both the "Force method" and the "Energy method" were used in modeling the tensile properties.

The peak stress values predicted using force method, were compared with the measured values. The agreement between the predicted and measured values of stress was good, the difference being less than a factor of two. Measured values were greater than the predicted values; this was attributed to the bonding at the cross-over points which were present in the actual web but were assumed to be absent in the modeled web.

This indicates that the next step in this field of research will be to consider bonding at the cross-over points and modify the model for predicting the tensile properties of the electrospun webs.

### 6.2 Recommendations for future work

Based on the research in this thesis, the following recommendations can be made to further the work in the area of the structural mechanics of the electrospun webs:

1. In the model, it was assumed that only fibers gripped at both ends contributed to the strength of the fabric. Friction or bonding between the fibers at cross-over points was ignored. However, the tests on actual webs show that some bonding does exist at the

cross-over points. Incorporating the bonding between the fibers will ameliorate the model and proved better prediction of the tensile properties of the webs.

2. In the model, the fibers were considered to be straight, but there is, no doubt, some crimp present. Including a curl or crimp factor in the model will be useful.

3. Electrospun web elongated up to 600% which indicated that the molecular chains were disoriented. X-ray diffraction also showed that web had crystalline structure but the crystals were not oriented. Drawing and annealing the electrospun web can be expected to orient the molecules and enhance the mechanical properties of the web as illustrated for one structure whose results are included in Appendix B. It is recommended that the drawing and annealing behavior of electrospun webs and its impact on tensile properties be examined in detail.

4. We only used one polymer (PEO) in this research. Mechanical properties being important in many different applications of electrospun webs, it is recommended that this work be extended to webs spun from other polymers, especially those used extensively in making durable and load bearing products.

# 7. REFERENCES:


Adanur, S., & Liao, T. (1999). Fiber arrangement characteristics and their effects on nonwoven tensile behavior. *Textile Research Journal, 69*(11), 816-824. doi:10.1177/004051759906901104

Backer, S., & Petterson, D. R. (1960). Some principles of nonwoven fabrics. *Textile Research Journal, 30*(9), 704-711. doi:10.1177/004051756003000912

Bhattarai, N., Cha, D. I., Bhattarai, S. R., Khil, M. S., & Kim, H. Y. (2003). Biodegradable electrospun mat: Novel block copolymer of poly (*p*-dioxanone-*co*-L-lactide)-*block*-poly(ethylene glycol). *Journal of Polymer Science Part B: Polymer Physics, 41*(16), 1955-1964. doi:10.1002/polb.10547

Britton, P. N., Sampson, A. J., Elliott, C. F., JR, Graben, H. W., & Gettys, W. E. (1983). Computer simulation of the mechanical properties of nonwoven fabrics: Part I: The method. *Textile Research Journal, 53*(6), 363-368. doi:10.1177/004051758305300607

Britton, P. N., Sampson, A. J., & Gettys, W. E. (1984). Computer simulation of the mechanical properties of nonwoven fabrics: Part II: Bond breaking. *Textile Research Journal, 54*(1), 1-5. doi:10.1177/004051758405400101

Chaikof, E. L. (2001). Engineered collagen–PEO nanofibers and fabrics. *Journal of Biomaterials Science -- Polymer Edition, 12*(9), 979. Retrieved from http://search.ebscohost.com/login.aspx?direct=true&db=aph&AN=5563182&site=ehost-live&scope=site

Dalton, P. D., Klinkhammer, K., Salber, J., Klee, D., & Moller, M. (2006). Direct in vitro electrospinning with polymer melts. *Biomacromolecules, 7*(3), 686-690. Retrieved from http://dx.doi.org/10.1021/bm050777q

Dersch, R., Liu, T., Schaper, A. K., Greiner, A., & Wendorff, J. H. (2003). Electrospun nanofibers: Internal structure and intrinsic orientation. *Journal of Polymer Science Part A: Polymer Chemistry, 41*(4), 545-553. doi:10.1002/pola.10609

Grindstaff, T. H., & Hansen, S. M. (1986). Computer model for predicting point-bonded nonwoven fabric strength, part I. *Textile Research Journal, 56*(6), 383-388. doi:10.1177/004051758605600607

Hearle, J. W. S., & Newton, A. (1967). Nonwoven fabric studies: Part XIV: Derivation of generalized mechanics by the energy method. *Textile Research Journal, 37*(9), 778-797. doi:10.1177/004051756703700908

Hearle, J. W. S., & Newton, A. (1968). Nonwoven fabric studies part XV: The application of the fiber network theory. *Textile Research Journal, 38*(4), 343-351. doi:10.1177/004051756803800404

Hearle, J. W. S., & Ozsanlav, V. (1979a). Studies of adhesive-bonded non-woven fabrics part iii: The determination of fibre orientation and curl. *Journal of the Textile Institute, 70*(11), 487. Retrieved from http://www.informaworld.com.www.lib.ncsu.edu:2048/10.1080/00405007908658890

Hearle, J. W. S., & Ozsanlav, V. (1979b). Studies of adhesive-bonded non-woven fabrics part I: A theoretical model of tensile response incorporating binder deformation. *Journal of the Textile Institute, 70*(1), 19. Retrieved from http://www.informaworld.com.www.lib.ncsu.edu:2048/10.1080/00405007908631511

Hearle, J. W. S., & Stevenson, P. J. (1963). Nonwoven fabric studies, part III: The anisotropy of nonwoven fabrics. *Textile Research Journal, 33*(11), 877-888.

Hearle, J. W. S., & Stevenson, P. J. (1964). Studies in nonwoven fabrics: Part IV: Prediction of tensile properties. *Textile Research Journal, 34*(3), 181-191. doi:10.1177/004051756403400301

Huang, L., McMillan, R. A., Apkarian, R. P., Pourdeyhimi, B., Conticello, V. P., & Chaikof, E. L. (2000). Generation of synthetic elastin-mimetic small diameter fibers and fiber networks. *Macromolecules, 33*(8), 2989-2997. Retrieved from http://dx.doi.org/10.1021/ma991858f

Huang, Z., Zhang, Y. Z., Ramakrishna, S., & Lim, C. T. (2004). Electrospinning and mechanical characterization of gelatin nanofibers. *Polymer, 45*(15), 5361-5368. doi:DOI: 10.1016/j.polymer.2004.04.005

Inai, R., Kotaki, M., & Ramakrishna, S. (2005). Structure and properties of electrospun PLLA single nanofibres. *Nanotechnology, 16*(2), 208-213.

Khil, M. S., Kim, H. Y., Kim, M. S., Park, S. Y., & Lee, D. (2004). Nanofibrous mats of poly(trimethylene terephthalate) via electrospinning. *Polymer, 45*(1), 295-301. doi:DOI: 10.1016/j.polymer.2003.09.049

Lee, K. H., Kim, H. Y., Khil, M. S., Ra, Y. M., & Lee, D. R. (2003). Characterization of nano-structured poly(ε -caprolactone) nonwoven mats via electrospinning. *Polymer, 44*(4), 1287-1294. doi:DOI: 10.1016/S0032-3861(02)00820-0

Lee, K. H., Kim, H. Y., La, Y. M., Lee, D. R., & Sung, N. H. (2002). Influence of a mixing solvent with tetrahydrofuran and *N,N*-dimethylformamide on electrospun poly(vinyl chloride) nonwoven mats. *Journal of Polymer Science Part B: Polymer Physics, 40*(19), 2259-2268. doi:10.1002/polb.10293

Li, D., & Xia, Y. (2004). Electrospinning of nanofibers: Reinventing the wheel? *Advanced Materials, 16*(14), 1151-1170. doi:10.1002/adma.200400719

Li, D., Wang, Y., & Xia, Y. (2003). Electrospinning of polymeric and ceramic nanofibers as uniaxially aligned arrays. *Nano Letters, 3*(8), 1167-1171. Retrieved from http://dx.doi.org/10.1021/nl0344256

Li, W., Laurencin, C. T., Caterson, E. J., Tuan, R. S., & Ko, F. K. (2002). Electrospun nanofibrous structure: A novel scaffold for tissue engineering. *Journal of Biomedical Materials Research, 60*(4), 613-621. doi:10.1002/jbm.10167

Moghe, A. K. (2008). *Core-sheath differentially biodegradable nanofiber structures for tissue engineering* Retrieved from http://www.lib.ncsu.edu/theses/available/etd-07022008-142257/unrestricted/etd.pdf

Moon, S., Ryu, B., Choi, J., Jo, B., & Farris, R. J. (2009). The morphology and mechanical properties of sodium alginate based electrospun poly(ethylene oxide) nanofibers. *Polymer Engineering & Science, 49*(1), 52-59. doi:10.1002/pen.21216

Ohgo, K., Zhao, C., Kobayashi, M., & Asakura, T. (2003). Preparation of non-woven nanofibers of bombyx mori silk, samia cynthia ricini silk and recombinant hybrid silk with electrospinning method. *Polymer, 44*(3), 841-846. doi:DOI: 10.1016/S0032-3861(02)00819-4

Ojha, S. S. (2007). *Fabrication and characterization of novel single and bicomponent electrospun nanofibrous mats* Retrieved from http://www.lib.ncsu.edu/theses/available/etd-06082007-125208/unrestricted/etd.pdf

Paradkar, A. M. (1987). *Structural mechanics of nonwoven fiber web*

Pedicini, A., & Farris, R. J. (2003). Mechanical behavior of electrospun polyurethane. *Polymer, 44*(22), 6857-6862. doi:DOI: 10.1016/j.polymer.2003.08.040

Petterson, D. R., & Backer, S. (1963). Relationships between the structural geometry of a fabric and its physical properties, part VII: Mechanics of nonwoven, orthotropic behavior. *Textile Research Journal, 33*(10), 809-816.

Ramakrishna, S. (2005). *An introduction to electrospinning and nanofibers.* Singapore ; Hackensack, NJ: World Scientific.

Subbiah, T., Bhat, G. S., Tock, R. W., Parameswaran, S., & Ramkumar, S. S. (2005). Electrospinning of nanofibers. *Journal of Applied Polymer Science, 96*(2), 557-569. doi:10.1002/app.21481

Tan, E. P. S., Goh, C. N., Sow, C. H., & Lim, C. T. (2005). Tensile test of a single nanofiber using an atomic force microscope tip. *Applied Physics Letters, 86*(7), 073115. doi:10.1063/1.1862337

Tan, E. P. S., & Lim, C. T. (2004). Physical properties of a single polymeric nanofiber. *Applied Physics Letters, 84*(9), 1603-1605. doi:10.1063/1.1651643

Tan, E. P. S., & Lima, C. T. (2004). Novel approach to tensile testing of micro- and nanoscale fibers. *Review of Scientific Instruments, 75*(8), 2581-2585. doi:10.1063/1.1775309

Tan, E. P. S., Ng, S. Y., & Lim, C. T. (2005). Tensile testing of a single ultrafine polymeric fiber. *Biomaterials, 26*(13), 1453-1456. doi:DOI: 10.1016/j.biomaterials.2004.05.021

Teo, . (2006). A review on electrospinning design and nanofibre assemblies. *Nanotechnology, 17*(14), R89.

Tianyi Liao, , & Adanur, S. (1999). Computerized failure analysis of nonwoven fabrics based on fiber failure criterion. *Textile Research Journal, 69*(7), 489-496. doi:10.1177/004051759906900705

Wnek, G. E., Carr, M. E., Simpson, D. G., & Bowlin, G. L. (2003). Electrospinning of nanofiber fibrinogen structures. *Nano Letters, 3*(2), 213-216. Retrieved from http://dx.doi.org/10.1021/nl025866c

Zong, X., Ran, S., Fang, D., Hsiao, B. S., & Chu, B. (2003). Control of structure, morphology and property in electrospun poly(glycolide-co-lactide) non-woven membranes via post-draw treatments. *Polymer, 44*(17), 4959-4967. doi:DOI: 10.1016/S0032-3861(03)00464-6

# APPENDICES

**<u>Appendix A:</u> Fabric stress-strain properties using the Energy method:**

To measure the fabric stress strain behavior from fiber properties, the energy method is useful. Principle of the energy method is based on the assumption that the work done on a specimen due to some deformation imposed is equal to the sum of the energy changes in the elements of that specimen. Consider a fabric specimen that is given displacements $S_1, S_2, .....S_i, .....S_n$ on $n$ points which lead to forces $P_1, P_2, .....P_i, .....P_n$ in the direction of the corresponding force. The work done by force $P_i$ for a change $dS_i$ is $P_i.dS_i$. This work must be stored in the fabric as elastic deformation energy. If the fabric is divided into $N$ elements or discs denoted by suffix $j$, and energy stored in an element is denoted by $E_j$,

Total stored energy $= \sum_{j=1}^{N} E_j$ .

$i=1,2,3.\ldots\ldots n$ and $j=1,2,3.\ldots\ldots N$, or the number of disks

When we consider the displacement only at $S_i$ where all other $S$ values are kept constant,

for a displacement $dS_i$ change in stored energy $= \left( \frac{\partial}{\partial S_i} \sum_{j=1}^{N} E_j \right)_{S_1, S_2, .....S_{i-1}, S_{i+1}.....S_n} dS_i$

$$= \left( \sum_{j=1}^{N} \frac{\partial E_j}{\partial S_i} \right)_{S_1, S_2, .....S_{i-1}, S_{i+1}.....S_n} dS_i$$

By equating work done and energy change, $P_i = \left( \sum_{j=1}^{N} \frac{\partial E_j}{\partial S_i} \right)_{S_1, S_2, .....S_{i-1}, S_{i+1}.....S_n}$ (3.33)

This is a general form of the equation for force in the specimen and can be applied to any level of deformation given to a specimen. The above equation can be modified to appear in different units or forms as shown below.

Force on point *i*:

in terms of energy in fibrous elements, $P_i = \sum_{j=1}^{N} \frac{\partial E_j}{\partial \varepsilon_j} \left( \frac{\partial \varepsilon_j}{\partial S_i} \right)$

in terms of energy in fibrous elements per unit mass $P_i = \sum_{j=1}^{N} \mu_j \frac{\partial U_j}{\partial \varepsilon_j} \left( \frac{\partial \varepsilon_j}{\partial S_i} \right)$

in terms of fiber stress-strain relation $P_i = \sum_{j=1}^{N} \mu_j \sigma_j \left( \frac{\partial \varepsilon_j}{\partial S_i} \right)$

where, $\sigma_j$ is stress in fibrous element *j*, $\varepsilon_j$ is strain in element *j*, $\mu_j$ is mass of element *j*, and $U_j$ is energy per unit mass.

The above equations can be further simplified if shape of the specimen is known and the forces and displacements can be converted into stresses and strains. Consider a rectangular specimen (shown in Figure 8.1) of length *L*, width *B* and mass *M*, and force $P_i$, applied to the edge of width *B*, causes displacement $S_i$, then *M*/*L* gives the mass per unit length.

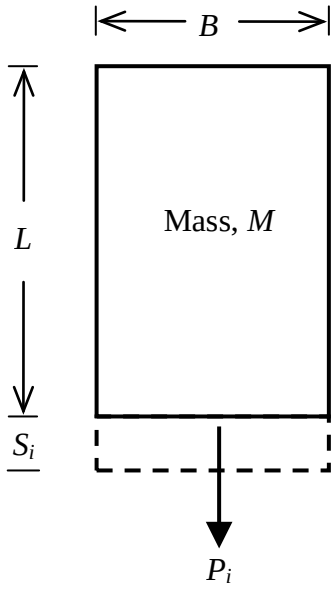


**Figure 8.1**: A rectangular specimen considered for simplification

Specific stress in the specimen = $\sigma_i = {}^{P_i}\!\Big/\!_{M/L}$

By substituting $P_i$ value from Equation 3.33, $\sigma_i = \left(\sum_{j=1}^{N} \frac{\partial E_j}{\partial S_i}\right)_{S_1, S_2, \ldots S_{i-1}, S_{i+1} \ldots S_n} \Big/ M/L$

Strain $\varepsilon_i = {}^{S_i}\!\Big/\!_{L}$ or $S_i = \varepsilon_i . L$.

$$\sigma_i = \left(\sum_{j=1}^{N} \frac{\partial E_j}{\partial(\varepsilon_i . L)}\right)_{S_1, S_2, \ldots S_{i-1}, S_{i+1} \ldots S_n} \Big/ M/L = \frac{1}{M} \sum_{j=1}^{N} \left(\frac{\partial E_j}{\partial \varepsilon_i}\right)_{\varepsilon_1, \varepsilon_2, \ldots \varepsilon_{i-1}, \varepsilon_{i+1} \ldots \varepsilon_n}$$

$$\sigma_i = \frac{1}{M} \sum_{j=1}^{N} \mu_j \left(\frac{\partial U_j}{\partial \varepsilon_i}\right)_{\varepsilon_1, \varepsilon_2, \ldots \varepsilon_{i-1}, \varepsilon_{i+1} \ldots \varepsilon_n} = \frac{1}{M} \sum_{j=1}^{N} \mu_j \frac{\partial U(\varepsilon_j)}{\partial \varepsilon_j} \left(\frac{\partial \varepsilon_j}{\partial \varepsilon_i}\right)_{\varepsilon_1, \varepsilon_2, \ldots \varepsilon_{i-1}, \varepsilon_{i+1} \ldots \varepsilon_n}$$

where, $\partial U(\varepsilon_j)$ is energy change per unit mass due to strain $\varepsilon_j$.

If $\sigma(\varepsilon_j)$ is specific stress in the element due to strain $\varepsilon_j$, $t_j$ is mass per unit length of element and $l_j$ is length of an element, then

$$dU(\varepsilon_j) = \left[ t_j \sigma(\varepsilon_j) l_j d\varepsilon_j \right] / \mu_j = \sigma(\varepsilon_j) d\varepsilon_j \qquad (\because t_j l_j = \mu_j)$$

$$\sigma_i = \frac{1}{M} \sum_{j=1}^{N} \mu_j \sigma(\varepsilon_j) \left( \frac{\partial \varepsilon_j}{\partial \varepsilon_i} \right)_{\varepsilon_1, \varepsilon_2, \ldots\ldots \varepsilon_{i-1}, \varepsilon_{i+1} \ldots\ldots \varepsilon_n} \tag{3.34}$$

Fiber strain due to fabric strain:

From Equation 3.25 in Section 3.4.1, $\mathrm{OC} = \left[ (y+\Delta y)^2 + \cot^2 \theta_j (y - \Delta y \nu_{LT})^2 \right]^{1/2}$

Fiber strain, $\varepsilon_j = \dfrac{(\mathrm{OC} - l)}{l} = \dfrac{\left[ (y+\Delta y)^2 + \cot^2 \theta_j (y - \Delta y \nu_{LT})^2 \right]^{1/2} - y / \sin \theta_j}{y / \sin \theta_j}$

since $\sin \theta_j = \dfrac{y}{l}$

$$\varepsilon_j = \left[ (1+\varepsilon_i)^2 \sin^2 \theta_j + (1 - \nu_{LT} \varepsilon_i)^2 \cos^2 \theta_j \right]^{1/2} - 1 \tag{3.35}$$

The above equation transforms fabric strain to fiber strains at different angles of orientation.

Differentiating the above equation with respect to fabric strain gives,

$$\left(\frac{\partial \varepsilon_j}{\partial \varepsilon_i}\right) = \frac{\left[(1+\varepsilon_i)\sin^2\theta_j - \nu_{LT}(1-\nu_{LT}\varepsilon_i)\cos^2\theta_j\right]}{\left[(1+\varepsilon_i)^2\sin^2\theta_j + (1-\nu_{LT}\varepsilon_i)^2\cos^2\theta_j\right]^{1/2}} \tag{3.36}$$

As mentioned earlier if we ignore the contribution to strength by bonding at cross-over points, then energy stored in fabric is equal to the energy stored in individual fibers gripped at the two ends. As shown in Section 3.3.2, the number of fibers gripped at both ends in a disc is (from Equation 3.15):

$$N_j = \frac{x|\sin j\gamma| - y|\cos j\gamma|}{S} \tag{3.37}$$

Accordingly, the stress in the fabric is

$$\sigma_i = \frac{1}{M}\sum_{j=a}^{b} N_j \mu_j \sigma(\varepsilon_j)\left(\frac{\partial \varepsilon_j}{\partial \varepsilon_i}\right) \tag{3.38}$$

Here $\mu_j$ is the mass of the fibers gripped at the two ends in a disc, or

$$\mu_j = \frac{\pi y d^2 \rho_f}{4\sin\theta_j} \tag{3.39}$$

By substituting Equations 3.36, 3.37 and 3.39 in the fabric stress Equation 3.38

$$\sigma_i = \frac{1}{M}\sum_{j=a}^{b} \frac{x|\sin j\gamma| - y|\cos j\gamma|}{S} \frac{\pi y d^2 \rho_f}{4\sin\theta_j} \sigma(\varepsilon_j) \frac{\left[(1+\varepsilon_i)\sin^2\theta_j - \nu_{LT}(1-\nu_{LT}\varepsilon_i)\cos^2\theta_j\right]}{\left[(1+\varepsilon_i)^2\sin^2\theta_j + (1-\nu_{LT}\varepsilon_i)^2\cos^2\theta_j\right]^{1/2}}$$

The angle $\theta$ varies from layer to layer and for $j^{th}$ layer or disc, it is given by $j\gamma$. Therefore,

$$\sigma_i = \frac{1}{M}\sum_{j=a}^{b} \frac{x|\sin j\gamma| - y|\cos j\gamma|}{S} \frac{\pi y d^2 \rho_f}{4|\sin j\gamma|} \sigma(\varepsilon_j) \frac{\left[(1+\varepsilon_i)\sin^2 j\gamma - \nu_{LT}(1-\nu_{LT}\varepsilon_i)\cos^2 j\gamma\right]}{\left[(1+\varepsilon_i)^2 \sin^2 j\gamma + (1-\nu_{LT}\varepsilon_i)^2 \cos^2 j\gamma\right]^{1/2}} \quad (3.40)$$

Calculating peak stress using Energy method:

Instead of Force method used in Section 3.4.1, Energy method also can be used to calculate peaks stress values.

Stress in fabric

$$\sigma_i = \frac{1}{W}\sum_{j=a}^{b} \frac{x|\sin j\gamma| - y|\cos j\gamma|}{S} \frac{\pi y d^2 \rho_f}{4|\sin j\gamma|} \sigma(\varepsilon_j) \frac{\left[(1+\varepsilon_i)\sin^2 j\gamma - \nu_{LT}(1-\nu_{LT}\varepsilon_i)\cos^2 j\gamma\right]}{\left[(1+\varepsilon_i)^2 \sin^2 j\gamma + (1-\nu_{LT}\varepsilon_i)^2 \cos^2 j\gamma\right]^{1/2}}$$

Peak stress in fabric is achieved by replacing $\varepsilon_j$ and $\varepsilon_i$ with $\varepsilon_{jp}$.

Peak stress in fabric

$$\sigma_i = \frac{1}{W}\sum_{j=a}^{b} \frac{x|\sin j\gamma| - y|\cos j\gamma|}{S} \frac{\pi y d^2 \rho_f}{4|\sin j\gamma|} \sigma(\varepsilon_{jp}) \frac{\left[(1+\varepsilon_{jp})\sin^2 j\gamma - \nu_{LT}(1-\nu_{LT}\varepsilon_{jp})\cos^2 j\gamma\right]}{\left[(1+\varepsilon_{jp})^2 \sin^2 j\gamma + (1-\nu_{LT}\varepsilon_{jp})^2 \cos^2 j\gamma\right]^{1/2}} \quad (3.41)$$

Equation 3.40 gives the stress in a fabric when strain $\varepsilon_i$ is applied. Stress-strain curve of the fabric can be generated by calculating stress values of fabric for strain values from 0 to breaking strain. Equation 3.41 can be used to compute peak stress value of fabric. The assumption involved in developing the model is that no bonding exists at the cross-over

points. Although an adhesive is not involved, some bonding does exist between fibers as they lay over each other during the electrospinning process. This bonding, howsoever small, can be expected to allow even loose and one end gripped fibers to contribute to the strength of the fabric. Accordingly, the model presented can only be considered as the first step towards characterizing the mechanical behavior of electrospun webs.

## **Appendix B:** Enhancement of orientation and crystallinity of electrospun fibers in a selected structure

The electrospun webs tended to elongate extensively, to values as much as 600%, which indicated that the molecular chains were not oriented. X-ray diffraction was performed to find the crystallinity and orientation of webs. Figure 8.2 obtained for PEO solution of 10% concentration shows the X-ray diffraction pattern of as spun random web. The circles indicate that the crystals present are randomly oriented.

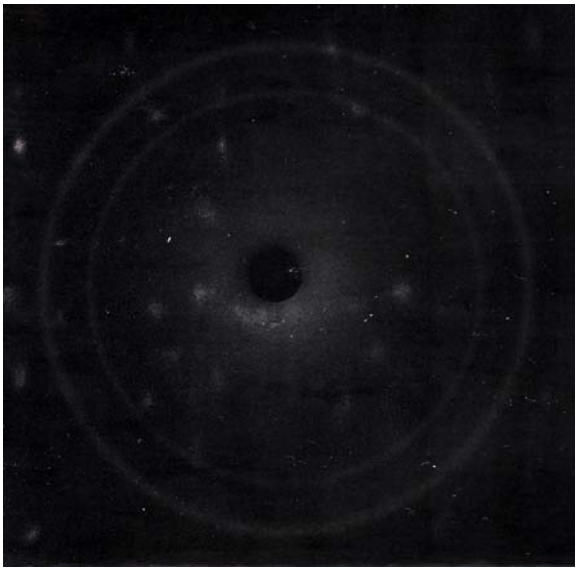

**Figure 8.2** X-ray Polaroid image of undrawn web

Drawing and annealing of such web can be expected to orient the molecules along with crystals and enhance the mechanical properties. To find the effect of drawing, X-ray diffraction patterns were collected for webs drawn at 150% and 300%. The X-ray diffraction

patterns, given in Figure 8.3, show that the circles changed to arcs. The greater the draw ratio, the smaller is the length of the arcs, which means that the degree of orientation increased with draw ratio. This result indicates that the electrospun webs are amenable to drawing and orientation of structure, and as a result to enhancement of the mechanical properties.

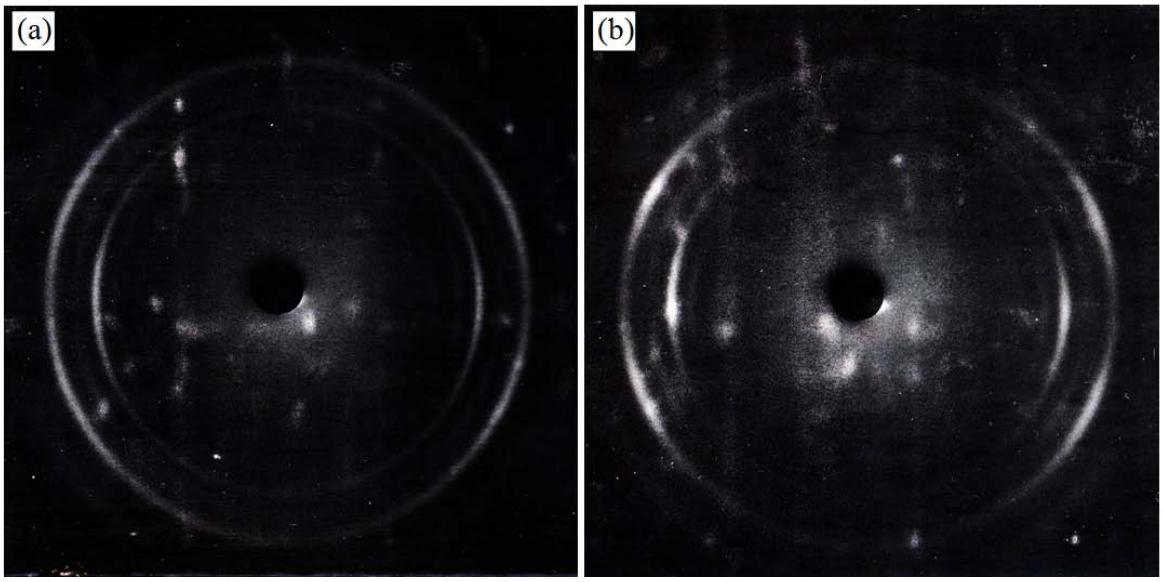


**Figure 8.3** X-ray Polaroid images of (a) 150% drawn and (b) 300% drawn webs